The Halogen Composition of the Proto-Iceland Plume Source Mantle

Dónal O' Farrell

Thesis submitted to the University of Dublin,

Trinity College in fulfilment for the degree

MASTER OF SCIENCE

Department of Geology
School of Natural Sciences
Trinity College Dublin
September 2017

Trinity College Dublin

The University of Dublin

Declaration

I declare that this thesis has not been submitted as an exercise for a degree at this or any other university and it is entirely my own work.

I agree to deposit this thesis in the University's open access institutional repository or allow the library to do so on my behalf, subject to Irish Copyright Legislation and Trinity College Library conditions of use and acknowledgement.

Summary

This study combined electron microprobe; ion microprobe and laser ablation- inductively coupled mass spectrometry to characterise the halogen composition of a suite of melt inclusions derived from 62Ma lavas from Baffin Island; products of the ancestral Icelandic mantle plume.

This reservoir retains primordial volatile compositions from the Earliest inception of the Earth. As such the characterisation this reservoir allowed for the determination of isotopic ($\delta^{37}Cl$) and elemental (Cl,Br) halogen composition of the Bulk Silicate Earth. This represents the first ever study to directly constrain the initial halogen inventory of the Earth via direct measurement of the primordial undegassed reservoir.

Additionally, this study discovered an enriched component within the Proto-Iceland mantle plume; a significant occurrence among a suite of highly primitive melts. The enriched component is akin to other younger enriched components within the younger Icelandic lavas; suggesting that the Proto-Iceland mantle plume is also heterogeneous with respect to its geochemical character at a very fine scale.

Abstract

The study of halogens in mantle-derived melts is allowing for new and unique insights into mantle geodynamics (e.g. Kendrick et al., 2017). The current dataset of mantle halogens record the compositions of both the depleted MORB mantle and the major re-enriched OIB deep mantle reservoirs (EMI, EMII and HIMU). However our understanding of the halogen geochemical cycle suffers from a major limitation; the lack of a direct and measurable constraint on the Bulk Silicate Earth halogen composition of the Earth. Without this constraint in place, it is impossible to assess properly, the overall mass balance of halogens between the major geochemical reservoirs.

This study has aimed to address this issue by characterising the halogen composition of the primordial 'undegassed' mantle reservoir. This 'undegassed' high $^{3}He/^{4}He$ mantle is sampled in the Vaigat formation; the oldest rocks of the 62-58Ma Baffin Island-West Greenland lavas; products of the ancestral Iceland plume (Stuart et al., 2003; Starkey et al., 2009). Based on tungsten isotopic measurements in lavas from the same locality; the formation of this reservoir is time constrained to the first fifty million years of solar system history (Rizo et al., 2016). It records primordial compositions with respect to Pb and Nd (Jackson et al., 2010); and has previously elucidated the primordial water content of the Earth (Hallis et al., 2015). As such characterising the halogen composition of this reservoir represents a unique opportunity to assess the halogen inventory of the earliest Earth.

Modelling for crustal contamination revealed that none of the inclusions studied display any evidence of having been obviously crustally contaminated. The most primitive inclusions, yielded near-chondritic trace element compositions, while more enriched inclusions, record comparative light-ion lithophile element enrichment consistent with their respective whole rock's more radiogenic Sr-Nd composition. Cl/K ratios suggest that only one of the inclusions studied records potential seawater contamination. This enriched inclusion also records very incompatible element (Nb, Th, U Ba) enrichment suggestive of derivation from a source with a more enriched (EMI or EMII) mantle-like derivation; present within younger Icelandic plume lavas (Stracke et al., 2003; Thirlwall et al., 2004; Halldorsson et al., 2016). This primary enriched melt then interacted with a deep contaminant such as altered oceanic crust or

seprentinized mantle endemic to the asthenospheric mantle beneath Baffin-Island and West Greenland.

Elemental (Cl,Br) halogen compositions were calculated for the primitive mantle using experimentally derived partition coefficients (Joachim et al., 2015; Joachim et al., 2016).The primitive mantle Cl composition is suggested to lie within the range of 8.38-20.84 ppm; generally lower than previous estimates for primitive mantle with the upper range within range of previous estimates (Sun and McDonough, 1995, Palme and O'Neill, 2013, Kendrick et al., 2017). As such these results must prefer lower estimates for the Cl composition of the depleted MORB mantle in agreement with recent estimates (eg. Urann et al., 2017). Br values range from 1.15 to 21.84 ppb agreeing well with the values of O'Neill and Palme (2003).

Remarkably, δ^{37}Cl compositions of the most primitive inclusions yield values averaging -0.21±0.4‰, which agrees closely with the average value (-0.2‰), previously inferred for the Bulk Silicate Earth (Sharp et al., 2007) and that of type 3 chondrites at -0.3±0.5‰ (Sharp et al., 2013). Considering the Baffin Island melt inclusions record primitive trace element and $^{3}He/^{4}He$ characteristics in combination with other primordially determinant geochemical proxies; the values presented here may represent the combined Br, Cl and δ^{37}Cl compositions of the Bulk Silicate Earth.

Table of contents

Acknowledgements

I would like to offer my sincerest thanks to my supervisor's Dr Emma Tomlinson and Dr John Caulfield for their invaluable assistance, patience and guidance throughout the duration of this project. Both are extremely gifted researchers with incredible work ethics and natural leadership abilities. Without their guidance, I would not have gotten very far. I am especially grateful to Emma for granting me this enormous opportunity. Science Foundation Ireland generously provided funding for this project. Dr Finlay Stuart kindly donated the Baffin Island samples which made this study possible. My sincerest thanks go to my parents for supporting my education and offering endless patience and emotional support. I will never understand the breadth of their patience; but I am certainly grateful for it.

The technical staff of TCD; Maura, Noel, Frank and especially the recently retired Neil; they made my lab work a possibility. I must also thank the very helpful and patient Dr Robbie Goodhue. Dr David Chew offered invaluable help during the final stages of polishing. Last minute SEM work was organized by Professor Balz Kamber and was guided by a very generous Paul Guyett. Dr Vicki Smith and all of her colleagues at the University of Oxford gave me expert advice on preparation and Dr Smith also carried out WDS work on my behalf for which I am very grateful. The staff at the SWISS SIMS facility carried out the chlorine isotope measurements for which I am deeply grateful; in particular to Dr Anne-Sophie Bouvier. I am grateful to have met all of my fellow postgraduate and post doctorate scholars over the past 2 years; some of the most dedicated and naturally gifted people I have ever encountered. In particular I am grateful to Foteini Drakou and Isadora Heinrichs for being supportive friends. I am also very grateful to my close friends Davy and Niamh who offered support throughout the duration of this effort.

Lastly, I must say thanks to the academic staff of TCD Geology. Over 4 years they have instilled me with a passion for geology that I will carry with me for a lifetime. I will certainly miss the museum building. In many ways, it was a second home.

Chapter 1 Introduction

The distribution and partitioning of volatile elements between mantle and surface reservoirs is an area of long-standing and active research (e.g. Schilling et al., 1978). The presence of volatile species in the mantle may impose first order controls on rheology; which can affect mantle convection, the driver of plate tectonics (Bürgmann et al., 2008). Volatiles degassed from mantle-derived magmas can also contribute to the formation of both the atmosphere and hydrosphere; of which the chemical compositions can potentially determine suitable conditions for the presence of life on Earth and other planetary bodies (Sharp and Draper, 2013). As such, elucidating the relative distribution of volatile species within the major geochemical reservoirs, and their modes of redistribution within a temporally resolvable architecture, is a critical facet of accurately modelling planetary evolution.

The halogens (F,Cl,Br and I) are a group of reactive volatile elements which are overwhelmingly concentrated in Earth's surface reservoirs; in particular, the oceans and evaporite deposits (Eastoe et al., 2007; Pyle and Mather, 2009). They represent major degassing products in volcanic emissions (Aiuppa et al. 2009) which can directly affect stratospheric chemistry (von Glasow et al., 2008). They range from moderate (F,Cl) to highly volatile (I) behaviour. The 'heavy' halogens (Cl.Br and I) behave incompatibly in basaltic systems as a result of their large ionic radii while F has a propensity to substitute for the hydroxyl group in nominally anhydrous minerals (Luth et al., 2003; Roberge et al., 2015). As such, their distribution in the Earth system is controlled by their incompatibilities, their volatility (degassing) and fluid mobility (Pyle and Mather, 2009). The halogens are highly effective chemical tracers capable of tracking the introduction of volatile elements incorporated in serpentinites, sediments and altered lithospheric components to the deepest portions of the mantle (John et al., 2010; John et al., 2011; Chavrit et al., 2015; Kendrick et al., 2017).

Significant progress has been made towards quantifying the distribution of halogens throughout the mantle (Kendrick et al., 2017). This has been achieved by analysing the halogen compositions of mid-ocean ridge basalts (MORBs); the passive upwelling products of the upper mantle, and Ocean Island Basalts (OIBs); often the products of mantle plumes which may sample the deepest mantle (White, 2010).

A remarkable feature of mantle-derived halogens is that Br/Cl and to a lesser degree I/Cl ratios are consistent in both MORBS and OIBs. This has led some authors to suggest that the mantle halogen composition is dominantly homogenous reflecting long-term recycling of halogens into the mantle with a dominant slab/subduction control. (Kendrick et al., 2017).
The mantle $\delta^{37}Cl$ composition is however significantly variable across all mantle domains. This variability has similarly been attributed to the addition of recycled materials to the mantle over time, however heterogeneity over homogeneity is the resultant interpretation (John et al., 2010).

Despite significant progress, our current understanding of the halogen geochemical cycle suffers from a major limitation, this being the lack of a direct and measurable constraint on the Bulk Silicate Earth halogen composition. The Bulk Silicate Earth, refers to a composition of the silicate portion of the Earth after core extraction but prior to crustal extraction (McDonough and Sun, 1995). The elemental halogen composition of the BSE has been determined by iteration; by comparing mass balance estimates of the major geochemical reservoirs (Kendrick et al., 2017) or by comparing elements of similar incompatibility such as Cl/K etc. (Jambon et al., 1995; Palme and O'Neill, 2003; Kendrick et al., 2017).

To date, no study has attempted to characterise the halogen composition of a mantle reservoir which directly preserves primordial volatile chemistry. This study presents the first ever combined elemental (Cl,Br) and isotopic ($\delta^{37}Cl$) constraints on the high $^{3}He/^{4}He$ mantle reservoir, a mantle reservoir which can provide direct constraints on the BSE halogen composition. The high $^{3}He/^{4}He$ ratio of volcanic rocks believed to be derived from mantle plumes is believed to represent evidence of a mantle volatile reservoir that has remained largely undegassed since the Earth's accretion (Kurz. et al., 1982, Hilton et al.,1999). 62-58 million year old lavas exposed at Baffin island and West Greenland; the initial products of the ancestral Iceland plume retain the highest $^{3}He/^{4}He$ values ever recorded in terrestrial lava samples; up to 50 times higher than the present day atmospheric value (Stuart et al., 2003; Starkey et al.,2009). This reservoir has already been shown to preserve primordial volatile chemistry additional to the noble gases in the form of primordial water based upon deuterium isotopic constraints (Hallis et al., 2015). The extreme age and primitive composition of this reservoir is supported by Sm-Nd and Pb-Pb isotopic evidence; temporally constraining its formation between 4.55 and 4.45Ga (Jackson et al., 2010). Tungsten isotopic evidence goes

further in suggesting that this reservoir was created during the first 50 million years of solar system history (Rizo et al., 2016).

It is anticipated that this reservoir may preserve a primordial cache of halogens from the earliest Earth. This may allow for the first ever direct constraints on the BSE halogen composition, by analysis of the high $^{3}He/^{4}He$ mantle reservoir, a uniquely primordial and enigmatic vestige of the earliest mantle constitution.

Chapter 2 Background

2.1 Overview

Halogens reside in very low abundances (ppm-ppb) in basaltic rocks. As such, the analytical challenges posed meant that progress was hampered in assessing their distribution in the mantle by way of mantle-derived basalts. However recent advances, such as the noble gas technique (Johnson et al., 2000), the foremost accepted analytical technique for elemental halogen analysis, and dramatic improvements with respect to in situ analysis, have meant that significant strides have been made in characterising the halogen compositions of the major geochemical reservoirs (Kendrick et al,, 2017).

Chlorine isotope determinations of mantle-derived samples have also evolved to a globally inclusive but limited dataset (Sharp et al., 2007; John et al., 2010). Isotope ratio mass spectrometry represents the best accepted analytical technique for the determination of $\delta^{37}Cl$. Continuous flow IRMS methodologies only require small sample aliquots; on the order of micrograms to tens of micrograms with uncertainties approaching ±0.2 ‰ (Barnes and Sharp., 2016 and references therein). However, this method is not practical for certain sample types. For example; glasses and to a greater extent melt inclusions which can be less than 100um in size; necessitate the usage of an in-situ technique such as secondary ion mass spectrometry (Layne et al., 2009). Ion probe analysis is particularly useful in that it allows for high spatial resolution that can allow for direct measurements of Cl and $\delta^{37}Cl$ in melt inclusions (Layne et al., 2009; Manzini et al., 2016). Significant improvements have been made favouring multi-collection mode which allows for the simultaneous detection of $^{35}Cl^-$ and $^{37}Cl^-$ signals allowing for errors on the order of ±0.4‰ provided Cl concentrations are greater than 400ppm; at which point errors become larger (e.g. John et al., 2010). However methodologies are evolving in this regard also (Manzini et al., 2017).

Presented here is a simplified schematic which summarises our current picture of the mantle halogen composition based upon $Br/Clx10^3$ ratios and $\delta^{37}Cl$ values determined for the major geochemical reservoirs (Figure 1). Potential subduction inputs are also highlighted in section; above both subduction zones.

$Br/Cl\ x10^3$ ratios have a very tight range in mantle-derived basalts (on the order of 2-4), while the mantle $\delta^{37}Cl$ composition is far more variable across all mantle domains. At the base of

this image, overlying the core is the high $^{3}He/^{4}He$ reservoir, the target in this study; halogen composition to date undefined.

What follows is a synopsis of our current understanding of the mantle halogen composition; first pertaining to the elemental halogen (Cl,Br) picture; followed by the picture provided by $\delta^{37}Cl$ compositions. Both of these overviews will serve to illustrate our current understanding of the halogen geochemical cycle pertinent to the mantle.

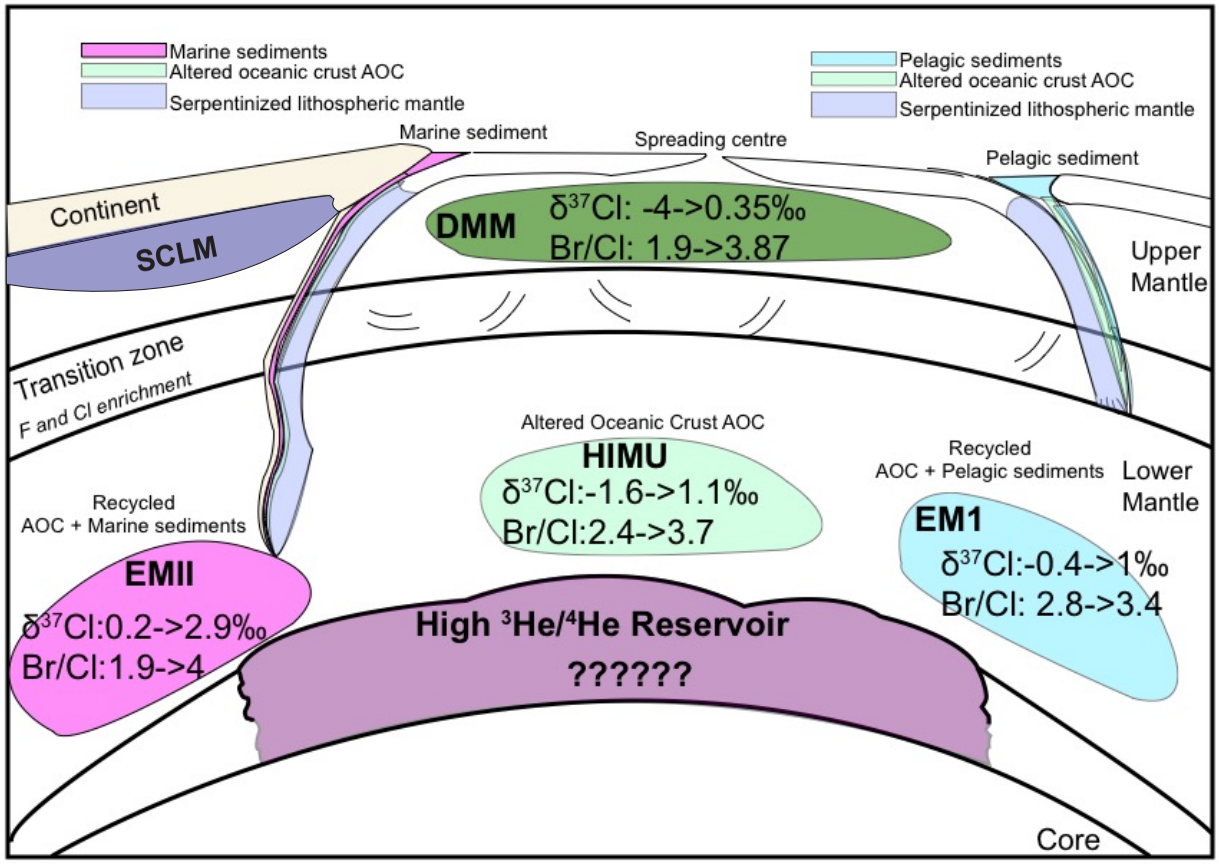

Figure 1: Schematic of the mantle halogen geochemical cycle. Potential source contributions to the mantle halogen budget are shown in section above the diagram. Transition zone enrichment inferred from Roberge et al,(.2015; 2017.). Data sources: δ37Cl MORB data: Sharp et al., 2007, Bonifacie et al. 2008, Layne et al. 2009. δ37Cl OIB data: John et al. 2010 Br and Cl data: Kendrick et al 2017. And references therein

2.2 Elemental Halogen (Cl, Br) composition of the mantle

As is evident from figure 1; the $Br/Clx10^3$ ratios of all the major mantle reservoirs are very similar within a tight range (2-4). $I/Clx10^3$ values are on the order of 25-90 (not shown). This has led some authors to suggest that the elemental halogen content of the mantle is controlled by slab mineralogy; which dictate the incorporation of recycled halogens through the subduction process (Kendrick et al., 2017). It should be pointed out however that from current calculated primitive mantle compositions; $Br/Clx\ 10^3$ ratio is 2.5 (based on the inferred BSE halogen composition of O'Neill and Palme; 2014); which is the average value of the contemporary global dataset. New high-resolution data on chondrites; the building blocks of planetary bodies demonstrate Br/Cl and I/Cl ratios indistinguishable from primitive mantle Br/Cl and I/Cl ratios (Clay et al., 2017). As such the Br/Cl and I/Cl composition of the modern mantle likely reflects an originally consistent Br/Cl and I/Cl composition that was overprinted by subduction additions, with little apparent deviation from the original chondritic composition.

Evidence for volatile and halogen subduction addition to the mantle is unequivocal. It was traditionally thought that volatiles (in this case the noble gases) could not be subducted deep into the mantle as result of the subduction barrier (Staudacher and Allégre, 1988); the inference being that most subducted volatiles were mobilised into the mantle wedge and degassed within arc magmas. However, the discovery that there is an air-like overprinting of primordial heavy noble gases in the mantle provides compelling evidence that there is indeed deep and pervasive recycling of volatiles into the mantle OIB source regions; all the way to the core-mantle boundary (Holland and Ballentine., 2006).

The recycling of halogens into the mantle has been demonstrated to directly affect mantle halogen compositions. For example, Scambelluri et al. (1997) demonstrated that hydrous ultramafic assemblages can host/transport significant quantities of seawater and elements such as the halogens into the deep mantle. Sumino et al. (2010) demonstrated that an exhumed portion of mantle from 100km depth, preserved marine pore fluid halogen and noble gas signatures. More evidence for halogen recycling stems from the fact that the OIB elemental Cl composition is enriched relative to primitive mantle estimates (Joachim et al., 2015; Kendrick et al., 2017). This is also supported by the considerable $\delta^{37}Cl$ variability (-4 to 2.9‰) expressed in the major mantle reservoirs (John et al., 2010).

2.3 Subduction inputs

The main carriers of halogens to the mantle represent subduction inputs and are likely to be sediments; altered oceanic crust and oceanic mantle serpentinites (Straub and Layne, 2003; John et al., 2011; Chavrit et al., 2016). In terms of serpentinites; mass balance indicates that they may be volumetrically significant contributors to the mantle halogen budget (John et al., 2011). Calculations by Barnes and Straub (2010) indicate Cl inputs at the Izu Bonin arc exceeds the outputs at arc volcanoes; suggesting that there is a net uptake by the mantle, which exceeds the output in the associated arc magmatism. The importance of serpentinized lithospheric mantle as a dominant halogen input to the mantle was re-iterated by Kendrick et al. (2017). Altered oceanic crust is also a volumetrically significant reservoir for Cl; due to formation of secondary Cl-bearing minerals such as chlorite and amphibole veins (Barnes and Cisernos, 2012) additional to the halogen host potential of the nominally anhydrous minerals. Chavrit et al. (2015) based on detailed halogen analysis of altered oceanic crust of varying depth profiles, estimated that altered oceanic crust alone fluxed to the mantle over a 3-billion-year timeframe (the postulated initiation of Wilson cycle style tectonics (Shirey and Richardson., 2011); could account for the whole Earth budget of halogens in the modern mantle.

2.4 Halogens in the mantle: mantle minerals

Silicate nominally anhydrous minerals (N.A.M.) such as olivine, orthopyroxene, clinopyroxene and aluminous phases only accept minor quantities of Cl in their crystal lattices, and in fact the lack of correlations between major elements and Cl may suggest that coupled substitution does not occur in many of the nominally anhydrous mantle minerals (Pyle and Mather 2009; Urann et al., 2017). As a consequence silicate minerals host only minor quantities of halogens; however the nominally anhydrous mantle minerals can retain sufficient quantities of Cl to account for the mantle halogen budget (Joachim et al., 2015); and indeed deeper mantle mineral polymorphs such as wadsleyite and ringwoodite may host even more abundant quantities of halogens (Roberge et al., 2015, 2017); meaning that the transition zone could represent a volumetrically significant repository for halogens (Figure 1). Experimental studies on the larger halogens Br and I are less frequent (Joachim et al., 2016) and more work is urgently needed in this regard.

2.5 BSE estimates for Br and Cl

All of the current estimates on the BSE halogen composition are in one way or another based on an iterative methodology rather than a direct measurement of a primordial reservoir (Table 1).

Reservoir	Chlorine	Bromine
Bulk Silicate Earth	17-37ppm	3.6-76ppb
MORB source mantle	0.14-21ppm	7.5-8ppb
OIB source mantle	21-71ppm	11-20ppb

Table 1: Compositions of the Bulk Silicate Earth relative to the MORB and OIB source mantles. Data sources: Joachim et al., 2015 and references therein,2016; Lyubetska and Korenga. 2007 McDonough and Sun. 1995; O'Neill and Palme 2003., Roberge et al., 2017.

Most commonly these values are arrived at by comparing lithophile elements of similar incompatibility to the volatile element in question; e.g. Cl/K (Palme and O' Neill, 2003). While other methodologies involve summing the relative proportions halogens contained within the major reservoirs (depleted mantle, continental crust and exosphere) to arrive at the original primitive mantle composition (Kendrick et al., 2017). The latter methodology is interesting with respect to this study. In order to calculate the primitive mantle halogen composition; an estimate was inferred postulating the ratio of processed mantle relative to primitive mantle. The authors arrived at this conclusion by suggesting that the proportion of unprocessed/primitive mantle correlates with incidences of high $^{3}He/^{4}He$ ratios recorded in oceanic basalts.

This study will in contrast directly measure the halogen composition of the high $^{3}He/^{4}He$ reservoir which preserves primordial volatile chemistry (Hallis et al., 2015).

2.6 $\delta^{37}Cl$ composition of the mantle

The fractionation of stable isotopes decreases with the square root of temperature and becomes nearly negligible in most cases at mantle temperatures (White, 2015) Stable isotopes measured

in OIBs as such can offer unequivocal evidence of recycling of ancient lithosphere, crust and sediments into the mantle (e.g. Cabral et al. 2013).

Chlorine has some 24 isotopes ranging from 22Cl to 51Cl. The two most abundant stable isotopes are ^{35}Cl and ^{37}Cl. $\delta^{37}Cl$ values (ratios of ^{37}Cl to ^{35}Cl) are reported in ‰ deviations relative to the standard SMOC (Standard Mean Ocean Chloride). Significant $\delta^{37}Cl$ fractionation from Standard mean Ocean Chloride (seawater) is not expected to occur at mantle or magmatic temperatures (Schauble et al., 2003). As such, highly fractionated $\delta^{37}Cl$ compositions measured in mantle-derived samples relative to standard mean ocean chloride at 0‰ (Eastoe et al., 2007) must reflect the addition of already fractionated surficial material to the mantle source (John et al., 2010). It is thought that the chlorine isotopic composition of the ocean has remained relatively constant through time; as there is no significant variation in measured $\delta^{37}Cl$ in Precambrian and Phanerozoic halites, cherts, barites and dolomites (Sharp et al., 2013 and references therein). Considering the ocean retains 80-90% of the Earth's halogen inventory (Pyle and Mather, 2009); this suggests that the value of the Bulk Silicate Earth should approach that of seawater at 0‰.

The mantle $\delta^{37}Cl$ composition shows considerable variability across each of the major mantle domains (Figure 1) The depleted MORB mantle records isotopically negative compositions which extend as low as -4‰ (Layne et al., 2009). While the re-enriched OIB mantle reservoirs show both isotopically heavy and lighter compositions. It should be noted that while this dataset covers the major OIB reservoirs; in most cases these are limited to just a handful of analyses from the same locality. For example, the EMI mantle reservoir $\delta^{37}Cl$ composition is based upon only two analyses of Pitcairn glasses. The most positive $\delta^{37}Cl$ glass in the global dataset is a Society glass of EMII character recording a $\delta^{37}Cl$ value of 2.9‰. Positive covariation is evident between more radiogenic $^{87}Sr/^{86}Sr$ compositions and more isotopically heavy $\delta^{37}Cl$ reflecting mixing of two different mantle sources (John et al., 2010).

Significantly, when the global dataset of $^{206}Pb/^{204}Pb$ and $\delta^{37}Cl$ compositions are plotted against the other; there is an obvious compositional zonation likely directly related to mantle source characteristics (Figure 2). As such there appears to be definable and conclusive $\delta^{37}Cl$ flavours within the mantle; quite distinct from Br/Cl and I/Cl ratios.

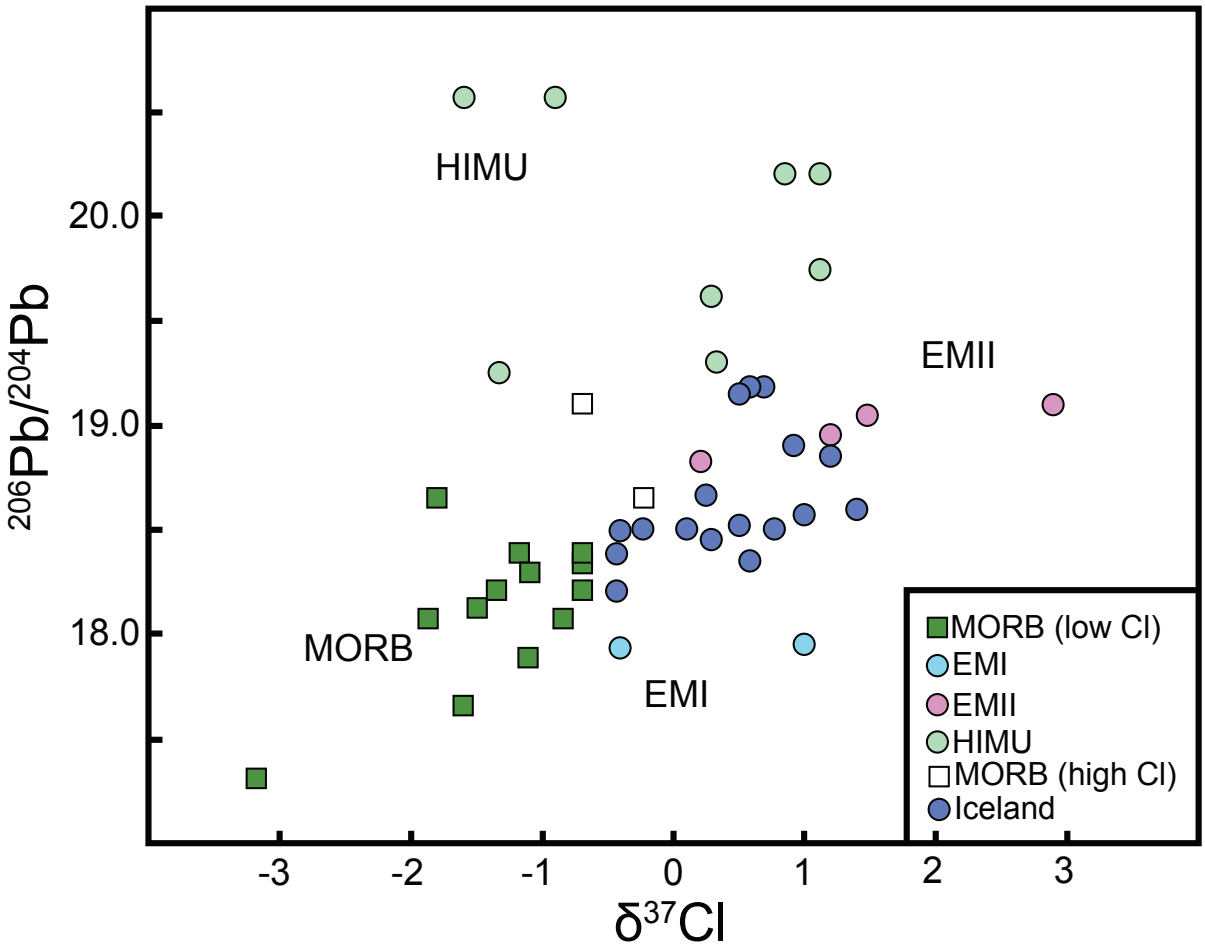

Figure 2: Global dataset of $^{206}Pb/^{204}Pb$ versus $\delta^{37}Cl$ in MORB and OIB. MORB data: Sharp et al., 2007, Bonifacie et al. 2008, Layne et al. 2009. δ37Cl OIB data: John et al. 2010. Icelandic data: Halldorsson et al. 2016

2.7 δ^{37}Cl Subduction inputs

A remarkable feature of the δ^{37}Cl composition of the earth is that in contrast to most other stable isotopes, more variability is observed within mantle samples than within surficial reservoirs (White, 2015).

This is unexpected as high temperature magmatic/mantle fractionations are negligible and hence the variability expressed in the respective mantle domains is a consequence of surficially fractionated materials being added to the source.

The greatest variation in the δ^{37}Cl composition of the surficial components is observed in marine pore waters extending to values as low as -8‰ (Bonifacie et al., 2008b). The δ^{37}Cl composition of sediments within the limited dataset does not record a dominant signal unique to this input (Barnes and Sharp, 2016) with mostly isotopically negative values. Sediments were thought to be fractionated during the subduction process; via the expulsion of ^{37}Cl-depleted pore fluid leaving the residual sediments with isotopically positive δ^{37}Cl compostions and accounting for the positive δ^{37}Cl signals observed in enriched mantle domains (John et al., 2010). However, comparative analyses of ultra-high pressure metamorphic rocks display a similar overlap in ranges (-3.6 to 0‰); suggesting that fractionation is not mediated by subduction metamorphism.

Fluid interaction seems to be the dominant mechanism of Cl isotope fractionation in sediments; as metamorphic rocks tend to retain the δ^{37}Cl values of their protoliths (Selverstone and Sharp, 2015). Altered oceanic crust is generally enriched in chlorine due to secondary alteration minerals; with recorded values in altered basalts of between -1.4 to 1.8‰ (Barnes and Cisernos, 2012). Serpetinites are well characterized with respect to δ^{37}Cl. John et al. (2011) demonstrated that during a complete sequence of serpentinization from oceanic environments to depleted harzburgite there is no discernible Cl isotopic fractionation. This is despite significant devolatilisation throughout prograde metamorphism of subducting serpentinites. Again the major source of fractionation of serpentinites is anticipated to be infiltrating fluids (Barnes and Sharp., 2016 and references therein).

2.8 Iceland

$\delta^{37}Cl$ values of the Icelandic NVZ (Neovolcanic Zone) glasses ranges from -1.8 to 1.4‰ (Halldorsson et al., 2016). Significant perturbations of the $\delta^{37}Cl$ signal by shallow level degassing or seawater contamination can be ruled out and as such the values presented therein are representative of the contemporary Iceland plume. The authors imply mixing between at least two major reservoirs in the modern Icelandic plume source mantle; a depleted reservoir characteristic of DMM with low Cl concentrations and slightly negative $\delta^{37}Cl$ compositions and also a reservoir of more enriched character, with high Cl concentrations and more positive $\delta^{37}Cl$. The degree of melting is thought to account for some of this variability based on correlations between La/Yb and $\delta^{37}Cl$; whereby the lowest degree melts (deepest within the melting column) will sample mantle with higher Cl and $\delta^{37}Cl$; becoming progressively diluted with a more DMM-like component as the degree of melting increases.

The $^{206}Pb/^{204}Pb$ versus $\delta^{37}Cl$ Icelandic data (Figure 2) appears to highlight a compositional bi-modality present in the Icelandic plume. Most obvious is an apparent continuum between a DMM component and an EMII-like component; end-members previously suggested to account for the mixtures/variabilities seen in Icelandic basalts (Stracke et al., 2003; Thirlwall et al., 2004; Halldrosson et al., 2016).
This led the authors to imply that the modern Icelandic plume has incorporated a section of altered subducted lithosphere with an associated sedimentary veneer (Halldorsson et al., 2016). As such this provides evidence that portions of the Iceland plume are variably contaminated with recycled material; in this case likely some quantity of terrigenous sediment. This speciation is as such potentially also present in the Proto-Iceland mantle plume.

2.9 Primitive mantle $\delta^{37}Cl$ composition

While pronounced variability exists in mantle-derived samples from the OIB and MORB reservoirs measured by ion probe (John et al., 2010); Sharp et al. (2007;2013) determined based on analyses on a diverse sample set (MORB, OIB, halites, carbonatites, unaltered peridotites) measured by IRMS that almost all of these samples recorded $\delta^{37}Cl$ values approaching 0‰. The suggestion as such was that the primitive mantle halogen composition is very close to that of the least altered chondrites at 0.3±0.5‰ (Sharp et al., 2007; 2013),

indicative of a consistent $\delta^{37}Cl$ nebular composition parental to chondrites and the Earth; with no obvious secular variation throughout the Earth's history.

No study to date has attempted to independently resolve the $\delta^{37}Cl$ composition of the Bulk Silicate Earth by analysing a reservoir which directly preserves primordial volatile chemistry (Hallis et al., 2015).

Chapter 3 Samples

3.1 Sample locality and association with the Iceland plume

The samples chosen for this study are derived from the Vaigat Formation of the 62-58Ma Baffin Island-West Greenland lavas. The lavas are exposed as coastal outcrops along the coastlines of both Padloping Island and Cape Searle; both situated in Merchant's Bay of the Davis Strait which lies off the Eastern coast of mainland Baffin Island (Figure 3).

They represent some of the initial products of the Iceland mantle plume. The thermal anomaly generated by the Iceland plume was thought to be centered within Western Greenland at around 65Ma. Plate migration for the following 20Myr meant the anomaly migrated westward (Mihalffy et al., 2008). Gill et al. (1995) postulated that the Baffin Bay lavas may in fact represent a 'startup' plume ancestral to the Proto-Iceland plume.

The first magmas of the North Atlantic Igneous province form the 62.5-61Ma Vaigat formation, of Baffin Island and West Greenland (Larsen et al., 2015). It is lavas from this formation that are targeted for this study. The Baffin Island and West Greenland (BIWG) magmas were erupted through rifting and thinning of Precambrian lithosphere contemporaneous with the opening of the Labrador Sea (Clarke and Upton, 1971). The lavas are emplaced upon Precambrian crust and Tertiary sediments.

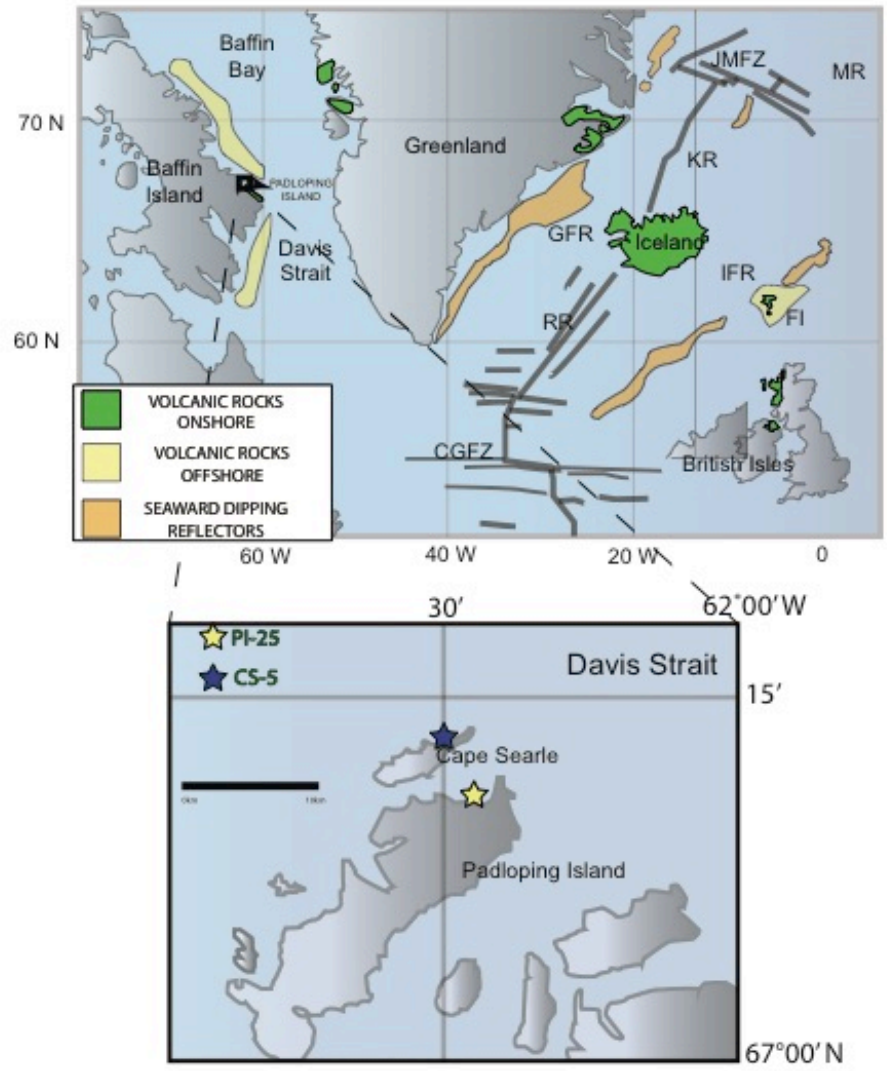

Figure 3:Location map of the North Atlantic Igneous Province and associated volcanism (after Saunders et al., 1997). CGFZ=Charlie Gibbs Fracture Zone, RR= Reykjanes Ridge, GFR= Greenlan-Faeroes Ridge, IFR=Iceland-Faeroes Ridge, Faeroes Islands Inset: Padloping Island and Cape Searle, both samples are taken from coastal outcrops.KR=Kolbeinsey Ridge, JMFZ=Jan Mayen Fracture Zone, MR=Mohns Ridge. Inset: Padloping Island Cape Searle; both samples are derived from coastal outcrops

3.2 Geochemistry of the lavas

The BIWG lavas are highly magnesian melts; their bulk major element chemistry strongly suggests derivation from high temperature melts consistent with a thermal anomaly generated by a mantle plume (Larsen and Pedersen, 2000; Herzberg et al., 2007). The samples are predominantly tholeiitic (Larsen et al., 2003). Sample PI25; one of the 2 samples targeted for this study recorded a whole rock MgO composition of 27.69 wt% while CS5 has an MgO composition of 15.69 wt%. The association of high MgO contents (15-30 wt%) and conspicuously abundant olivine phenocrysts could potentially serve to define these lavas as picrites (le Bas., 2000). These lavas are plotted on a le Bas diagram in Figure 4. Sample CS-5 plots in the basalt sector. Sample PI-plots on the line dividing picro-basalts and basalts.

Two magma types can be recognised based on their trace-element geochemistry; N-type and E-type (Robillard et al.,1992). N-type magmas, predominantly high-MgO, have depleted LREE patterns $(La/Sm)_N$ typical of N-MORB, and $^{87}Sr/^{86}Sr < 7.032$. E-type magmas, which cluster in the lower MgO magmas have flat to slightly enriched LREE patterns typical of E-MORB and $^{87}Sr/^{86}Sr$ between 0.7032-0.7039. These two magma types are virtually indistinguishable in terms of major elements and many other trace elements (Robillard et al., 1992; Starkey et al., 2009). Both samples chosen for this study resemble E-MORB type compositions.

The olivine phenocrysts contain rare olivine-hosted melt inclusions. It is these inclusions which are targeted to characterize the volatile composition of the mantle domain from which they are sourced. Previous studies on Padloping Island melt inclusions suggested that melt inclusions in that study were subject to up to 15% contamination with broadly granitic partial melts derived from Precambrian lithosphere of predominantly Paleoproterozoic age (Clarke and Upton, 1971; Yaxley et al., 2004). Starkey et al. (2012) demonstrated however that olivine hosted melt inclusions derived from the broad Baffin Island-West Greenland suite displayed no obvious evidence for crustal contamination based upon La/Yb versus Nb/Zr ratios. As such, this will require investigation in the melts studied.

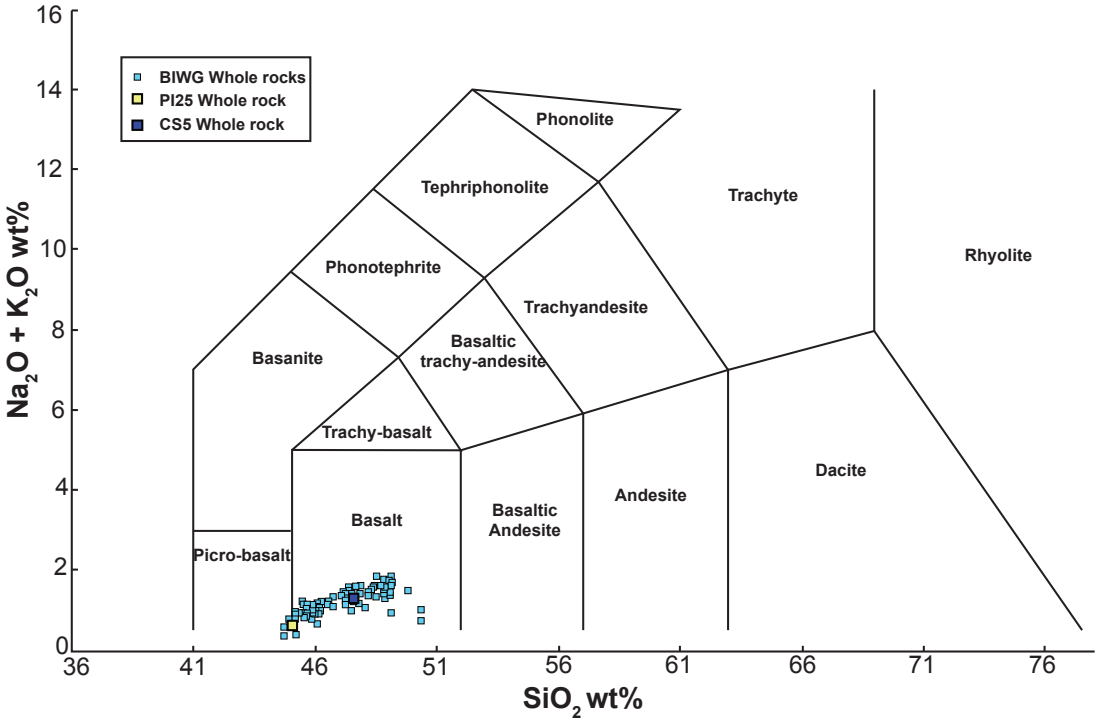

Figure 4: Total alkali-silica (TAS) diagram after le Bas (2000). The Baffin Island- West Greenland basalts from Starkey et al. (2009) predominantly plot in the basalt sector (including CS-5). PI-25 plots on the border of basalts and picro-basalts.

3.3 Sr-Nd-He isotopic systematics

Careful consideration of the available samples led to the choice of sample PI25 of the BIWG suite from Starkey et al. (2009). This sample records a particularly unfractionated Sr-Nd radiogenic isotopic composition (Figure 5) and the highest $^{3}He/^{4}He$ composition (50Ra) (Figure 6) and as such it is the best possible representation of the undegassed and unperturbed primordial volatile reservoir (Porcelli and Elliot., 2008; Starkey et al., 2009). A separate sample; CS5 with more radiogenic $^{87}Sr/^{86}Sr$ and $^{143}Nd/^{144}Nd$ and moderately high $^{3}He/^{4}He$ was chosen as a more radiogenic contrast.

The melts retaining the highest $^{3}He/^{4}He$ values represent the most ideal candidates for the stated goals of this study. Combined with other primordially determinant compositional vectors; such as deuterium, tungsten, lead, and neodymium isotopic constraints, means that these samples represent the ideal candidates for assessing the halogen composition of the primordial mantle reservoir; and by inference that of the Bulk Silicate Earth (Jackson et al., 2010; Hallis et al., 2015., Rizo et al., 2016).

-

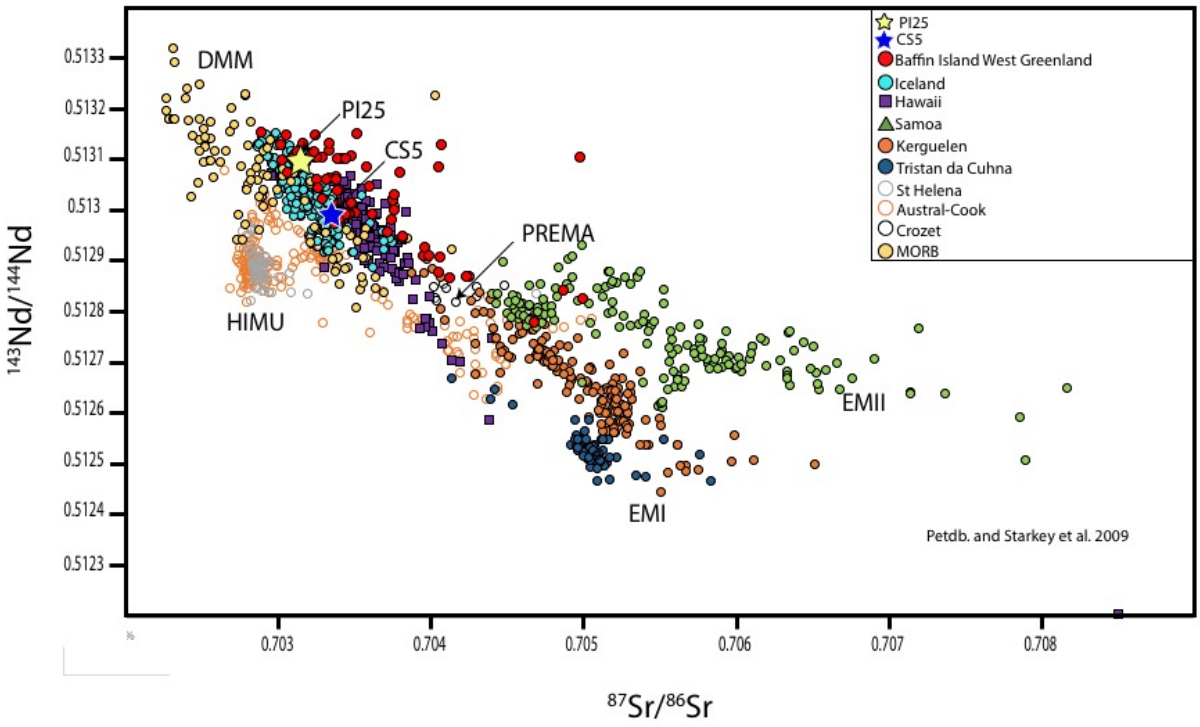

Figure 5: Gloabl Sr-Nd array. Representative samples from the major mantle reservoirs are taken from Petdb within the Earthchem databases. Baffin island and West Greenland lavas are from Starkey et al. (2009). The samples chosen for this study: PI25 and CS5 are represnted by yellow and blue stars respectively; a format which will be retained throughout the manuscript.

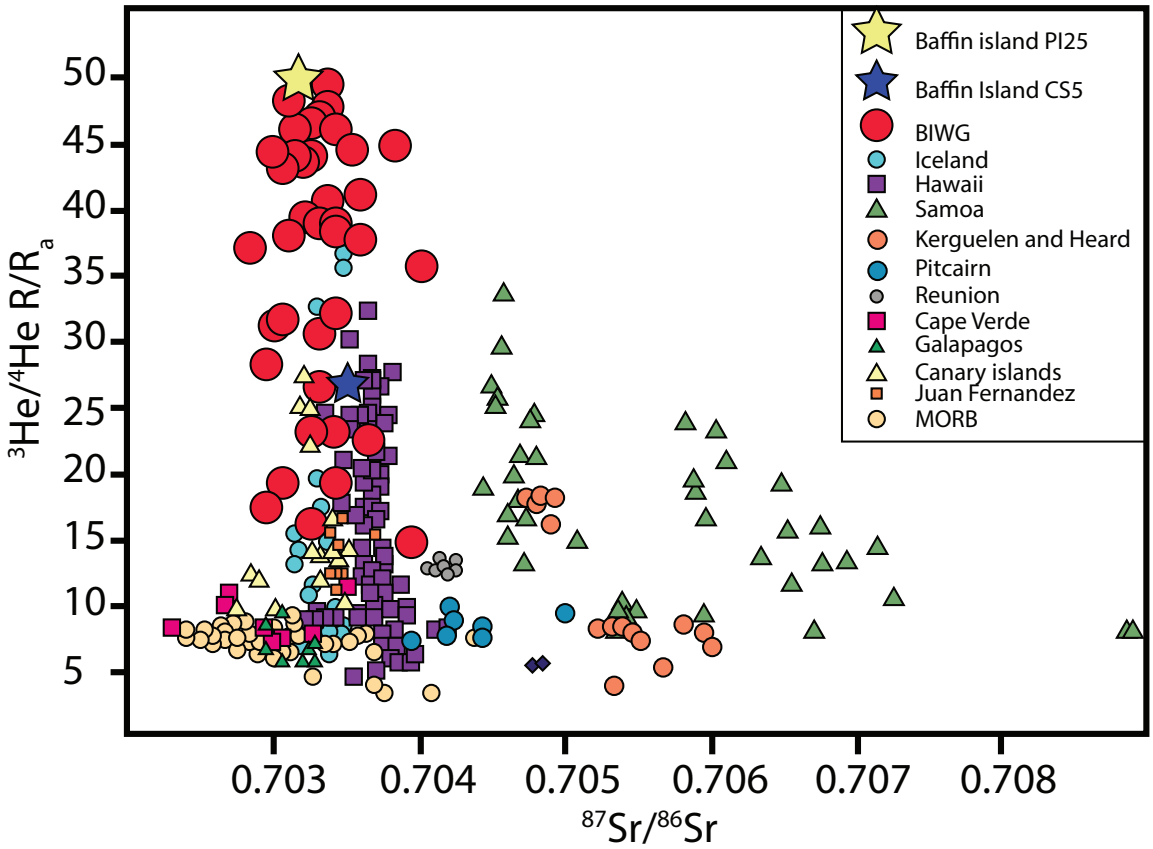

Figure 6: Global array for Sr-He. Note that OIB values do not exceed 35 times the atmospheric value with some extending to values as low as 5Ra.. MORB samples average 8Ra. The BIWG samples are uniquely high within the global dataset up to 50Ra. Both samples are again represented with star figures. Replotted from Starkey et al. (2009). Data sources OIBs: Abdeini et al. (2006). MORB: Petdb from the Earthchem databases.

3.4 Melt inclusions

3.4.1 Melt inclusion background

Olivine hosted melt inclusions (OHMIs) are small volumes of quenched silicate melt which are encapsulated in a crystallizing olivine phenocryst. They are usually less than 100 μm in size. OHMIS are in effect chemical and temporal snapshots of the parental magmatic system at the time of encapsulation (Danyushevsky et al., 2002) Olivine, being an early crystallizing phase in mafic systems, should encapsulate MIs during an early phase of melt evolution. The MIs are potentially shielded from further magmatic processes. Dissolved volatiles are lost from an ascending magma as they have pressure dependent solubilities. This makes it difficult to investigate pre-eruptive volatile contents of magma by direct analysis of erupted material (Mackwell, 2015). Melt inclusions are protected from degassing and as such can offer more reliable insights into the volatile composition of the magma and ultimately that of the source (Jennings et al., 2016).

Variability in OHMIS is often far more pronounced than that seen in their parental whole rocks, and it may suggest that erupted whole rocks represent an average of a variety of different primary melts that were mixed prior to eruption. However, any inferences made about the source must be scrutinized carefully as MI major element compositions can be significantly altered by post entrapment modification processes, rendering their interpretation more problematic (Sobolev, 1996). OHMIs are often affected by a secondary process referred to as post-entrapment crystallization (PEC). This involves secondary micro-crystallization of olivine along the interface between the inclusions and the host phenocryst. This can significantly perturb the major element chemistry of the inclusion (Yaxley et al., 2004), most notably with respect to FeO and MgO. These processes can be accounted for by reverse modelling the chemical effects of PEC. Generally, it is accepted that trace element concentrations will increase proportionally due to the reduction in volume of the inclusion as a result of PEC, as olivine is a very poor repository for trace elements (Peate et al 2012; Starkey et al., 2012). Due to the highly incompatible nature of the heavy halogens (Cl,Br); the halogen composition and ratios expressed in the measured MI compositions should be unaffected by PEC. Cl is also not known to diffuse out of melt inclusions; as such both measured Cl and δ^{37}Cl should be representative of the source (Layne et al., 2009; Le Voyer et al., 2014; Manzini et al., 2017).

3.4.2 Description of the inclusions in this study

Sample PI-25 contains rare glassy inclusions. The majority have a round shape and are optically clear with a mean long axis length of 30μm (Supplementary Figure 1A). There was also a considerable amount of long cylindrical inclusions of varying lengths and widths (Supplementary Figure 1B). Some rare glassy inclusions display a slightly orange/pink tinge and were preserved with more complicated morphologies (Supplementary Figure 1C). Sample PI-25 also contained an anomalous inclusion which was a deep brown in colour (supplementary figure 1D). Attention is drawn to this inclusion at this stage, as it's chemistry was unique among all inclusions studied; often referred to herein as the 'enriched' PI25 melt inclusion.

Sample CS-5 contained far less pristine glassy inclusions. Many showed evidence of some degree of recrystallization (Supplementary Figure 1E).

Chapter 4 Methodology

Methods are outlined in the order of the preparation/data acquisition. Reference material compositions were obtained from GeoREM for accuracy measurements (Jochum et al., 2006), along with the Smithsonian diopside microbeam standard: NMNH 11733 (Jarosewich et al., 1980). Precision measurements have also been included in this section.

4.1 Preparation

Olivine-hosted melt inclusions contained within individual olivine phenocrysts were sought out by careful picking using a transmitted light microscope. Clear glassy inclusions were deemed the most suitable candidates for electron microprobe and ion probe analysis. Ion probe analysis was deemed essential as it is the only viable method to study low abundance volatiles in situ in olivine-hosted melt inclusions (Hauri., 2002; Layne et al., 2009; Manzini et al., 2016). This is due to the small size of OHMIs (most <100 μm) necessitating an in-situ technique. Ion probe analysis also provides unrivalled sensitivity (ppm-ppb) for low abundance volatiles (Hauri., 2002).

Individual crystals were placed in clove oil which has a refractive index similar to that of olivine (~1.635). This helped to demarcate any inclusions present in the olivine crystals. High magnification (50-100x) was necessary to determine potential candidate inclusions. Inclusions adhering to opaque minerals were avoided as were inclusions connected to cracks or any aberrant internal architecture present in the olivine phenocrysts. Inclusions not fully encapsulated in their host phenocrysts were also avoided. These were quality control steps to ensure that the volatile signature being analysed was closest to that of the source and that no de-volatilisation of the melt inclusion had occurred.

Suitable olivine hosted-melt inclusions were picked and subsequently mounted in Crystalbond 509 on individual glass slides. The use of Crystalbond was necessary as target inclusions had to exposed individually in their host phenocrysts. Crystalbond can be removed by heating, or by dissolution in an organic solvent, allowing for further work to be carried out on the

individual inclusions subsequent to liberation. Blotches of Crystalbond were placed on the edges of the glass slides in order to aid in keeping the slide level when polishing.
Manual polishing by hand was then carried out to expose surfaces just above the respective melt inclusions in preparation for mounting in epoxy. Samples were wet polished using progressively fining grit SiC papers (p800, p1200, p2000 and p4000 papers). Manual polishing was deemed necessary for two main reasons:
1. Despite the time-consuming nature of manual polishing; Crystalbond 509 has a tendency to degrade when subjected to repeated and intense friction on an automatic polishing lap, which can lead to breakdown in the integrity of the adhesive; often resulting in loss of crystal, or adhesion of polishing compound to the Crystalbond.
2. Manual polishing allowed for more control in the amount of material being removed during polishing.
In order to minimise scoring and etching on the surface of the phenocryst particular care was taken to polish in 'figure 8s'; taking care to change the orientation of the sample every 10-20 rotations. A number of inclusions were damaged or plucked during the coarse polishing phase despite appropriate care. Polishing with too low a grade of SiC paper tended to round or impart a slope upon the grains.

Crystals with a pre-exposed or partly exposed melt inclusion were then liberated from the Crystalbond by heating the Crystalbond to c.100 °C on a hotplate. Every effort was made to remove as much Crystalbond as possible in this stage by edging the crystal along the width or length of the glass slide. Crystals were then bathed in acetone for 5 minutes to remove potentially adhering resin or polishing material. Crystals were then oriented onto their target surfaces aided by reference photographs and sketches taken prior to liberation. The target surface of the crystal was then placed face down on double-sided sticky tape in preparation for mounting in epoxy. A silicate glass standard StHs6/80 was placed onto each of the 3 sample pucks for later accuracy and reproducibility controls (Jochum et al., 2006). Epoxy mounts were poured and then placed into a vacuum chamber to minimise bubble formation. This step was necessary to prevent the release of volatiles from the epoxy mount into the analytical chambers of the respective apparatuses under vacuum. The pucks were then placed in an incubator for a 48-hour period to allow them to set.

The final polishing step involved simultaneously exposing melt inclusions hosted in different crystals contained within the pucks.

Automatic polishing was necessary at this stage as epoxy mounts responded poorly to polishing with silicon carbide papers. Polishing was carried out using a Labopol 21 automatic lap in the Fission Track Laboratory at Trinity College Dublin. Progressively fining grits of Diapro polishing solution were used to polish to the target surfaces. A fine polishing step using 1um Diapro solution followed this to reduce any scratches remaining on the surface of the olivines and exposed inclusions. Each individual crystal and inclusion was then photographed using a mounted digital camera under transmitted light using a Nikon Eclipse LV100 light microscope.

4.2 Major element analysis

Samples were characterised for major element oxides by SEM-EDX at the Centre for Microscopy and Analysis, Trinity College Dublin to target the most suitable inclusions for ion probe analysis, and also to assess the extent of crystallisation in the melt inclusions. The pucks were carbon coated before analysis on a Tescan MIRA XMU FE-SEM operating under high vacuum conditions. The SEM was equipped with an Oxford X-Max 80 nm^2 detector running Oxford Aztec analysis software and compositional data were obtained with an acceleration voltage of 20kV, a beam current diameter of 30 μm at a magnification of 31,000x. The standards employed were pyrope for Fe and Mn, augite for Al,Ca and Mg, anorthoclase for Na and K, in-house synthetics were used for TiO_2 and CrO_2 (Jarosewich et al., 1980). Totals acquired were all within ±1% of 100%. Accuracy and precision measurements for selected oxides can be viewed in table 2. Back-scattered electron images were taken of all samples and of all of the individual inclusions to aid in assessing the highest priority (i.e. the most pristine) inclusions for SIMS analysis. The C coating was then removed by further polishing using 1 μm Diapro solution on a Labopol 21 automatic polishing lap.

Diopside, NMNH 11733	Accuracy 1 (in %)	Accuracy 2 (in %)	Precision
SiO2	0.58	0.84	0.41
MgO	1.04	1.15	0.73
CaO	0.04	-0.35	0.33

Table 2: Accuracy and precision measurements for major element analysis conducted by SEM-EDX. Diopside, NMNH 11733 is a Smithsonian microbeam standard from Jarosewich et al. (1980).

4.3 δ^{37}Cl analysis

Due to size of the inclusions a high spatial resolution; an in-situ technique was required for δ^{37}Cl data acquisition. As such, ion probe analysis was carried out on a CAMECA IMS 1280HR instrument at Swiss Sims facility (University of Lausanne) to determine δ37Cl values of the melt inclusions.

In order to maintain a constant secondary ion beam current, potential difference between the extractor lens and the sample must be kept constant; a gold coat can help to absorb any charge build-up on the surface. As such; sample pucks were coated with a 20nm gold coat.

Calibration against low Cl-glass standards B-21, B-20D (basalts) and T-1G (granodiorite) was required to quantify the analytical runs. In order to monitor instrumental mass fractionation (IMF), standard B20D, which was compositionally similar to the samples in this study was used to correct for this fractionation. StHs6/80-G was used to assess drift and as a reproducibility monitor.

In order to minimise all possible Cl contamination from the sample surface, a pre-sputtering of 250s with a 25um raster applied to the beam was employed. Samples were sputtered with a Cs^+ primary beam accelerated through a nominal potential of 10kV. The energy slit of the mass spectrometer was set to 50eV width. Mass resolving power was set to 4004. Count cycles were set to 70 seconds to improve count statistics.

Accuracy was controlled with reference to in house values for standards T-1G and StHs80. Reproducibility (2 standard deviations) reported in per ml deviations was 0.25‰ for T-1G, and 1.1‰ and 1.09‰ for B2-1 and B20D respectively.

4.4 Major element analysis by Wavelength-dispersive X-ray spectroscopy

In preparation for SEM-WDS (wavelength-dispersive spectroscopy) analysis the gold coats were removed by polishing on an auto lap using Diapro solution. Major and selected low abundance element chemistry of host olivine's and melt inclusions was determined using a wavelength-dispersive JEOL 8600 electron microprobe in the Research Laboratory for Archaeology and the History of Art, University of Oxford. The samples were first coated with a 12nm carbon coat. Three separate analytical runs were carried out in total. The olivine crystals were analysed for major elements with a 15-20 nA current with a beam diameter of 1um. The melt inclusions underwent two analytical runs, the first intended to determine major element chemistry. This was carried out with a 6nA beam current with a beam diameter of 5-10um with 30s count times for each peak. The second run was intended to characterise low abundance elements F, Cl, P, Cr and S at a higher beam current with a 5-10um beam diameter and 60 second plus count times for each element. Well characterised standards StHs6/80-G and GOR128 were used to calibrate the instrument.

Accuracies for all oxides were generally within the ranges of ±5% for all oxides in StHs6/80-G and ±1% for GOR-128-G. Cl and F were below detection limits in the volatile analysis. Precision measurements for the major element oxides analysed can be seen in table 3. Precision measurements for selected low-abundance volatile elements can be seen in table 4. Poor totals on some inclusions necessitated combining the major element data acquired by WDS with the previously determined EDS data. Both sets of data showed very good agreement when normalised and as such this substitution was deemed satisfactory.

Precision/ Relative Standard Deviation (in %)	StHs6/80-G	GOR128-G
Ox%(Na)	6.25	11.63
Ox%(Mg)	1.6	0.39
Ox%(Al)	0.83	1.27
Ox%(Si)	0.36	0.82
Ox%(K)	1.52	65.83
Ox%(Ca)	0.93	2.29
Ox%(Ti)	7.21	7.59
Ox%(Mn)	74.04	30.91
Ox%(Fe)	4.34	1.55

Table 3: Precision measurements for major element oxides analysed by SEM-WDS.

Precision/ Relative Standard Deviation (in %)	StHs6/80-G_	GOR128-G	Durango	Morb-gl
F	<LOD	<LOD	2.86225944	<LOD
P	20.70	23.09	0.37	3.89
S	<LOD	<LOD	2.92	8.88
Cl	<LOD	<LOD	2.32	38.49
Cr	<LOD	4.05	49.49	42.55

Table 4: Precision measurements for selected low-abundance volatile elements analysed by SEM-WDS.

4.5 Trace element analysis by LA-ICPMS

Selected trace and rare earth elements of the olivine-hosted melt inclusions were analysed in situ by laser ablation inductively coupled plasma mass spectrometry at the geochemistry laboratory at Trinity College Dublin. The apparatus used was a Teledyne Photon Machines Excite 193nm Excimer UV Ar-F laser system with a Helex 2-volume ablation cell and He-Ar carrier gas (.4/min He) coupled to a thermo iCapQs quadrupole mass spectrometer. Data acquisition on the mass spectrometer was performed with Qtegra2.2 software (Thermo Fisher Scientific Inc.)

Si29 was chosen as the internal standard; assigning GSD-1G as the calibration standard. Concentration values in all analysed melt inclusions were obtained by electron microprobe for use as an internal standard.

BHVO-2G and BCR were used as reproducibility and accuracy monitors. The mapping area was defined with chromium 2.1 software (Photon Machines Inc.) 16x25mm rectangular laser spots were defined.

An additional 40ml/M N was added to the cell. The repetition rate was 10Hz with 350 counts per second.

40 second washout periods were allowed between ablations to avoid carry over. An in-house signal smoothing device (posh dog) was used to improve signal between the laser and mass spectrometer.

2 separate analytical runs were carried out, the first analysed pucks 1 and 2 containing PI25 olivine hosted melt inclusions. The second analytical run was carried out on Puck 3 (CS5).

Data was reduced using Iolite V2.5 software (Paton et al., 2011). Iolite software is designed to reduce large datasets of mass spectrometric data running in the Igor Pro environment.

The respective laser log files of both experiments were used to synchronise the ICP-MS data. After importing the data into Iolite, baseline integrations were defined and subtracted from reference material and sample integrations.

Once all integrations for the unknowns, reference materials and baselines were defined the data was reduced with the applicable 'data reduction scheme'; in this case 'Trace elements IS'; the I.S. representing 'internal standard'. Percentage error/accuracy relative to well characterized quality control standards for all elements ranged between -5 to -28% for BHVO and -13 to 13% for BCR. Precision measurements for the first and second analytical runs conducted can be viewed in tables 5 and 6 respectively.

Some of the analyses involved inclusions which were either small (<30um) or that had previously been analysed by ion probe, as such partial olivine incorporation meant that a simple nickel correction factor was employed for some of the analyses; the principal being that olivine recorded up to 2wt% Ni, while melt inclusion Ni compositions were in most cases lower than 50ppm. As such integrations recording high Ni concentrations had included an analysis of a portion of the phenocryst.

Precision/ relative standard deviation (in %)	BCR	BHVO
Li	0.968	9.225
Ca	1.724	3.980
V	0.360	8.592
Ni	5.882	4.911
Rb	1.669	4.195
Sr	0.447	7.568
Y	1.010	8.834
Zr	0.998	6.818
Nb	1.358	6.612
Cs	1.653	36.800
Ba	1.372	8.807
La	2.680	2.236
Ce	1.268	9.754
Pr	1.254	5.655
Nd	0.000	6.867
Sm	1.066	4.247
Eu	3.980	3.047
Gd	6.676	10.879
Yb	4.690	2.328
Hf	5.747	12.094
Pb	5.528	40.158
Th	0.247	10.073
U	2.804	12.220

Table 5: Precision measurements for trace elements in the LA-ICPMS run (all of puck 1 and 2 inclusive; see supplementary tables).

Precision/ relative standard deviation (in %)	BCR	BHVO
Li	5.378	0.763
Ca	6.238	1.318
V	1.361	1.771
Ni	2.347	6.115
Rb	1.535	0.370
Sr	1.208	0.416
Y	1.156	5.021
Zr	2.495	3.522
Nb	4.417	1.623
Cs	8.730	4.118
Ba	1.118	0.347
La	0.210	0.691
Ce	1.619	1.949
Pr	0.695	0.887
Nd	1.727	7.143
Sm	8.494	3.604
Eu	1.493	2.591
Gd	0.074	1.712
Yb	8.140	5.753
Hf	3.049	0.952
Pb	0.935	36.986
Th	1.757	1.322
U	4.878	1.114

Table 6: Precision measurements for trace elements in the second LA-ICPMS run (all of puck 3 inclusive; see supplementary tables).

4.6 Elemental halogen (Cl,Br) acquisition by LA-ICPMS

Using an in-house methodology developed at T.C.D.; Cl and Br compositions were determined (Caulfield et al., 2017). The apparatus used is the same as described for trace element acquisition. Glass standards NIST610 and NIST612 were used to calibrate for the halogens. Data reduction was also carried out in the Iolite software. Selected percentage biases/accuracies relative to well characterized standards for Cl were calculated -9 and -17% for NIST 612 ,-2 and -9% for GS-C 1-G and finally -5 and -9% for GS-D 1-G. Br biases were significantly higher; -43 and -46% for NIST-612; -57 and-51% for GSC 1-G and -62 and -59&

for GSD-1G (Jochum et al., 2006). Precision measurements for this technique can be seen in table 7.

Precision/ relative standard deviation (in %)	Mg	Ni	K	Cl	Br
nist612	0.84	4.09	2.52	0.76	3.23
GS-C	0.4	3.14	0.15	3.34	5.86
GS-D	1.21	2.05	0.13	2.22	3.58
STHS	2.01	4.39	1.81	19.6	14.2
ATHO	2.38	6.24	5.55	13.2	1.03
BHVO	1.21	1.41	1.66	4.29	32.7

Table 7: Precision measurements for Mg, Ni, K, Cl and Br analysed by LA-ICPMS.

Chapter 5 Results

5.1 Olivine major element chemistry

Major element analyses carried out by WDS are displayed in supplementary Table 1. Forsterite contents for all phenocrysts are in the range of Fo_{86} to Fo_{88}.

5.2 Melt inclusion major element chemistry

5.2.1 Uncorrected major element chemistry

Major element data for the olivine-hosted melt inclusions analysed in this study are presented in supplementary table 2. Harker variation diagrams with the inclusions analysed in this study were compared with BIWG inclusions from Starkey et al. (2012), (Figure 7).

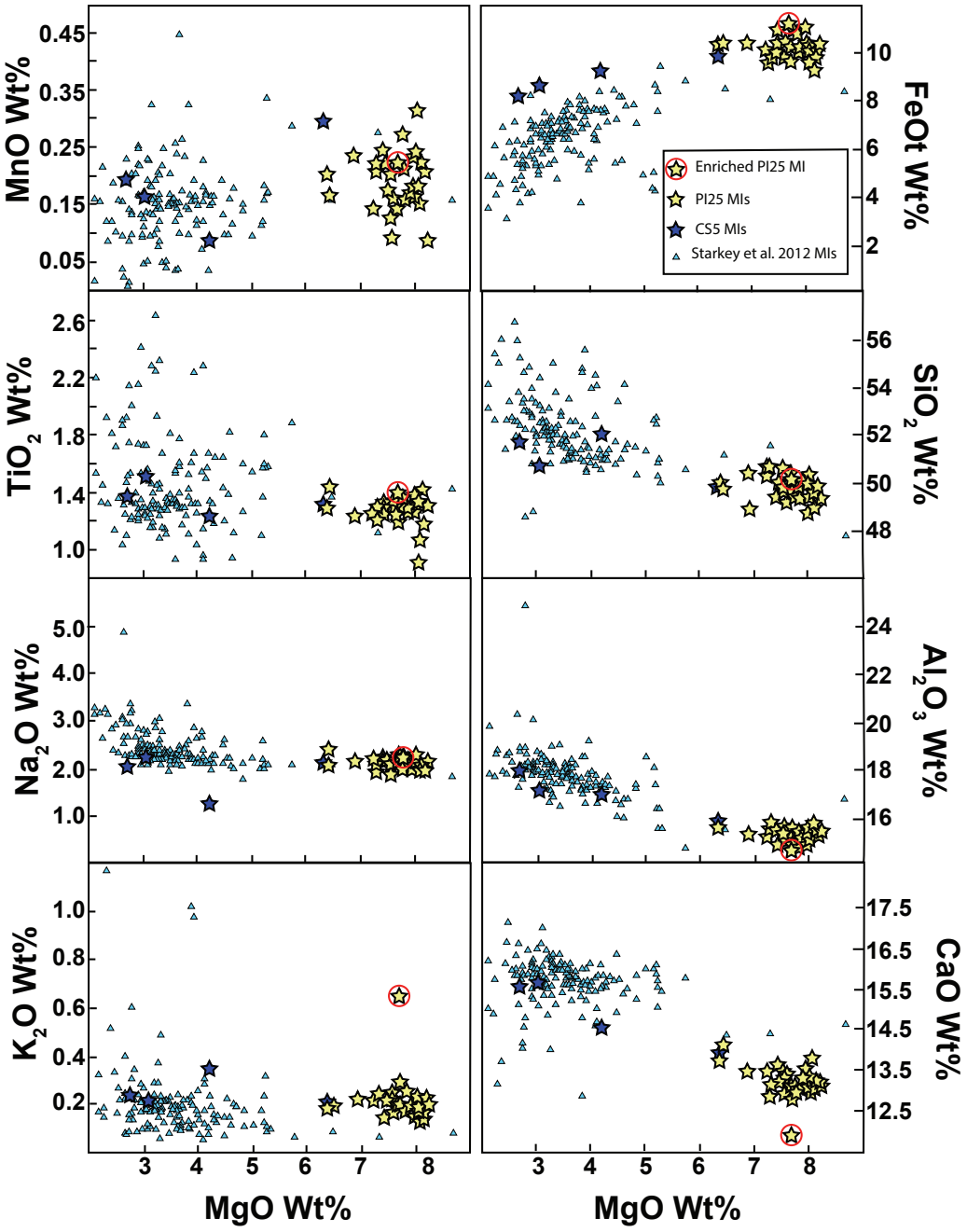

Figure 7: Uncorrected major element melt inclusion compositions. BIWG melt inclusions from Starkey et al. (2012) are included for reference.

5.2.2 Post-entrapment crystallisation correction

Major element data in these phenocrysts is likely unrepresentative of the primary magmatic composition due to secondary processes which alter the major element chemistry of the encapsulated melt. In order to potentially derive meaningful petrological data from the MIs , the effects of post-entrapment modification must be accounted for. One of the most significant is that of post entrapment crystallization. Effectively the encapsulated melt begins to crystallize olivine along the inclusion/phenocryst interface during cooling (Sobolev. 1996). These rims are often visible in back-scattered electron images and this is indeed the case for the majority of the inclusions analysed in this study (Supplementary Figure 1F).

In order to investigate whether post-entrapment crystallisation has affected these inclusions, they are compared to the whole rocks and inclusions from the BIWG suite of Starkey et al. (2012).

Equilibrium olivine was added in 0.1% increments according to a constant K_d of 0.3 (Roedder and Emslie, 1970) to the inclusion 1.PI-25 5 in order to simulate the re-introduction of olivine to the melt. The BIWG whole rocks plot along this line, an olivine control line which represents a liquid line of descent. The reverse calculation extends compositions from an olivine in equilibrium with the PI-1-5 melt down to Fo_0.

The inclusions were then corrected by using the correct MI composition option in PETROLOG (Danyushevsky et al., 2000). The first experiment made usage of the olivine MI option. This feature requires the input of the forsterite Mg no. of the host olivine of each inclusion, and also the initial trapped FeO*/FeOt content. This correction is only appropriate if the FeOt content of the inclusions and their whole rocks are consistent. 10.5wt% was chosen in line with the content chosen for correction by Starkey et al. (2012) and very close to the composition chosen by Yaxley et al. (2004) for correction of the Baffin island melt inclusions. 10.5wt% was deemed appropriate for sample PI25 OHMIS as this is close the FeOt content of the whole rock (10.65wt.%) and the average composition of the uncorrected melt inclusions. The PI25 MI inclusions range in value from 9-11.5 wt. %; with an average of 10.5 wt. %. CS5 inclusions had lower FeOt contents ranging from 8.6 to 9.8wt.%. However the whole rock value for CS5 was higher at 10.65 wt. %. As such this disparity may suggest this correction is perhaps less suitable for the CS5 melt inclusions. Corrected values are displayed in figure 8.

This correction was not favoured for two main reasons.

1.Both the FeO and MgO values are too low to represent the original trapped melt.

2.Crucially also; the inferred CS5 MgO Values are higher than that of PI25.

Neither of these scenarios seem realistic when compared to the major element chemistry of their respective whole rocks.

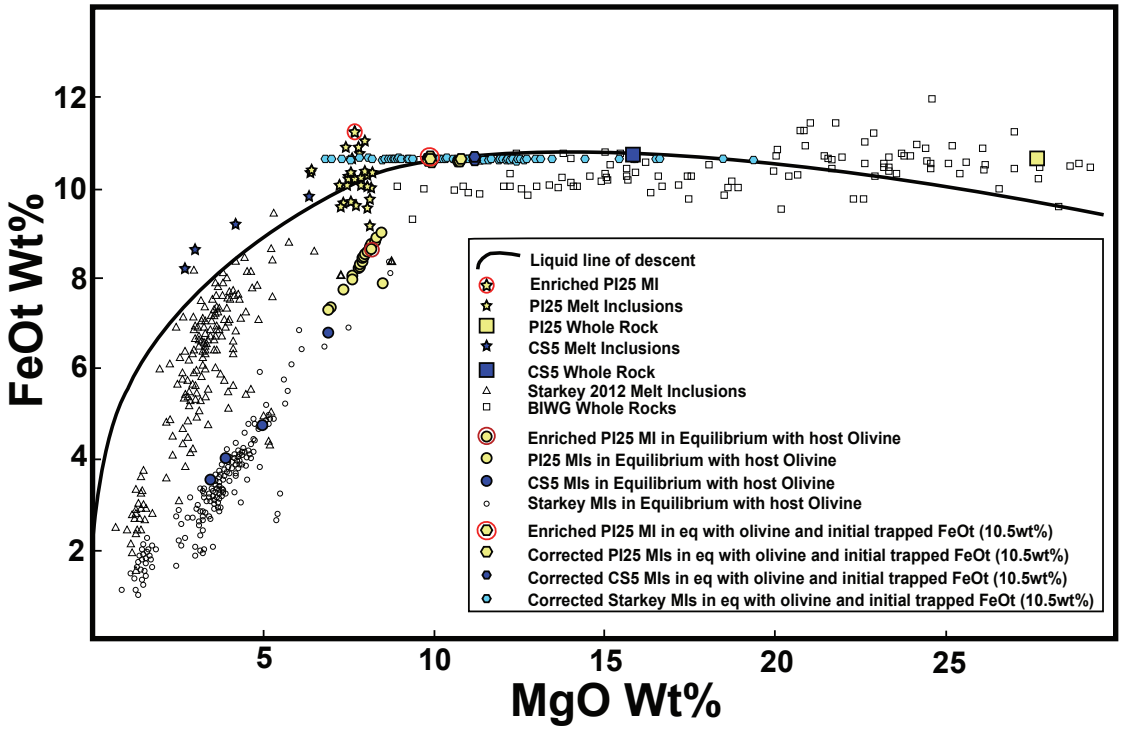

Figure 8: FeO wt% versus MgO wt%. Plotted values include the Starkey et al. (2009) whole rocks and the Starkey et al. (2012) melt inclusions. The black curve represents an olivine control line which represents a liquid line of descent Corrected melt inclusion major element compositions are shown; major elements corrected to be in equilibrium with the host olivine (large circles), and corrected to be in equilibrium with the host olivine and an initial FeOt content of 10.5 wt%.

As such an alternative methodology was explored. Still within the PETROLOG3 software, the reverse crystallisation option was used in order to correct the major element composition of the inclusions to be back in equilibrium with primary compositions. Using the same principle that generated the LLD curves; equilibrium olivine was added to the respective melt inclusions until the melts of CS5 and PI25 were in equilibrium with mantle olivine of Fo_{93} , a value close to that previously used to reconstruct the primary trace element composition of sample PI25 (Fo_{92}); indicative of primary melting conditions (Jackson et al., 2010).

The results obtained using this methodology are compared with primary melt compositions determined for both the PI25 and CS5 whole rocks using the PRIMELT software (Hole and Millet. 2016). Notably , all trends observed in the uncorrected compositions are preserved through this correction (Figure 9). The values presented also agree very well with calculated primary melt compositions independently determined for both whole rocks (Hole and Millet. 2016). While this correction produced values more consistent with inferred primary magmatic compositions; the uncertainty associated with this iterative correction procedure meant that major element chemistry was not considered further in the discussion. K_2O values are considered but due to the incompatible nature of K; it was accepted that concentrations of K would vary proportionally with the other trace elements.

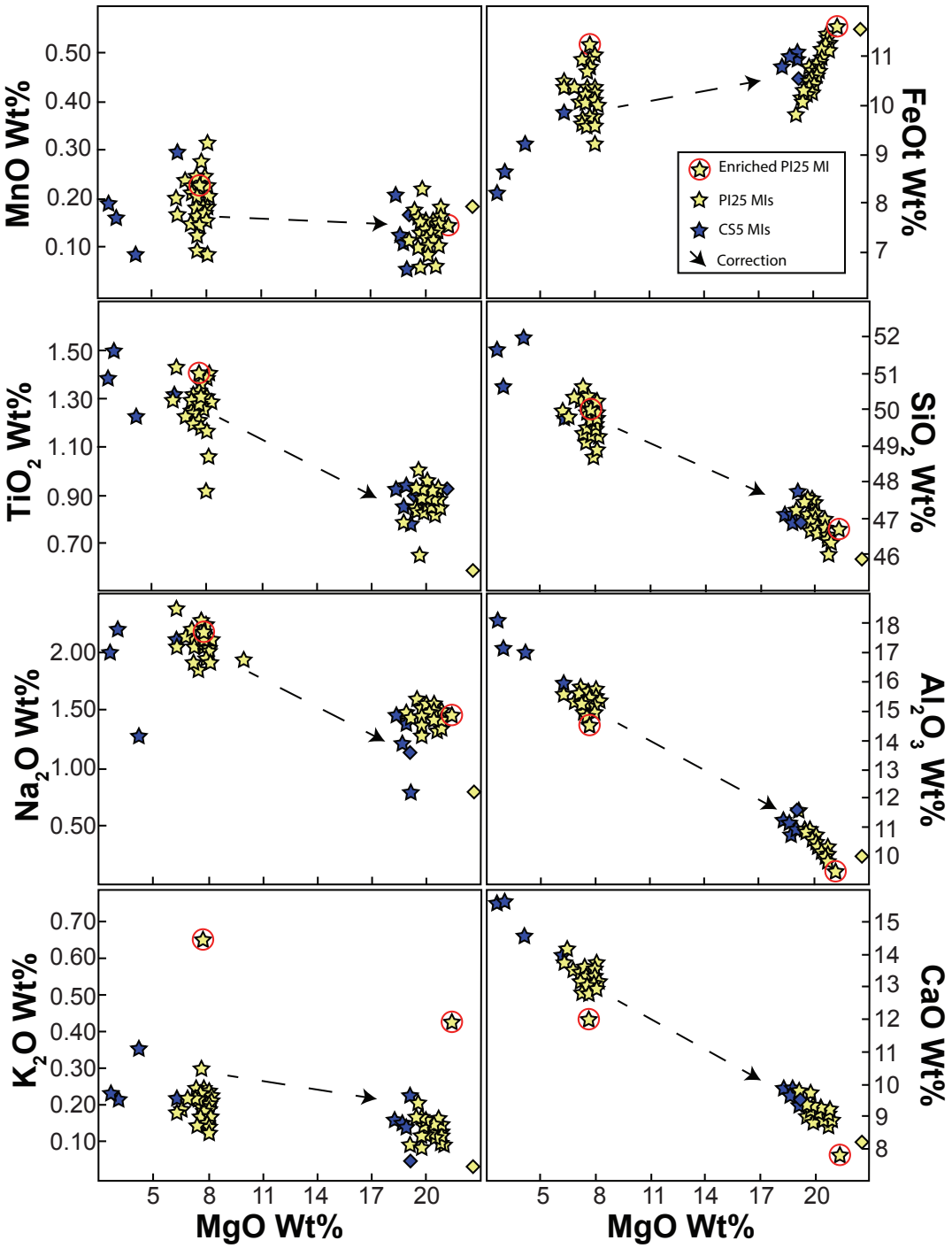

Figure 9: PETROLOG corrected melt inclusion major element values (Dnayushevskey et al., 2000). 0.01% increments of equilibrium olivine were added until the melts were in equilibrium with a mantle olivine with a forsterite content of Fo93. Included for comparison are reconstructed primary melt compositions of the PI25 and CS5 whole rocks using

5.3 Trace element results

Trace element values not corrected for post-entrapment crystallization were considered in this study. This was decided due to the fact that olivine is a very poor repository for trace elements. In line with predictions made in Starkey et al. (2012), trace element concentrations are expected to increase due to the reduction of the volume of the inclusion during post entrapment crystallization. As such, trace element concentrations and especially ratios can still offer meaningful information about the source. Due to the fact that some of the inclusions were smaller than the laser spot size, olivine was at times incorporated in an analysis. The inclusions had very low concentrations of Nickel, while phenocrysts recorded concentrations exceeding 2 wt.% Ni. As such, a simple correction factor making use of nickel concentrations was employed. While this correction does potentially alter concentrations, ratios should be unaffected. A trace element spidergram with these corrected values is presented in figure 10 along with NMORB plotted on the spidergram; all values being normalised to primitive mantle (McDonough and Sun., 1989).

As expected, trace element concentrations are higher in the inclusions than their respective whole rocks. PI25 inclusions in general conform to the pattern of the whole rock. The uranium anomaly is not a feature present in all inclusions, and a solitary inclusion records a pronounced Th anomaly. Rb in the PI25 OHMIs differs from the whole rock value, the whole rock displaying a pronounced depletion. The ‘enriched’ PI25 inclusion shows light rare earth element enrichment as well as enrichments in the very incompatible elements (VICE) Ba; Th, U and Nb (Hofmann et al., 1996). CS5 inclusions conform very well to the whole rock compositions, but they too display slight enrichment in Ba and Rb.

In general, the PI25 inclusions have a dominantly flat profile on the extended spidergram, consistent with derivation from a source which has a trace element composition close to that of primitive mantle. Nickel corrected trace element values are recorded in supplementary table 4.

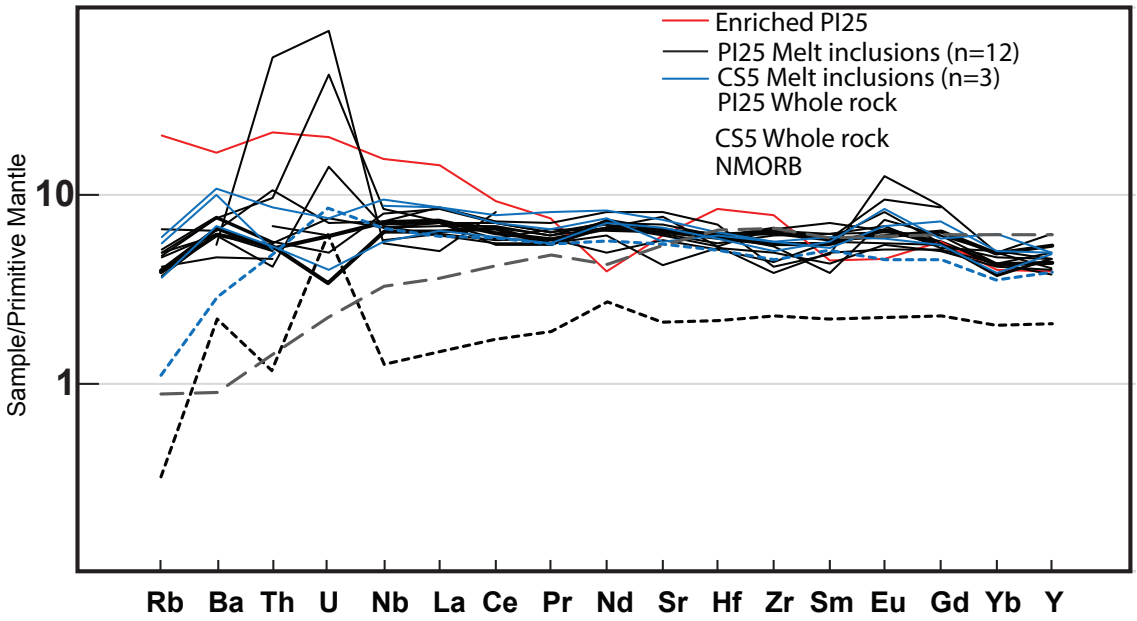

Figure 10: Extended trace element spidergram normalized to primitive mantle (McDonough and Sun., 1989). Included for reference are the whole rock compositions of both PI25 and CS5. NMORB is also plotted for reference (McDonough and Sun 1989). The outlier PI25inclusion is demarcated in red. The trace element profile for the PI25 olivine-hosted melt inclusions have a dominantly flat profile; suggestive of derivation from a source with a trace element character consistent with primitive mantle.

5.4 Elemental halogen results

Cl and Br compositions were analysed in six of the PI25 olivine hosted melt inclusions. Cl values range from 62.5 to 123.3 ppm Cl with the enriched outlier recording a Cl value of 923 ppm. Br values ranged from 110 to 440 ppb with the outlier recording a composition of 1,290 ppb.

5.5 Chlorine Isotope δ^{37}Cl Results

δ^{37}Cl compositions for all inclusion ranged from -0.97 to 1.01‰, with a single exception which recorded an anomalously high δ^{37}Cl composition of 2.19‰. PI25 inclusions are dominantly negative with an average composition of -0.2‰.

CS5 inclusions recorded isotopically heavier compositions than those of PI25 (0.67, 0.81 1.01‰), with the exception of the anomalously enriched δ^{37}C composition recorded in a solitary PI25 OHMI. A solitary inclusion from CS5 recorded a lower value of 0.04‰, however it is believed that this inclusion may have been subject to volatile loss as the inclusion lies in close proximity to a crack in the host phenocryst; a feature permissive of volatile leakage. As such it will not be considered further. Combined halogen results and ratios are recorded in supplementary table 3.

Chapter 6 Discussion

6.1 Assessing the primary magmatic signature of the Baffin Island source mantle

In order to investigate the origins of the melts studied; this study has employed the Nb-Zr-Y correlations; designed by Fitton et al. (1997); which can discriminate between Icelandic plume and asthenospheric components (Figure 11).This works along the principle of the conspicuous over-depletion of Nb in both the depleted mantle and the continental crust due to its unexpected behaviour during the melting process. Mass balance calculations can determine depleted MORB mantle compositions by simply subtracting average continental crust from primitive mantle, however Nb is unresolvable using this methodology. The missing Nb is suggested to be stored within subducting slabs and is ultimately recycled in mantle plumes. The consequence is that NMORB is more depleted in Nb, than most other Icelandic basalts which are not. This calculation as such can be used to constrain the source mantle derivation of Icelandic lavas. The inclusions of this study and their respective whole rocks have been plotted along with the Starkey et al. (2009; 2012) whole rocks and melt inclusions. Also included are the Icelandic Neovolcanic Zone glasses analysed for $\delta^{37}Cl$ (Halldorsson et al., 2016).

The upper and lower bounds of the Iceland array are defined by the following

Upper: log(Nb/Y)- 1.92log(Zr/Y) -1.176
Lower: log(Nb/Y)=1.91log(Zr/Y)-1.740

This measure is insensitive to the degree of melting and also crustal contamination. While samples of primitive mantle composition plot within the upper and lower bounds, estimated crustal compositions plot on or below the lower bound. As such N-MORB magma contaminated with continental crust cannot result in N-MORB magmas which plot above the lower bound. However depleted Icelandic basaltic magmas which recorded crustal interaction, could potentially have delta Nb less than 0 which would mean that it could plot below the Icelandic lower bound.

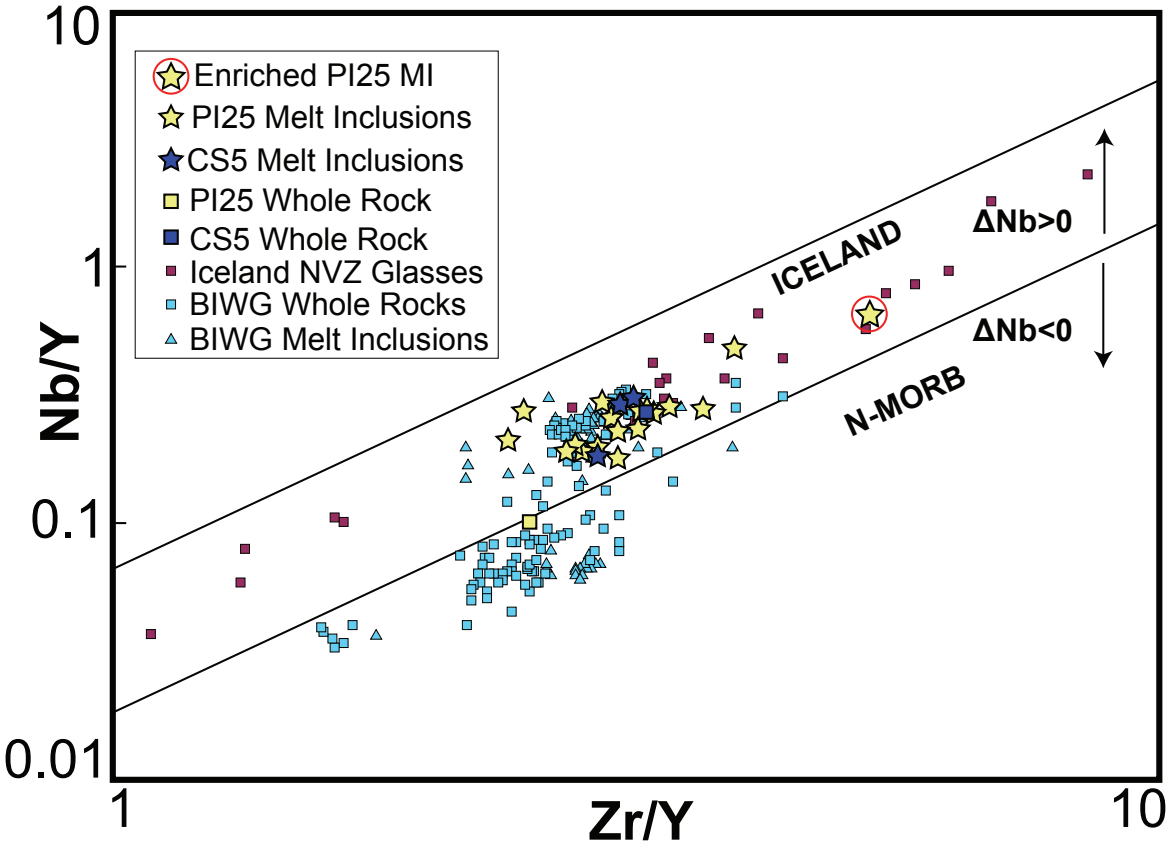

Figure 11: Nb/Y plotted against Zr/Y for the melt inclusions in this study (after Fitton et al., 1997). Also plotted are the BIWG whole rocks from Starkey et al. (2009,2012)., and the Neovolcanic zone glasses analysed for δ37Cl (Halldorsson et al., 2016). See text for discussion.

This appears to be the case for the whole rock PI25. Noticeably the whole rock plots just below the lower bound, while its inclusions all plot within the Icelandic array. As such this may suggest that the melt inclusions have for the most part been protected from crustal interaction while the magma may indeed have assimilated a crustal component subsequent to melt inclusion encapsulation. This is the more likely scenario as if sample PI25 represented an asthenospheric melt it would not display comparative enrichments in the LREE and notably Ba and U, this is in fact the case (Figure 10). The PI25 OHMIs all plot within the Icelandic array lending further support to the interpretation that the bulk primary magmas which constitute the PI25 whole rock were Icelandic plume components, and later in the bulk PI25 magmas evolution, it may have interacted with a crustal component. The CS5 whole rock plots within the Icelandic array as does all of the olivine-hosted melt inclusions analysed from this sample; suggesting that both samples are indeed derived from the Icelandic plume component rather than a more depleted asthenospheric component either endemic to the plumes architecture (Fitton et al., 1997) or a resident upper mantle domain independent of the plume. The enriched PI25 melt inclusion, plots well within the Icelandic array but trends to higher Zr values. Following inferences made by Starkey et al. (2012), samples which record higher Zr/Y values may suggest that the melt forming this inclusion crystallised clinopyroxene in which Y is moderately compatible.

6.2. Crustal contamination

6.2.1 La/Yb versus Nb/Zr

Before any definitive conclusions can be drawn about the source chemistry of the respective olivine-hosted melt inclusions; it must first be established whether or not any of the samples in question have been subject to crustal contamination.

Nb/Zr variations are characteristic of source variation. While deviations towards higher La/Yb values is qualitatively suggestive of crustal contamination (Starkey et al., 2012). Nb/Zr versus La/Yb is as such plotted for the inclusions and associated whole rocks of this study (Figure 12). Included for comparison are the BIWG whole rocks and melt inclusions from Starkey et al. (2009;2012). Also included are Padloping Island melt inclusions from Yaxley et al. (2004). Most inclusions from this study appear to follow the ‘source variation’ trend; while the enriched PI25 deviates towards relatively high La/Yb. This may be an indication of some degree of contamination. Unfortunately, this method is not quantifiable and is highly

susceptible to interpretation. As such a quantitative measure of contamination was sought to assess crustal contamination in the melts studied. Notably the PI25 whole rock shows no evidence for contamination within this framework.

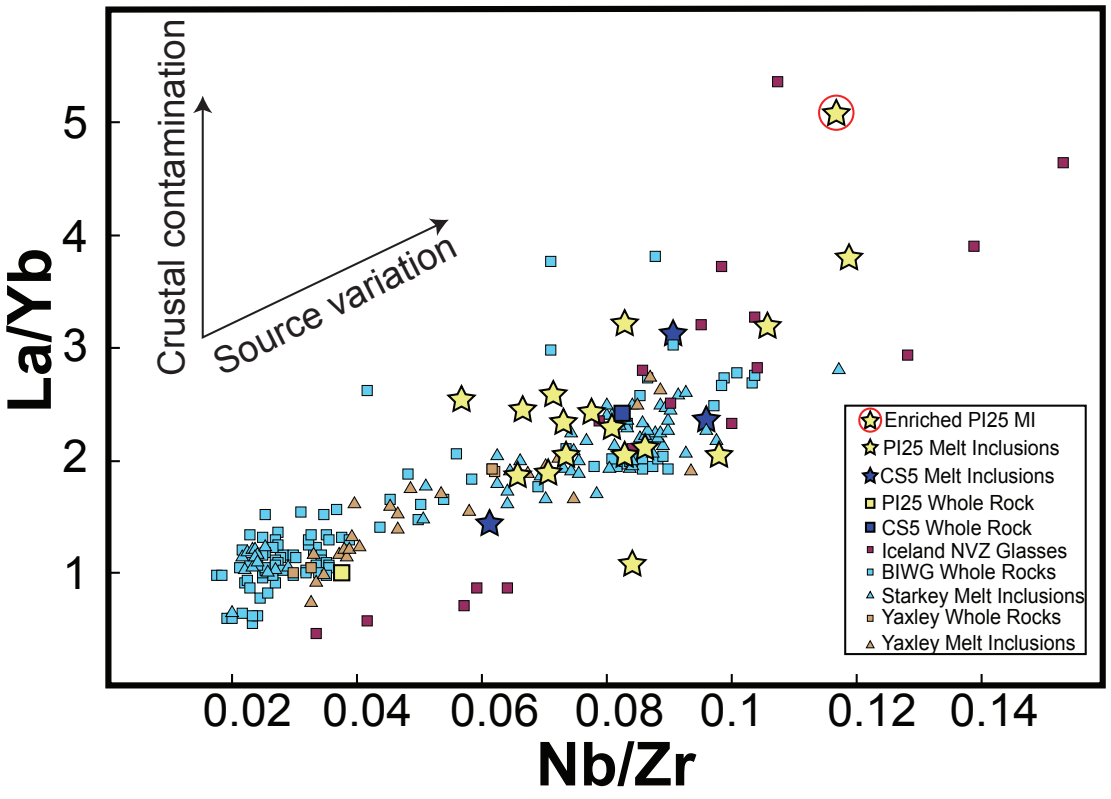

Figure 12: La/Yb plotted against Nb/Zr. Included for comparison are the BIWG whole rocks and melt inclusions from Starkey et al. (2012). Also included are Padloping Island melt inclusions from Yaxley et al. (2004).

6.2.2 Semi-quantitative crustal contamination modelling

Modelling was carried out in order to assess if discernible crustal contamination could be recognised and partially quantified using mixing calculations (e.g. Powell 1984). Following Yaxley et al. (2004); crustal rocks from the nearby onshore Baffin Island were considered as potential contaminants (Thérialut et al., 2001). This dataset comprises both Palaeoproterozoic metasediments and Palaeoproterozoic granitoids. The mixing calculation was carried out within the FC-AFC-FCA and mixing modeller: a Microsoft Excel spreadsheet program (Ersoy and Helvaci., 2010). The starting composition was the PI25 whole rock (Figure 13). 10%; refers to the first instance of 10% contamination on both diagrams; dots then record progressively more contamination in 10% increments. No evidence of contamination of the inclusions studied could be verified using this methodology. One might question the validity of using the PI25 whole rock as the initial composition; however, modelling from other starting compositions; including the inclusions and the CS5 whole rocks also yielded no discernible contamination (not shown). The possibility does of course exist that the contaminants employed here are not representative of the conditions experienced by the erupting Padloping Island/Cape Searle magmas.

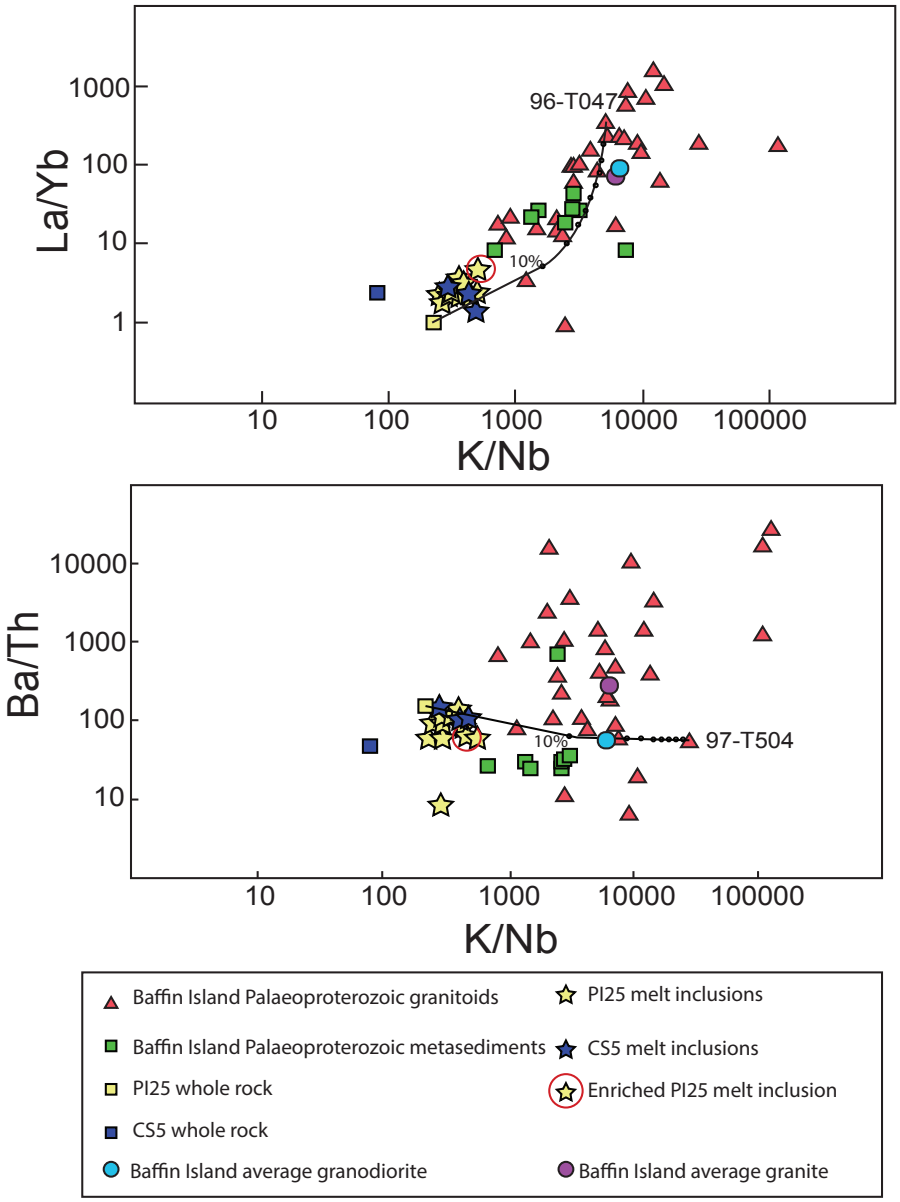

Figure 13: Crustal contamination models after Yaxley et al. (2004). Starting composition is the PI25 whole rock, the contaminants are representative Palaeoproterozoic rocks from nearby coastal Baffin Island (Thériault et al. (2001). Also shown are averaged compostions for the onshore Baffin Island Palaeoproterozoic granites and granodiorites. The models were generated within FC-AFC-FCA and mixing modeller: A Microsoft Excel spreadsheet program (Ersoy and Helvaci., 2010).

6.2.3 Summary of potential crustal contamination

Based on both methodologies employed; it must be concluded that there is no definitive evidence for crustal contamination in these samples; however, both methods appear to be contradictory in nature. Graphing La/Yb agaist Nb/Zr might suggest that as these samples for the most part follow the 'source variation' trend, and that they do not display evidence for crustal contamination. However, the Yaxley et al. (2004) samples which display up to 15% contamination using the modelling method do not display any such evidence on the plot of Nb/Zr versus La/Yb and plot within the trend of 'source variation'.

The interpretation of contamination or lack thereof must as such rely upon the trace element profiles on the extended trace spidergrams. The dominantly flat trace element profiles indicate that the majority of the inclusions analysed do not display evidence of crustal contamination. These flat profiles of the PI25 melts are also consistent with derivation from an unfractionated source nearing chondritic composition. The U spikes are unresolved; maybe suggestive of some source of seawater interaction? This is unresolved within this study.

As already pointed out; the enriched PI25 displays notable enrichments in Ba,Th, Nb and La; the significance of which will be explored in later sections.

6.3 Seawater contamination

6.3.1 Cl/K variation

With respect to the study of volatiles and in particular halogens, it is imperative to establish that the inclusions have not been contaminated by volatile rich material; most notably seawater or a component containing appreciable quantities of seawater (eg Michael and Schilling, 1989 Lassitier et al., 2002). The similar compatibility of K relative to Cl makes this proxy a suitable determinant of Cl enrichment or depletion. Elements with similar incompatibilities in the mantle are not easily fractionated and as such enrichments of Cl suggest some extraneous source of Cl incorporation such as contamination with a seawater-rich lithological component or interaction with a brine (Kendrick et al. 2015).

The samples from this study along with a global dataset of halogens are plotted according to this framework in Figure 14. The consistency between Cl/K values and their broad consistency with other trace elements suggests that these inclusions have not been subject to shallow level degassing (Lassitier et al., 2002). Cl/K values range from 0.032 to 0.076 in the PI25 melt inclusions, while the enriched PI25 has a Cl/K composition of 0.17.

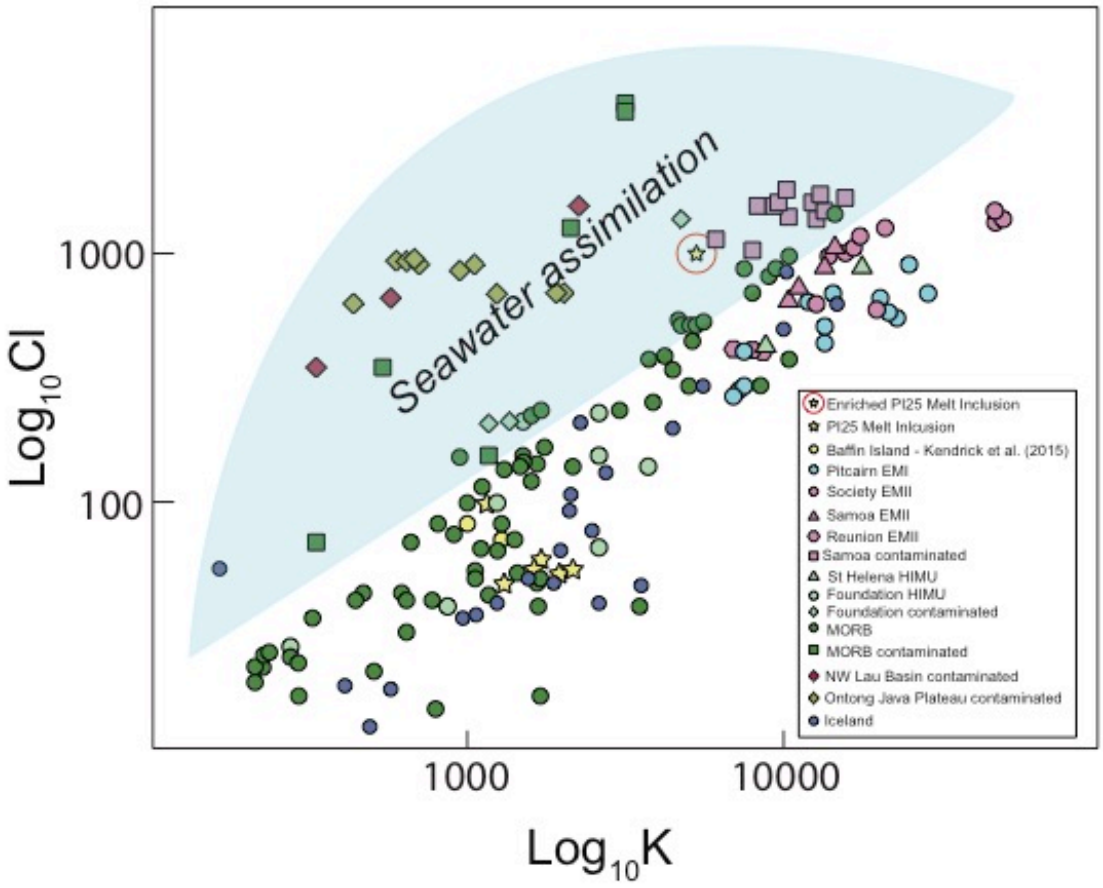

Figure 14: Global dataset of Cl/K values. Similar incompatibilities of both element mean that elements with high Cl/K values likely record interaction with a volatile rich contaminant such as seawater. Axes are both log10. The blue field is based upon samples that Kendrick et al. (2017) suggested have been contaminated with seawater. The 'enriched' PI25 melt inclusion plots among the the contaminated Samoan EMII samples.
Datasets: Global MORB, HIMU, EMI ,EMII Ontong Java and NW Lau basin glasses (Kendrick et al., 2017 and references therein). Icelandic glasses (Halldorsson et al. 2016). Baffin island glasses are from Kendrick et al. (2015).

The majority of the inclusions Cl/K compositions fall well below the 'cutoff' of 0.06, an indication that they have not been contaminated with respect to Cl (Lassitier et al., 2002 ; Shimizu et al., 2016; Rose-Koga et al., 2017). However, some of the inclusions studied plot marginally above the 0.06 'cutoff' (Lassitier et al., 2002). Kendrick et al. (2017) is more liberal with this figure; generally, only indicating contamination afflicts samples with Cl/K values exceeding 0.1. Unfortunately, Cl compositions were not obtained for all of the inclusions analysed for δ^{37}Cl so it is not possible to definitively rule out that some of these inclusions may have been subject to contamination with a volatile rich-source. The lack of contamination is inferred however based upon the overwhelming consistency of the δ^{37}Cl compositions obtained for sample PI25 melt inclusions and the lack of Cl contamination evident in the unenriched inclusions (supplementary table 3).
The enriched inclusion displays very high Cl/K composition of 0.17 that can only be explained by some form of interaction with a volatile-rich source, such as seawater bearing crust (altered oceanic crust) or a portion of serpentinized mantle (John et al., 2011; Chavrit et al., 2016). It should be pointed out the the δ^{37}Cl composition recorded in this inclusion is the second heaviest within the global dataset at 2.19‰, only exceeded by a Samoan glass of EMII derivation; at 2.9‰ (John et al., 2010).

The depths suggested for melt initiation (6.9GPa) and arrest for the PI25 whole rocks (Hole and Millet, 2016) preclude the possibility of direct melt-seawater interaction; the conclusion is thus that the Cl enrichment observed in this inclusion may record some interaction with a Cl-enriched input such as mantle serpentinite (John et al., 2011) or AOC (Chavrit et al., 2015) which are either endemic to the plume or the are subducted components in transit which were present beneath Baffin Island-West Greenland prior to plume impingement. However based upon the combined trace element profile (LREE and very incompatible element enrichment VICE) of this inclusion; this melt may reflect partially primary enrichment resembling in composition enriched-mantle like basalts evident in younger Icelandic lavas such as the <10Ka Theistareykir basalts; which also display light rare earth and very incompatible element (VICE; Ba,Th,Nb and La) enrichment (Hofmann et al., 1996; Stracke et al 2003). VICE are less subject to magmatic variations; and are as determinant in some cases as lithophile radiogenic isotopes in determining source mantle character (Hofmann et al., 1996).

6.3.2 Th/La versus Cl/K

In order to further investigate the potential for this enriched inclusion having a distinct mantle source to the other PI25 melts; Cl/K was plotted against Th/La (Figure 15) This diagram was in its original iteration (Shimizu et al., 2016) was intended to display magmatic variation on the x-axis; however, here it is employed with mantle source variation under consideration. The rationing of two highly incompatible elements such Th/La means that source variations can be observed; this determinant appears to demarcate the various OIB reservoirs adequately well in this case. MORB is expected to be variable as these rocks are taken from representative spreading centres globally (Kendrick et al., 2012). Of high significance is the presence of enriched PI25 inclusion plotting closer to the more enriched mantle reservoirs; however it's Cl/K value is obviously suggestive of contamination with a Cl-rich source. For the purposes of investigation; this sample will be treated in determining mantle source compositions characteristic of enriched mantle; while it's potential origins will be revisited in a later section.

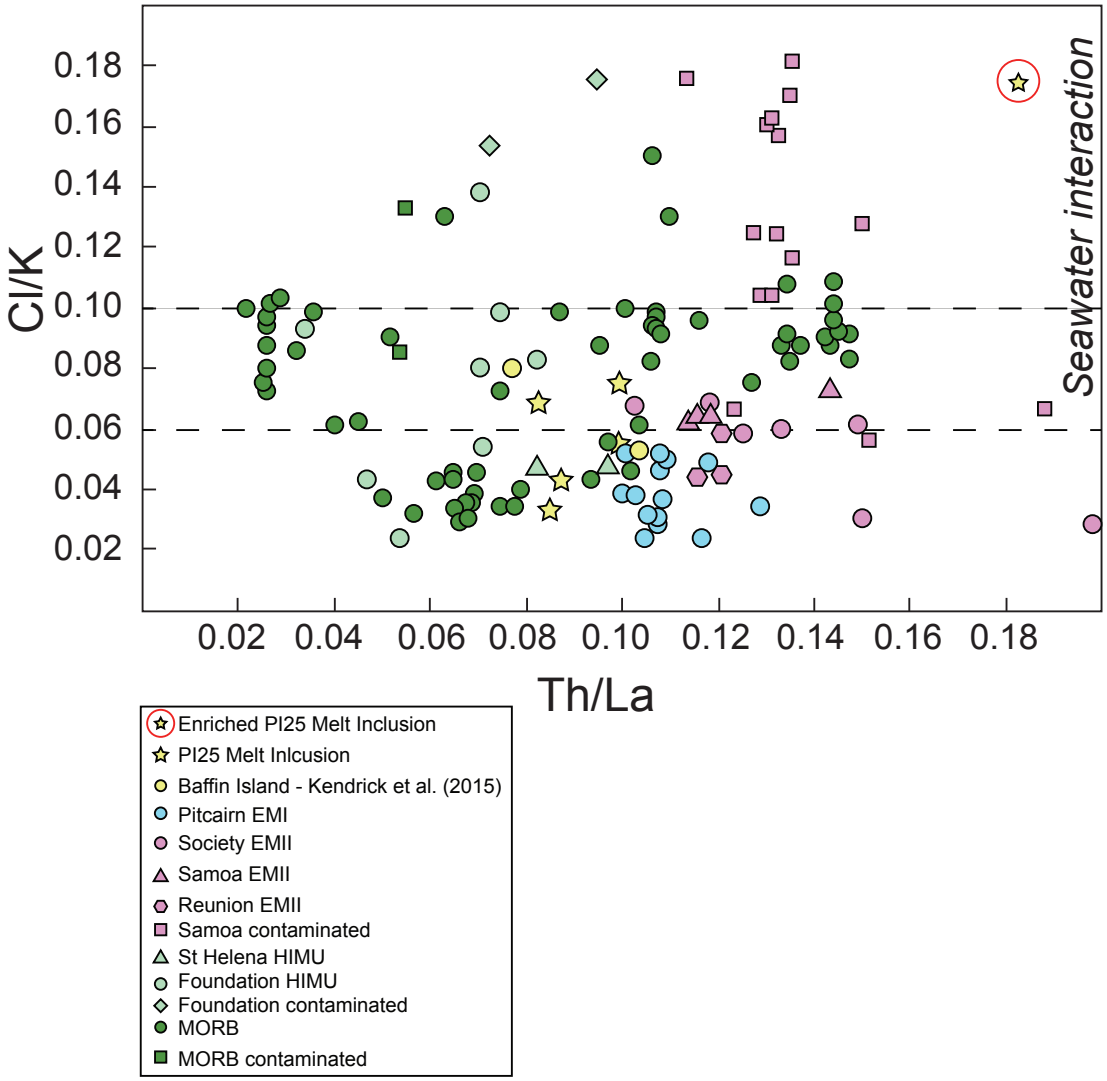

Figure 15: K/Cl plotted against Th/La after Shimizu et al. (2016). Th/La in the graphs original usage (Shimizu et al., 2016) was intended to display magmatic variation on a local scale, however this ratio appears to delineate the compositions of the major OIB reservoirs adequately well. MORB variability is expected as the MORB plotted are from an array of geographical locations. All data (Kendrick et al., 2017 and references therein). The dashed lines represent the 2 suggested 'cut-offs' for Cl contamination.

6.4 Elemental halogen (Br,Cl) composition of the high $^{3}He/^{4}He$ mantle

6.4.1. Elemental chlorine concentrations

Chlorine concentrations from this study and the other major mantle reservoirs are presented in figure 16. The bulk of the inclusions (62-123 ppm) measured in this study are consistent with previous analyses of Baffin Island glasses (67 and 79 ppm) which in combination with good accuracies relative to well characterized standards lend confidence to the method of acquisition by laser ablation (Caulfield et al., 2017). HIMU glasses (Kendrick et al., 2017) have Cl compositions predominantly below 200 ppm with some exceptional compositions exceeding 1000ppm; which likely have been subject to seawater contamination. An abundance of MORB samples also low Cl concentrations but their ranges extend to much higher concentrations (Kendrick et al., 2012). The samples of this study also fall within the range observed for Icelandic Cl compositions. Of note; enriched PI25 sample (923 ppm) has a Cl composition similar to those of some EMII basalts.

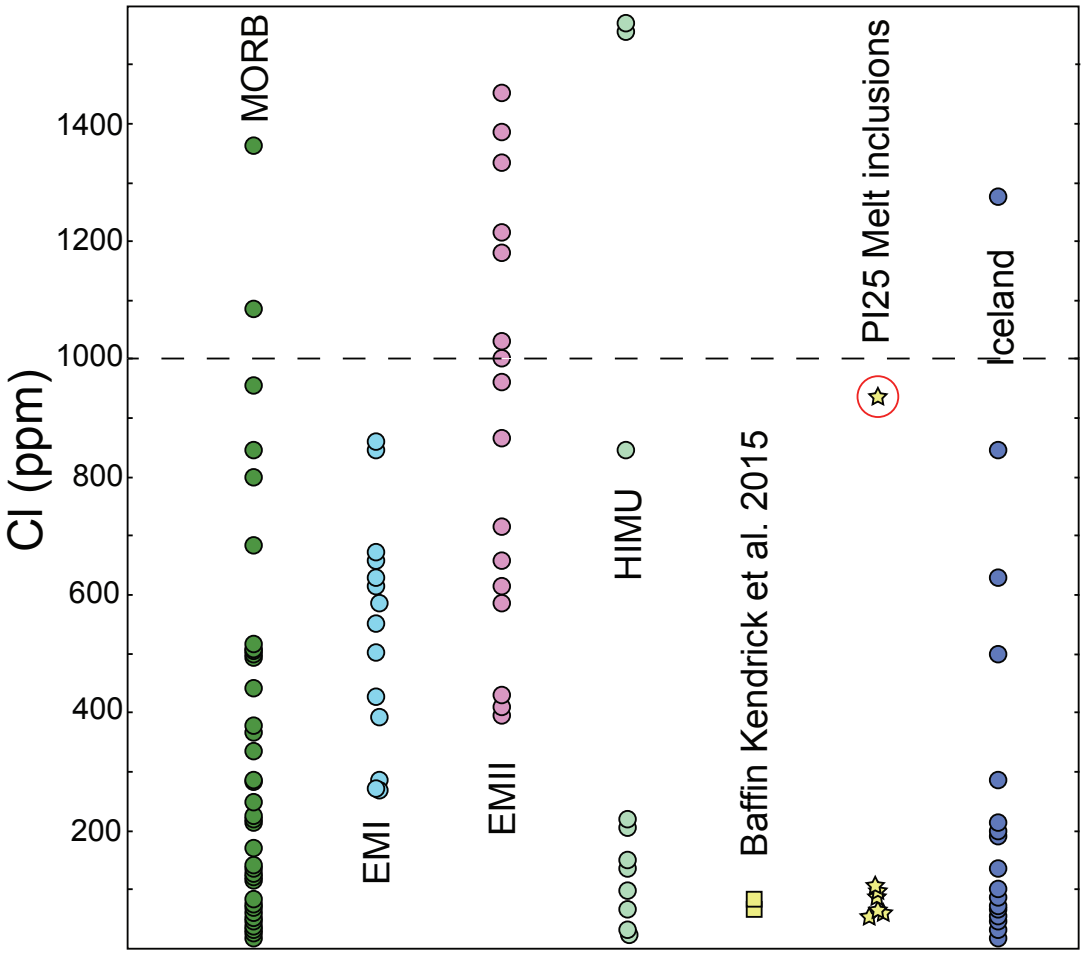

Figure 16: Global Cl dataset. The dashed line represents an approximate 'contamination' line. Samples exceeding this 1000ppm values are generally suggested to be contaminated (Kendrick et al., 2017). Icelandic data (Halldorsson et al., 2016). MORB, OIB and Baffin Island glasses (Kendrick et al., 2017). The PI25 inclusion with the red circle surrounding the icon is the 'enriched PI25' melt inclusion.

6.4.2 Elemental bromine concentrations

The same format is presented for the global Br dataset (Figure 17). Br values range from 114 to 433 ppb for the 'unenriched' melt inclusions; while the enriched melt inclusion records a Br concentration of 1285 ppb.

The fact that two analyses were unresolvable (below the limits of detection) might suggest that Br values are even lower than the minimum recorded here at 110ppb. The unenriched samples agree well with previous Br values determined for Baffin Island glasses (Kendrick et al., 2015) at 130 and 327 ppb. However, the considerably higher percentage biases relative to well characterized standards; in most cases higher than 40%; mean that the determinations for Br in this study are less reliable and caution must be observed when interpreting these values. The immediately obvious feature is that the Br compositions of the unenriched melt inclusions in this study and the Baffin glasses (Kendrick et al., 2015) are uniquely low in Br relative to the OIB reservoirs. Some MORB samples are within this range; however again the Br compositions of the MORB mantle extend to much higher compositions. (Kendrick et al., 2012; 2017). These values are not mantle compositions; they are concentrations recorded in glasses; however a first order interpretation may be that Br is pervasively enriched in the OIB mantle. The unenriched samples analysed for this study are derived from a more primordial mantle reservoir; preserving primordial volatile chemistry; as such they perhaps do not display this subduction mediated enrichment. While the HIMU glasses exhibited similar Cl compositions to the unenriched PI25 inclusions; their associated Br values are considerably higher (exceeding 1600ppb and ranging as high as 3700ppb). This might suggest preferential incorporation of Br over Cl in the HIMU mantle. Again, the Br composition of the enriched inclusion (1285 ppm) is within the range for EMII derived glasses.

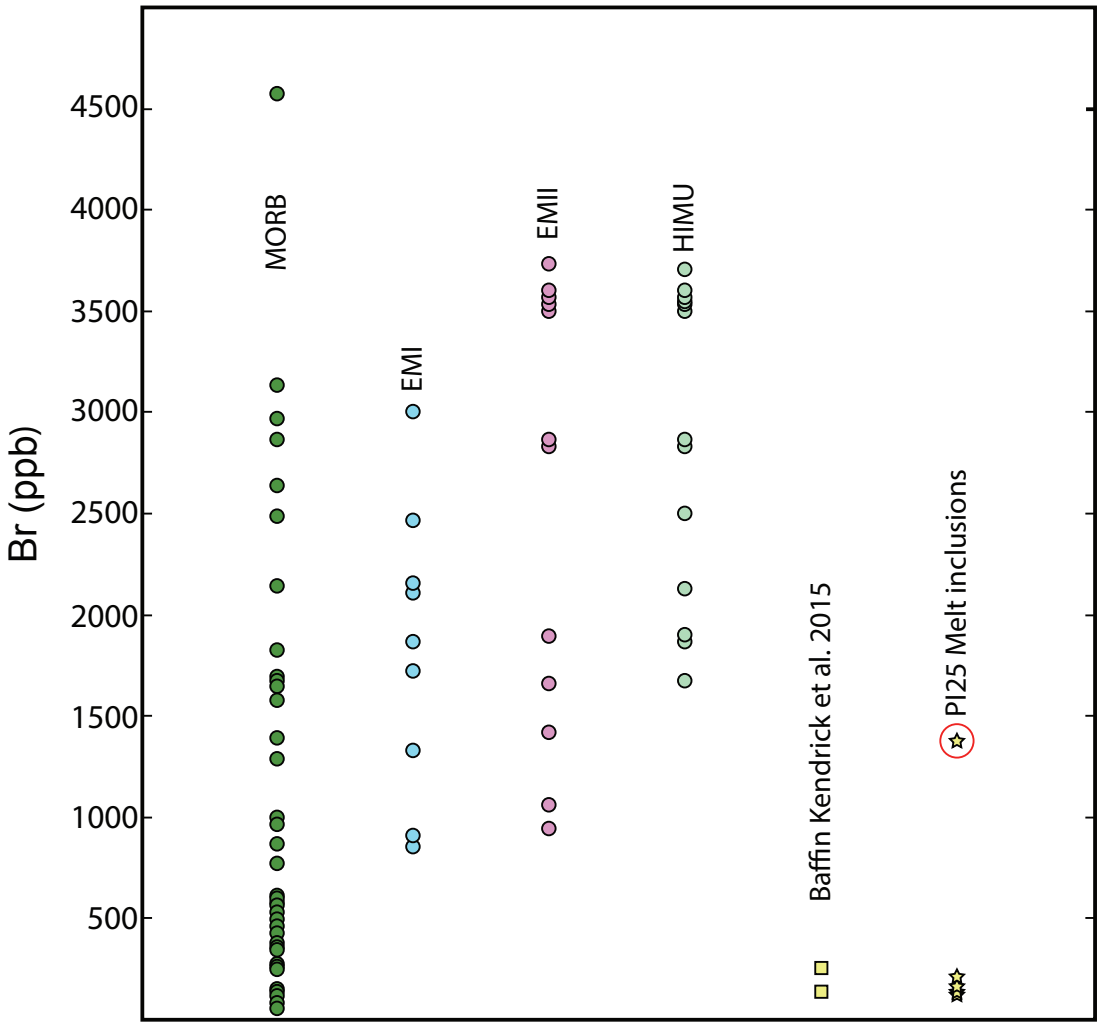

Figure 17: Global Br dataset. OIB and MORB and previous Baffin island glasses (Kendrick et al., 2017 and references therein).

6.4.3. Br/Cl ratios

Presented here is the global dataset of Br/Cl x10^3 ratios (Figure 18). As already indicated; this study does not favour Br/Cl ratios as particularly sensitive means to examine mantle halogen heterogeneity as result of subduction addition; δ^{37}Cl isotopic values have far more utility in this regard (John et al., 2010). Nevertheless, presented here; is a low (1.7) Br/Cl x 10^3 ratio that agrees with a previously determined low Br/Cl value (1.94) for the Baffin Island glasses; which is unique among the global dataset and may be a feature of the high ^{3}He/^{4}He mantle reservoir. The poor accuracies cited for Br acquisition in this study also dictates that this value may be a consequence of inaccurate Br data acquisition.

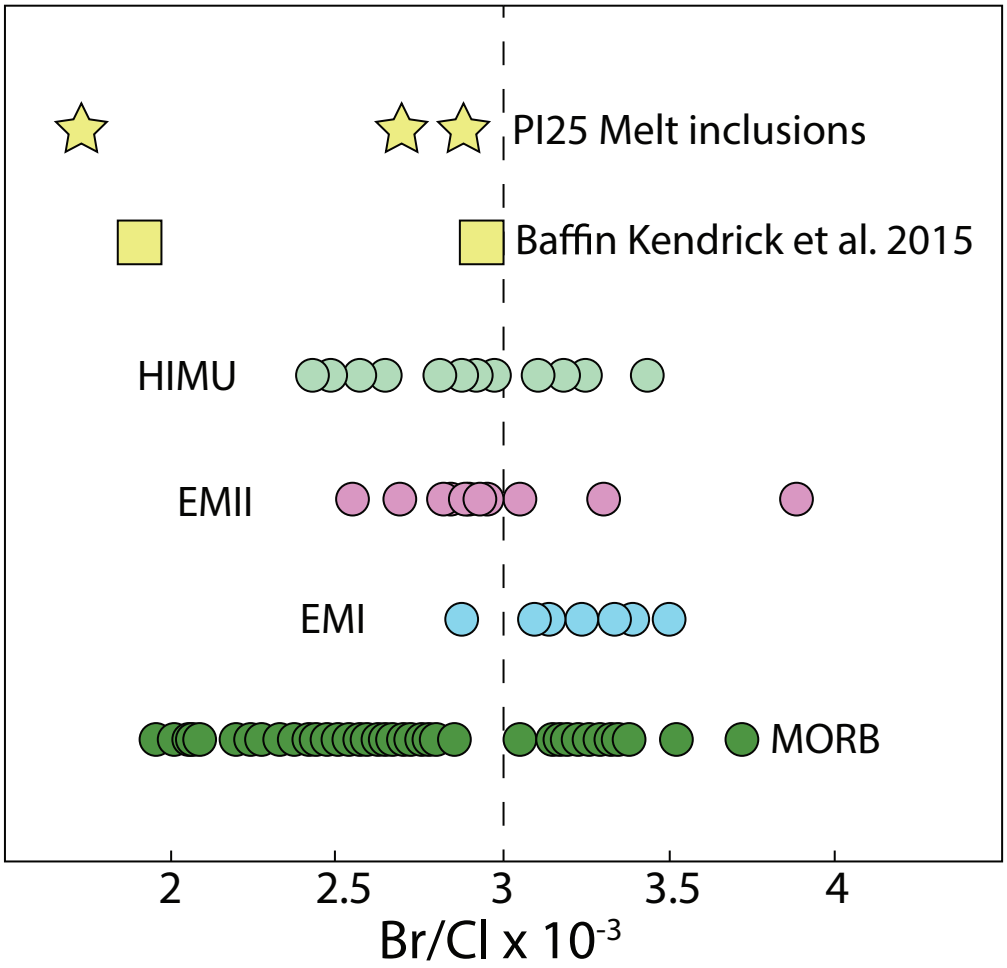

Figure 18: Br/Cl ratios complied for the major geochemical reservoirs. Br/Cl values are multiplied by 10-3. Remarkable consistency is observed in the mantle dataset. A single data point from this study and single data point from Kendrick et al. 2015 plot towards lower Br/Cl values, unique among the global dataset. MORB and OIB reservoir data (Kendrick et al., 2017).

6.5. Bulk Silicate Earth halogen calculations

6.5.1. Cl composition of the high $^{3}He/^{4}He$ mantle

Having established that the samples in this study display no evidence for crustal contamination; and aside from one very obvious outlier; the majority so samples analysed for Cl do not show potential for seawater interaction. These pristine, uncontaminated samples were chosen to calculate the Cl and Br compositions of the high $^{3}He/^{4}He$ mantle. For the sake of discussion; the enriched inclusion was used to determine the potential composition of the enriched mantle like end-member in the Icelandic plume (Stracke et al., 2003; Thirlwall et al., 2004 ; Halldorsson et al., 2016).

Experimentally derived partition coefficients were used to back calculate the Br and Cl compositions of the mantle source. A bulk distribution coefficient for Cl was calculated by combining datasets from experiments by Joachim et al. (2015), and Dalou et al. (2012). Joachim et al. (2015) calculated the distribution coefficients for Cl in olivine and orthopyroxene with experimental conditions simulating pressures ranging from 1-2.3 GPa and temperatures between 1350-1600ºC. Samples with the highest temperatures and pressures from this study were employed to derived the bulk K_d for the PI25 melts as melt initiation occurred at approximately 6.9 GPa with termination within the garnet stability field (Hole and Millet., 2016). Clinopyroxene and garnet partition coefficients were obtained from Dalou et al. (2012); at conditions of 1430ºC and a pressure of 1.6 GPa.

The high pressures and temperatures of melting for PI25 primary melts have not been simulated in any experiments to date.
As such the suitability of using the currently available K_d values is definitely not ideal and incites the potential for error. Nonetheless we can likely predict the major sources of potential error when combining K_d values from various experimental conditions to derive one suitable for the purposes of this study.
With respect to olivine; pressure demonstrably does not affect chlorine partitioning behaviour between the pressure interval of 1-2.3 GPa. It has been demonstrated however that the partitioning of chlorine into olivine is temperature dependent, increasing by about 1.5-2 orders of magnitude between the 1350-1600 ºC temperature interval (Joachim et al., 2015). As such we might assume that this trend continues towards higher temperatures. The average

temperature of melting predicted for this magma is 1679ºC (Hole and Millet., 2016). As such the K_d may be lower than is appropriate based on the increased average temperature predicted for these melts. Uncertainty exists as to whether partitioning into orthopyroxene decreases with increasing pressure (Dalou et al., 2012; Joachim et al., 2015). Chlorine partitioning in orthopyroxene increases by 1-1.5 orders of magnitude every 100ºC between the temperature interval 1300 to 1600ºC again suggesting the the K_{dCl} may be lower than that expected for melt initiation depth. Clinopyroxene distribution experiments were conducted at P/T conditions of between 8 Kbars at 1265ºC and 16 Kbars at 1430ºC. D_{Cl} is lower at higher temperatures and pressures likely indicating that at the P/T conditions of PI25 melting; the Cpx K_{dCl} would be even lower.

To the knowledge of this study there is only one data point for garnet; calculated for T/P conditions at 2.5GPa and 1430ºC (Dalou et al., 2012).

Selected K_{dCl} vaues for each mantle mineral are as follows 0.14 ,0.16, 0.0017 and 0.0029 for olivine, orthopyroxene, clinopyroxene and garnet respectively (Joachim et al., 2015; Dalou et a., 2012). For the purposes of this study; the water content of the mantle source was not taken into consideration. Water however, apparently has no demonstrable effect on the partitioning of Cl in olivine (Joachim et al., 2017).

Following Joachim et al. (2015), In order to calculate a bulk distribution coefficient representative of the PI25 source, a simplified mantle composition was considered according to McDonough (1990). The relative proportions of the mantle minerals according to these constraints are 62%, 24%, 12% and 2% for olivine, orthopyroxene, clinopyroxene and the aluminous phase (in this case garnet) respectively. The Bulk K_d of the source mantle was calculated according to the following formula:

$$BulkKd_{Cl} = x_1Kd_1 + x_2Kd_2 + x_3Kd_3 + x_4Kd_4$$

where x_1, x_2, x_3 and x_4 refer to the. Percentages of olivine, orthopyroxene, clinopyroxne and garnet respectively.

This yielded a bulk $K_{d\,Cl}$ value 0.125426. For calculations; melt fractions of 1-5% were employed; implied melt fractions for the OIB mantle (Dasgupta et al., 2007).

An equilibrium batch melting model was used to determine the original source composition (equation 4.6; Rollinson. 1993); which is as follows:

$$\frac{C_l}{C_0} = \frac{1}{BulkKd_{Cl} + F(1 - BulkKd_{Cl})}$$

Where C_l= composition of Cl within the melt. C_0 refers to the composition of Cl in the original unmelted source. F refers to melt fraction. Values are presented for the PI25 melt inclusions that are back calculated employing melt fractions of 1 and 5%. These range from 8.38-20.84 ppm. These estimates are lower from most previously determined values for BSE Cl composition. The upper limit however is close to that determined by McDonough and Sun (1995).

Calculations for the EMII like enriched PI25 melt inclusion; results in a value of 123-156 ppm for the enriched mantle like component of the Icelandic mantle. These values are double the value for upper limits of the OIB mantle previously considered (Joachim et al., 2015). Contamination may of course have inflated overprinted the primary Cl value of this melt, hence resulting in an inflated mantle source Cl composition.

6.5.2. Bromine composition of the high $^3He/^4He$ mantle

Unfortunately, distribution coefficient data for Br is limited to olivine only (Joachim et al., 2016). As such mantle Br calculations are based upon olivine alone. The distribution coefficient for bromine in olivine at T/P conditions of 1500ºC and 2.3 GPa is determined to be 0.000437 ± 0.000196. As already stated; Br was unresolvable (below the level of detection) in two of the inclusions analysed so minimum values may be even lower than those presented here. Bromine compositions for the high $^3He/^4He$ mantle and as such the primitive mantle range from 1.14 ppb to 21.67 ppb. The lower limit is in good agreement with other predicted values; e.g. 3.6 ppb (Lyubyetska and Korenaga., 2007). However, there is a considerable range of values with respect to the BSE Br composition with some studies placing this value as high as 76 ppb (Palme and O'Neill., 2014 ; Kendrick et al., 2017).

Br values for the enriched mantle-like melt are 13.4 ppb and 64.5 ppb at melt fractions of 1 and 5% respectively. Interestingly the lower limit agrees well with previous estimates for the EM1 and EMII reservoirs at 11 and 20 ppb respectively (Joachim et al., 2016). Again the suitability of these experimental conditions for the melts in this study are subject to a source of

potential error in calculating the Br composition of the source.

6.5.3. Implications for the mantle Cl and Br cycles

Chlorine values determined for the high $^{3}He/^{4}He$ mantle reservoir are generally lower than previously determined values for the primitive mantle although Cl values agree quite well the estimate of McDonough and Sun at 17ppm (1995). If the primitive mantle Cl values is indeed as low as 8.38ppm; then it necessitates the MORB source mantle concentration must have a low value for Cl consistent with recent estimates as low as 0.14ppm (Urann et al., 2017). The OIB source is enriched by a factor of 2.5 to almost 9 fold relative to the primitive mantle; consistent with significant fluxes of Cl into the OIB source reservoirs via subduction of sediment; serpentinites and altered oceanic crust (John et al., 2011; Chavrit et al., 2016) With respect to bromine, estimates are within the low end of ranges determined for the primitive mantle composition. It would again dictate that Br concentrations in the MORB mantle should be lower than the primitive mantle value; with suggested significant fluxes of Br into the mantle over time. Considering the lowest value calculated in this study of 1.14; there is a 10 and 20-fold enrichment factor for the EMI and EMII OIB mantles respectively (Joachim et al., 2016).

It is entirely possible that the Cl and Br values presented here for the high $^{3}He/^{4}He$ mantle are not representative of the Bulk Silicate Earth. Clay et al. (2017) suggest that halogens may have had to be efficiently extracted from the mantle early in their evolutionary history to account for their overwhelming concentration in the Earths accessible reservoirs (Pyle and Mather., 2009). Perhaps these values represent a snapshot somewhere within the progression of this process, and at this point more than half of the primitive mantle inventory of Cl could have repartitioned to the surface reservoirs by 4.5Ga as result of their fluid mobilities (Aiuppa et al., 2009; Rizo et al., 2016; Clay et al., 2017).

The compositions predicted for the enriched mantle reservoir seem unreasonably high for Cl at either 123.88 or 156.18 ppm at 1 and 5% melt fractions respectively. However, the Br values obtained 13.41 and 64.79 ppb for 1 and 5% melt fractions respectively; are potentially realistic (Joachim et al., 2016).

6.6 δ^{37}Cl composition of the high ^{3}He/^{4}He mantle

6.6.1 Comparison to other mantle reservoirs and subduction inputs

Presented here is the data from this study combined with δ^{37}Cl data for all of the major mantle reservoirs and also the potential subduction inputs (Figure 19). As already discussed in the background section; the variability in mantle-derived basalts exceeds that of the inputs with the exception of marine pore waters. This is atypical of a mantle stable isotopic system; as stable isotopic fractionation varies inversely with temperature; meaning that fractionation becomes almost negligible at mantle temperatures. This means that mantle-derived basalts acutely fractionated relative to 0‰; the composition of seawater (Eastoe et al., 2007); have sources that are contaminated with surface-fractionated material.

Excluding the enriched PI25; the CS5 inclusions record more isotopically heavy δ^{37}Cl compositions (0.67-1.01‰). These values are comparable to some of the more isotopically heavy Icelandic glasses. However they are also within the ranges of the enriched mantle reservoirs and indeed the upper limits of the HIMU reservoirs. It should be reiterated that data for the major geochemical reservoirs are quite limited (John et al., 2010).

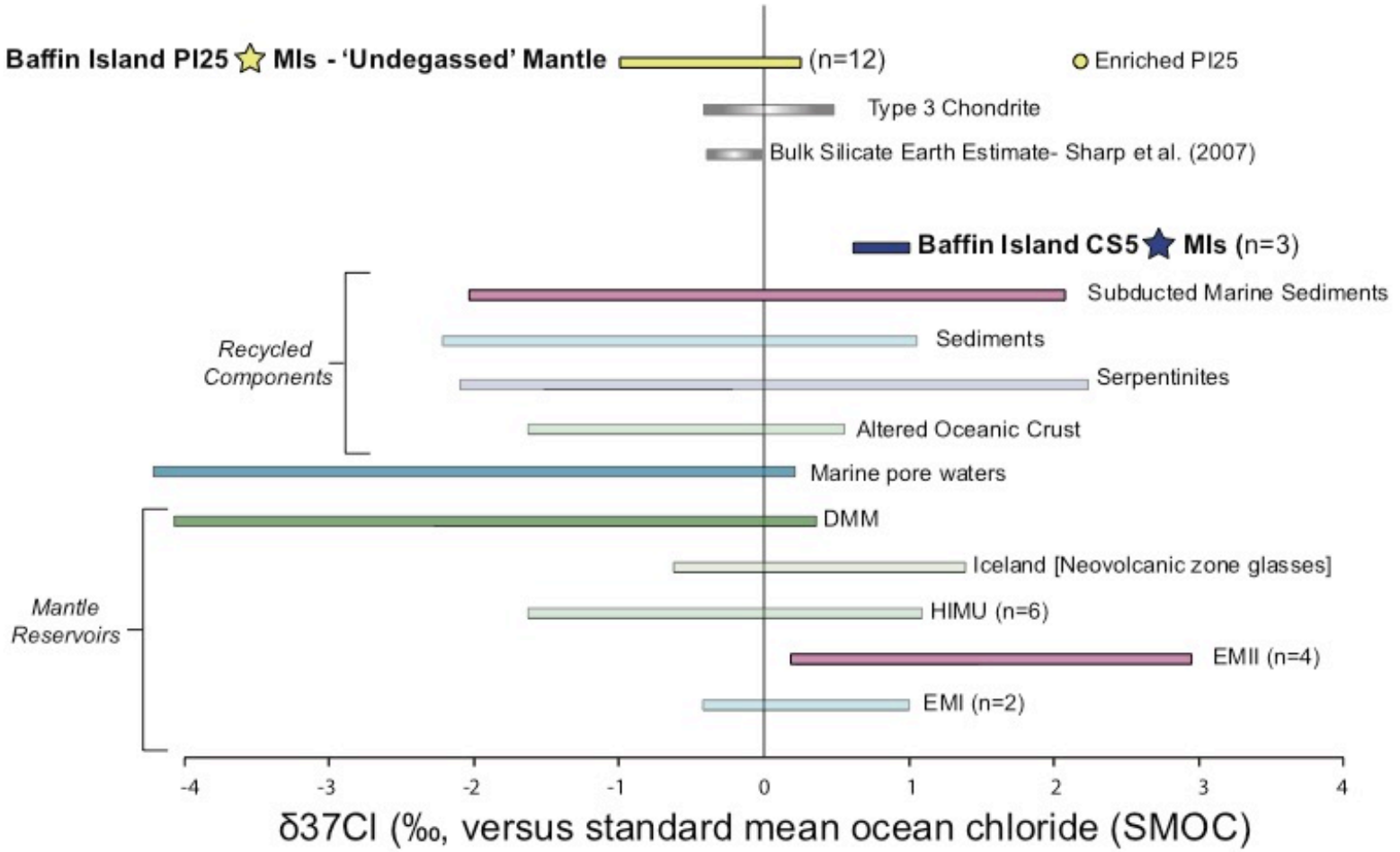

Figure 19: Global δ37Cl dataset for mantle reservoirs (OIB:John et al., 2010; MORB: Sharp et al., 2007., Bonifacie et al., 2008a., Layne et al., 2009) subduction inputs(AOC; Barnes and Cisneros 2012; Serpentinites; Barnes and Sharp (2006); Barnes et al. (2006, 2008, 2009a); Bonifacie et al. (2008b) (Barnes et al. 2014); Sediments; Barnes et al. (2009a, 2008); 5 Barnes and Cisner os (2012); SMS; John et al., 2010 and marine pore waters; Ransom et al. (1995); Spivack et al. (2002) Godon et al., 2004a,b; Boni facie et al. 2007 Also shown are type 3 Chondrites (Sharp et al., 2013) and the previous estimate for the Bulk Silicate Earth (Sharp et al., 2007).

In terms of comparable inputs; subducted marine sediments; sediments and serpentinites all have positively fractionated compositions comparable or exceeding the values in the CS5 melts.

The enriched PI25 sample is the second most isotopically positive sample within the global dataset (2.19±0.31‰); exceeded only by a Society EMII glass at 2.9‰. Comparable inputs which approach this degree of fractionation are the upper limits of serpentinites and subducted marine sediments (John et al., 2010; Barnes and Sharp 2016 and references therein).

The most remarkable feature of the presented data however relates to the compositions of the unenriched PI25 melt inclusions. The PI25 melt inclusions range in composition from -0.97 to 0.21‰; averaging -0.21‰. These values are in strong agreement with previous estimates for BSE halogen and chondritic compositions (Sharp et al.,2007; 2013). As such, this study has potentially isolated the primitive mantle $\delta^{37}Cl$ composition within the high $^{3}He/^{4}He$ mantle reservoir.

A critic may observe that the dominantly low $\delta^{37}Cl$ compositions obtained for the PI25 melt inclusions are very similar to the depleted end-member of the Halldorsson et al. (2016) Icelandic glass data. However; trace element compositions are dominantly chondritic for the melts in this study, and $^{3}He/^{4}He$ values derived from crushed olivines in this sample are the highest ever recorded in a terrestrial lava (Stuart et al., 2003;Starkey et al., 2009); a feature distinct from the Icelandic Neovolcanic Zone sample set (low helium is inferred by the authors), which therefore supports the likelihood of melt derivation from a less degassed primordial volatile reservoir.

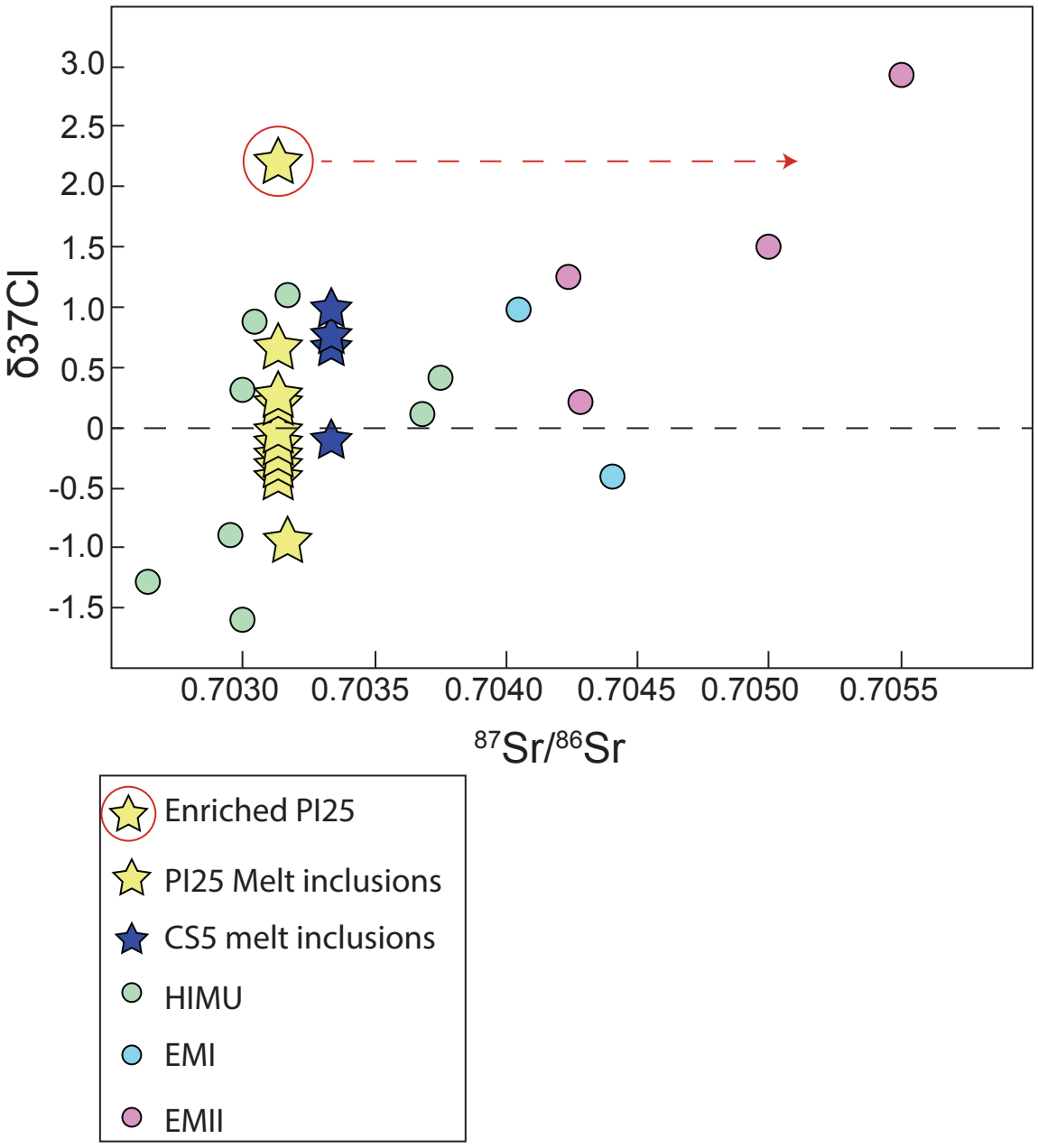

Figure 20: δ37Cl versus 87Sr/86Sr after John et al. (2010). The 87Sr/86Sr values for the PI25 and CS5 melt inclusions are the value of the whole rocks; as such caution must be advised in over interpretation. The red dashed line indicates than the enriched PI25 inclusions likely has a much more fractionated 87Sr/86Sr composition.

Use of whole rock isotopic composition data for melt inclusion data must obviously be treated with caution as OHMI variability relative to the whole rock is often highly variable. Indeed this is consistent with the conclusions of Harlou et al. (2006) when high resolution $^{87}Sr/^{86}Sr$ analyses were carried out on individual olivine hosted melt inclusions of the Baffin island suite; acutely radiogenic $^{87}Sr/^{86}Sr$ compositions being attributed to crustal contamination. With these limitations considered, the Baffin Island data appears to follow the same positive trend reflecting the relationship of heavier $\delta^{37}Cl$ in association with more radiogenic $^{87}Sr/^{86}Sr$; a trend which may reflect the relative addition of recycled sedimentary materials to the source mantle (Figure 20), (John et al., 2010). This figure serves emphasizes to that as expected, the more radiogenic whole rock sample CS5; records an isotopically heavier $\delta^{37}Cl$ composition. The notable exception to this trend is of course the anomalously enriched PI25. It is expected that this sample would exhibit a far more radiogenic $^{87}Sr/^{86}Sr$ composition which would place it closer to the EMI/EMII portion of the graph consistent with its VICE composition (red arrow).

Aside from seawater influx acting as a contaminant which could alter the $\delta^{37}Cl$ composition of the inclusions; late stage degassing can result in kinetic fractionations as HCL degasses at shallow levels (Sharp et al 2010). As already demonstrated the samples analysed for Cl, correlate in a linear fashion with K and Nb with no demonstrable Cl depletion relative to K, suggesting that degassing has not affected these samples. By inference, considering the overwhelmingly consistent results obtained for the remainder of the inclusions, neither degassing nor seawater assimilation is not expected to have affected the bulk of the $\delta^{37}Cl$ compositions of the majority of either the PI25 or CS5 melt inclusions; and as such these compositions should be considered primary.

6.6.2 Revisiting the enriched PI25 melt inclusion

The combined appearance of apparently contaminated Cl/K composition with an isotopically positive $\delta^{37}Cl$ composition is a highly erroneous association in a deep-seated melt. Halldorsson et al. (2016) pointed out that the degree of melting at Iceland could have an effect on the type of mantle being sourced; with lower degree melts at the base of the melting column sampling more enriched mantle with higher Cl and $\delta^{37}Cl$. As the degree of melting increases; asthenospheric melting would prevail which record low Cl and $\delta^{37}Cl$ compositions. In order to investigate whether or not this this phenomenon has affected the enriched melt; Cl has been plotted against $\delta^{37}Cl$ for the Halldorsson et al. (2016) sample set and the samples in

this study (Figure 21) Also included are global MORB compositions; simulating the asthenospheric component inherent to the prediction. Correlations are limited to 3 data points which have both Cl and $\delta^{37}Cl$ analyses available but it could be argued that the enriched inclusion conforms to this trend. As such degree of melting may be partly responsible for the high Cl and $\delta^{37}Cl$ of this sample. However, the degree of melting alone cannot account for the trace element enrichments seen in this sample which may be characteristic of other EMI/EMII like magmas previously observed in much younger Icelandic lavas based on enrichment in the very incompatible elements. These elements are not usually fractionated according to degree of melting and are indicative of the source (Hofmann et al., 1996 ;Stracke et al., 2003). Based on these facts; this study may conclude that this $\delta^{37}Cl$ composition of $2.19 \pm 0.31‰$ may be in part a primary signal reminiscent of the EMI/EMII-like component based upon the enrichment of this melt in the very incompatible elements La, Ba, Th and U (Hofmann et al., 1996) evident in the contemporary Iceland plume (Stracke et al., 2003., Thirlwall et al. 2004., Halldorsson et al., 2016;). This melt has interacted with a fractionated source deep in the mantle such as AOC or serpentinzed mantle endemic to the asthenosphere and not the Icelandic plume accounting for Cl contamination. This study as such anticipates; despite the apparent contamination, that more positive $\delta^{37}Cl$ compositions may be partially primary and more isotopically positive $\delta^{37}Cl$ values could potentially be discovered in Icelandic lavas with enriched mantle affinities like those at Theistareykir (Stracke et al., 2003).

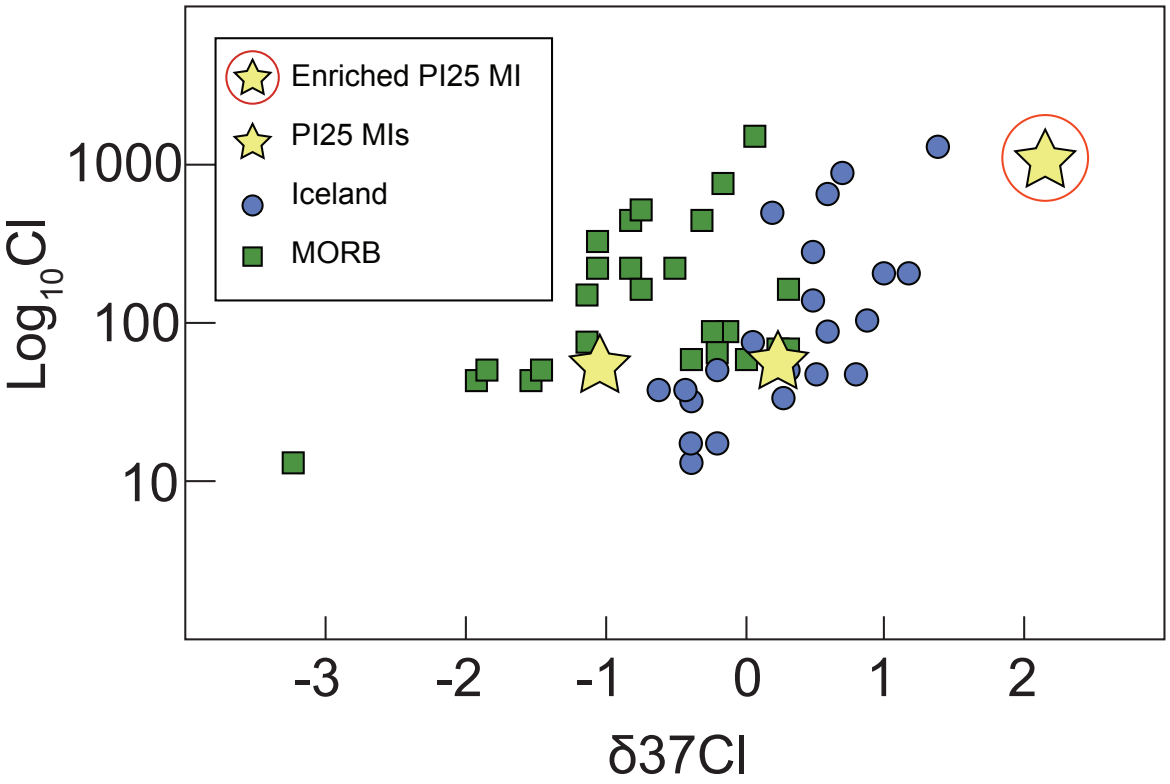

Figure 21: Cl versus δ37Cl after Halldorsson et al. (2016). Included data is the Icelandic NVZ glasses (Halldorsson et al., 2016). MORB data (Sharp et al., 2007 ; Bonifacie et al., 2008 ; Layne et al., 2009).

6.6.3. A closer look at the PI25 $\delta^{37}Cl$ signal

A closer look at the $\delta^{37}Cl$ compositions of the PI25 melt inclusions (Figure 22) compared to previous estimates for the BSE shows that there is very strong agreement between both datasets (Sharp et al., 2007; Sharp et al., 2013).

Previous estimates for the Bulk Silicate Earth are based on a diverse array of samples averaging 0.2 ‰ (Sharp et al., 2007; 2013).

This agrees closely with the least altered (Type 3) chondrites at -0.3 ±0.5‰ (Sharp et al., 2013).The Baffin Island PI25 melt inclusions record an average $\delta^{37}Cl$ composition of -0.21 ‰ (n=12; excluding the enriched melt inclusion). These inclusions record primitive trace element and $^{3}He/^{4}He$ compositions and display no definitive evidence for either crustal or seawater contamination. They represent the first attempt to directly analyze the composition of a reservoir which directly preserves primordial volatile chemistry (Hallis et al., 2015). It is thus suggested that the values presented here for the unenriched PI25 melt inclusions; may represent the BSE $\delta^{37}Cl$ composition.

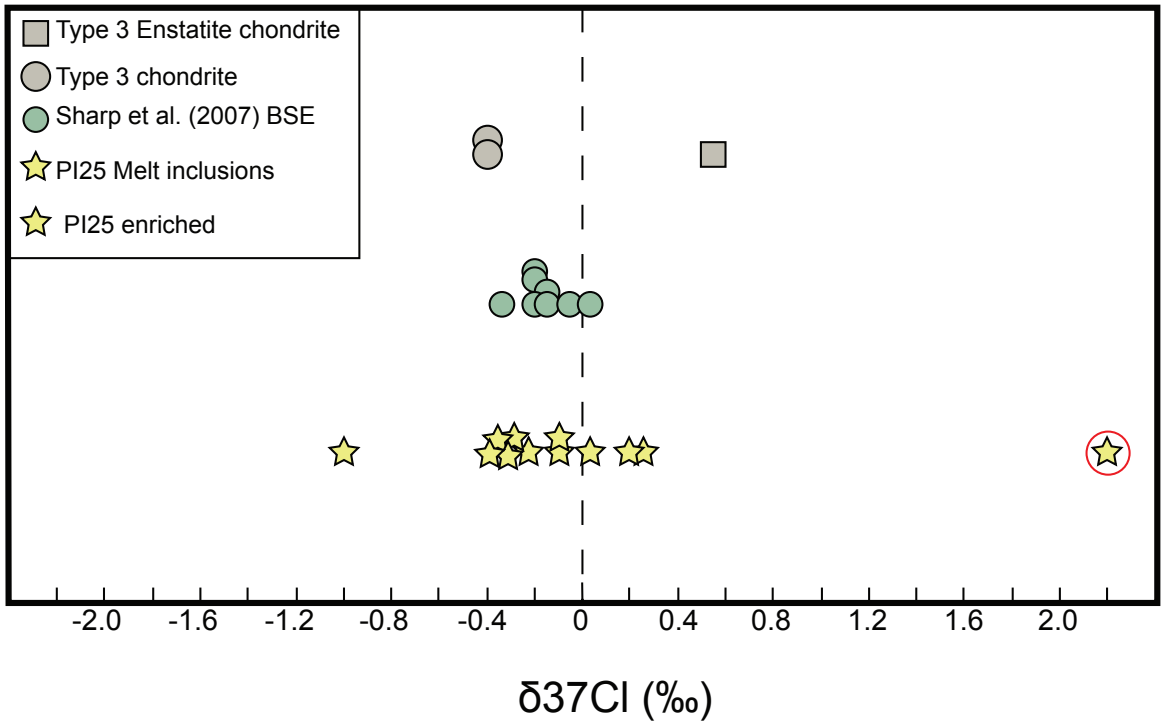

Figure 22: Comparisons between the δ37Cl compositions of type 3 Chondrites (Sharp et al., 2013); previous measurements of a variety of samples (MORB, OIB, halites, carbonatities, unaltered peridotites) used to infer the BSE δ37Cl composition (Sharp et al., 2007; 2013.). The PI25 melt inclusions of this study are very similar in value to the previous estimate for BSE.

Conclusions

Olivine-hosted melt inclusions derived from the high $^{3}He/^{4}He$ mantle reservoir (Stuart et al., 2003; Starkey et al., 2009) sampled in the 62Ma Vaigat formation lavas have potentially elucidated the combined elemental (Cl,Br) and isotopic ($\delta^{37}Cl$) halogen composition of the Bulk Silicate Earth. Lavas sampling this reservoir record primordial characteristics based on combined lead, neodymium; xenon, tungsten and deuterium isotopic constraints (Jackson et al., 2010; Mukhopadhyay et al., 2012; Rizo et al 2016; Hallis et al., 2015). The inclusions selected for this study preserve the highest $^{3}He/^{4}He$ values recorded in terrestrial samples and are as such considered the best possible representatives of the primordial mantle reservoir and by inference the Bulk Silicate Earth.

The samples considered show no obvious crustal or seawater contamination and are as such considered representative of the mantle source. Using experimentally derived partition coefficients (Joachim et al.,2015; Joachim et al., 2016) a Cl composition of 8.38-20.84 ppm is suggested for the primitive mantle. Br compositions are suggested to lie within the range of 1.84 to 28.14 ppb.

This lower value for primitive mantle Cl concentration requires that the MORB mantles composition Cl falls to the lower end of calculated values to allow for its depletion relative to BSE in agreement with recent measurements (e.g. Urann et al., 2017).The OIB reservoir is enriched by a factor of 2.5 to 9 relative to primitive mantle; suggesting long term subduction mediated enrichment of the OIB mantle since the likely onset of Wilson Cycle type tectonics at 3Ga (Shirey and Richardson, 2011;John et al., 2011; Chavrit et al., 2015).

Previous estimates for the Bulk Silicate Earth $\delta^{37}Cl$ value are based on a diverse array of samples averaging -0.2 ‰ showing no secular variation throughout the history of the Earth (Sharp et al., 2007; 2013).
This agrees closely with the least altered (Type 3) chondrites at -0.3 ±0.5‰ (Sharp et al., 2013).The Baffin Island PI25 melt inclusions record an average $\delta^{37}Cl$ composition of -0.21 ‰ (n=12; excluding an enriched melt inclusion). These inclusions record primitive trace element and $^{3}He/^{4}He$ compositions and display no definitive evidence for either crustal or seawater contamination. It is thus suggested that the values presented in this study for the non-enriched

PI25 melt inclusions; may represent the BSE $\delta^{37}Cl$ composition; which strongly agree with previous estimates.

The modern mantle $\delta^{37}Cl$ composition as such is one that reflects variable redistribution of recycled material to the mantle, accounting for the wide scale variability (John et al., 2010). This variability exceeds that of surface inputs. It may be that our input database in particular with respect to $\delta^{37}Cl$ is limiting this range and further studies may discover ever more isotopically fractionated input; as there is a noticeable lack of studies on sediments (Barnes and Sharp., 2016 and references therein). If the suggestion of (Clay et al., 2017) is correct, there would have been quick and efficient redistribution of the halogens from the BSE to surface reservoirs as a consequence of the halogens fluid mobilities (Aiuppa et al., 2009). Seawater being the most volumetrically significant reservoir for Cl; has retained the original nebular $\delta^{37}Cl$ composition of 0 ‰ (Sharp et al., 2013).

This study also potentially characterised the composition of a more enriched end member present within the Proto-Iceland mantle plume. Despite having an elevated Cl/K value of 0.17; indicating probable Cl enrichment; this inclusion records the second highest $\delta^{37}Cl$ composition within the global dataset (2.19‰). Enrichment in very incompatible elements (Ba ,Th U and Nb) suggests source variation similar to enriched-mantle type basalts observed in younger Icelandic lavas (Stracke et al., 2003; Thirlwall et al., 2004 ; Halldorsson et al., 2016). This melt then interacted with a volatile rich source; possibly altered oceanic crust or serpentinized mantle which was endemic to the Baffin Island-West Greenland asthenosphere; thereby inflating the Cl/K value of the melt (John et al., 2011; Chavrit et al., 2015).

References

Aiuppa, A., Baker, D. R., & Webster, J. D. (2008). Halogens in volcanic systems. *Chemical Geology*. https://doi.org/10.1016/j.chemgeo.2008.10.005

Barnes, J. D., & Cisneros, M. (2012). Mineralogical control on the chlorine isotope composition of altered oceanic crust. *Chemical Geology*, *326–327*, 51–60. https://doi.org/10.1016/j.chemgeo.2012.07.022

Barnes, J. D., & Straub, S. M. (2010). Chorine stable isotope variations in Izu Bonin tephra: Implications for serpentinite subduction. *Chemical Geology*, *272*(1–4), 62–74. https://doi.org/10.1016/j.chemgeo.2010.02.005

Barnes, J. D., Selverstone, J., & Sharp, Z. D. (2006). Chlorine isotope chemistry of serpentinites from Elba, Italy, as an indicator of fluid source and subsequent tectonic history. *Geochemistry, Geophysics, Geosystems*, *7*(8). https://doi.org/10.1029/2006GC001296

Barnes, J. D., Sharp, Z. D., & Fischer, T. P. (2008). Chlorine isotope variations across the Izu-Bonin-Mariana arc. *Geology*, *36*(11), 883–886. https://doi.org/10.1130/G25182A.1

Barnes, J. D., Paulick, H., Sharp, Z. D., Bach, W., & Beaudoin, G. (2009). Stable isotope (δ18O, δD, δ37Cl) evidence for multiple fluid histories in mid-Atlantic abyssal peridotites (ODP Leg 209). *Lithos*, *110*(1–4), 83–94. https://doi.org/10.1016/j.lithos.2008.12.004

Barnes, J. D., & Sharp, Z. D. (2017). Chlorine Isotope Geochemistry, *82*(2014).

Bonifacie, M., Monnin, C., Jendrzejewski, N., Agrinier, P., & Javoy, M. (2007). Chlorine stable isotopic composition of basement fluids of the eastern flank of the Juan de Fuca Ridge (ODP Leg 168). *Earth and Planetary Science Letters*, *260*(1–2), 10–22. https://doi.org/10.1016/j.epsl.2007.05.011

Bonifacie, M., Busigny, V., Mével, C., Philippot, P., Agrinier, P., Jendrzejewski, N., … Javoy, M. (2008). Chlorine isotopic composition in seafloor serpentinites and high-pressure

metaperidotites. Insights into oceanic serpentinization and subduction processes. *Geochimica et Cosmochimica Acta*, *72*(1), 126–139. https://doi.org/10.1016/j.gca.2007.10.010

Bürgmann, R., & Dresen, G. (2008). Rheology of the Lower Crust and Upper Mantle: Evidence from Rock Mechanics, Geodesy, and Field Observations. *Annual Review of Earth and Planetary Sciences*, *36*(1), 531–567. https://doi.org/10.1146/annurev.earth.36.031207.124326

Cabral, R. A., Jackson, M. G., Rose-Koga, E. F., Koga, K. T., Whitehouse, M. J., Antonelli, M. A., Hauri, E. H. (2013). Anomalous sulphur isotopes in plume lavas reveal deep mantle storage of Archaean crust. *Nature*, *496*(7446), 490–493. https://doi.org/10.1038/nature12020

Caulfield J.C., Tomlinson.E.L.,Marks.M.A.W.,Chew., D.M.,Mckenna., Ubide., T (2017) Microanalysis of Cl , Br and I in apatite , scapolite and silicate glasses by LA-ICP-MS. *Goldschmidt 2017 Abstracts,* 2017

Chavrit, D., Burgess, R., Sumino, H., Teagle, D. A. H., Droop, G., Shimizu, A., & Ballentine, C. J. (2016). The contribution of hydrothermally altered ocean crust to the mantle halogen and noble gas cycles. *Geochimica et Cosmochimica Acta*, *183*, 106–124. https://doi.org/10.1016/j.gca.2016.03.014

Clarke, D. B., & Upton, B. G. J. (1971). Tertiary Basalts of Baffin Island: Field relations and tectonic setting. *Canadian Journal of Earth Sciences*, *8*(2), 248–258. https://doi.org/doi:10.1139/e71-025

Clay, P., Burgess, R., Busemann, H., Ruziè-Hamilton, L., Joachim, B., Day, J., & Ballentine, C. (2017). Process of volatile addition to Earth revealed by halogens in chondrites. *Goldschmidt 2017 Abstracts*, *87*, 2017.

Dalou, C., Koga, K. T., Shimizu, N., Boulon, J., & Devidal, J. L. (2012). Experimental determination of F and Cl partitioning between lherzolite and basaltic melt. *Contributions to Mineralogy and Petrology*, *163*(4), 591–609. https://doi.org/10.1007/s00410-011-0688-2

Danyushevsky, L. V, Della, F. N., & Sokolov, S. (2000). Re-equilibration of melt inclusions trapped by magnesian olivine phenocrysts from subduction-related magmas : petrological implications, 68–83.

Danyushevsky, L. V, Sokolov, S., & Falloon, T. J. (2002). Melt Inclusions in Olivine Phenocrysts : Using Diffusive Re-equilibration to Determine the Cooling History of a Crystal , with Implications for the Origin of Olivine-phyric Volcanic Rocks. *Journal of Petrology*, *43*(9), 1651–1671. https://doi.org/10.1093/petrology/43.9.1651

Dasgupta, R., Hirschmann, M. M., & Smith, N. D. (2007). Partial melting experiments of peridotite + CO2 at 3 GPa and genesis of alkalic ocean island basalts. *Journal of Petrology*, *48*(11), 2093–2124. https://doi.org/10.1093/petrology/egm053

Eastoe, C. J., Peryt, T. M., Petrychenko, O. Y., & Geisler-Cussey, D. (2007). Stable chlorine isotopes in Phanerozoic evaporites. *Applied Geochemistry*, *22*(3), 575–588. https://doi.org/10.1016/j.apgeochem.2006.12.012

Ersoy, Y., & Helvaci, C. (2010). FC-AFC-FCA and mixing modeler: A Microsoft® Excel© spreadsheet program for modeling geochemical differentiation of magma by crystal fractionation, crustal assimilation and mixing. *Computers and Geosciences*, *36*(3), 383–390. https://doi.org/10.1016/j.cageo.2009.06.007

Fitton, J., Saunders, A., Norry, M., Hardarson, B., & Taylor, R. (1997). Thermal and chemical structure of the Iceland plume. *Earth and Planetary Science LettersEarth and Planetary Science Letters*, *153*(153), 197–208. https://doi.org/10.1016/S0012-821X(97)00170-2

Godon, A., Jendrzejewski, N., Eggenkamp, H. G. M., Banks, D. A., Ader, M., Coleman, M. L., & Pineau, F. (2004). A cross-calibration of chlorine isotopic measurements and suitability of seawater as the international reference material. *Chemical Geology*, *207*(1–2), 1–12. https://doi.org/10.1016/j.chemgeo.2003.11.019

Halldórsson, S. A., Barnes, J. D., Stefánsson, A., Hilton, D. R., Hauri, E. H., & Marshall, E. W. (2016). Subducted lithosphere controls halogen enrichments in the Iceland mantle plume source. *Geology*, *44*(8), 679–682. https://doi.org/10.1130/G37924.1

Hallis, L. J., Huss, G. R., Nagashima, K., Taylor, G. J., Halldórsson, S. A., Hilton, D. R., Meech, K. J. (2015). Evidence for primordial water in Earth's deep mantle. *Science (New York, N.Y.)*, *350*(6262), 336–339. https://doi.org/10.1126/science.aac4834

Harlou, R., Pearson, D.G., Davidson, J.P., Kamenetsky, V.S., Yaxley, G.M., 2006. Source variability and crustal contamination of the Baffin Island picrites — coupled Sr isotope and trace element study of individual melt inclusions. *Geochimica et Cosmochimica Acta,* 70, A231–A.

Hauri, E. (2002). SIMS analysis of volatiles in silicate glasses, 2: isotopes and abundances in Hawaiian melt inclusions. *Chemical Geology*, *183*(1–4), 115–141. http://doi.org/10.1016/S0009-2541(01)00374-6

Hilton, D. R., Grönvold, K., Macpherson, C. G., & Castillo, P. R. (1999). Extreme $^{3}He/^{4}He$ ratios in northwest Iceland: Constraining the common component in mantle plumes. *Earth and Planetary Science Letters*, *173*(1–2), 53–60. https://doi.org/10.1016/S0012-821X(99)00215-0

Hofmann, A. W., & Jochum, K. P. (1996). Source characteristics derived from very incompatible trace elements in Mauna Loa and Mauna Kea basalts, Hawaii Scientific Drilling Project. *Journal of Geophysical Research*, *101*(B5), 11831–11839. https://doi.org/10.1029/95JB03701

Hole, M. J., & Millett, J. M. (2016). Controls of mantle potential temperature and lithospheric thickness on magmatism in the North Atlantic igneous province. *Journal of Petrology*, *57*(2), 1–20. https://doi.org/10.1093/petrology/egw014

Holland, G., & Ballentine, C. J. (2006). Seawater subduction controls the heavy noble gas composition of the mantle. *Nature*, *441*(7090), 186–191. https://doi.org/10.1038/nature04761

Jackson, M. G., Carlson, R. W., Kurz, M. D., Kempton, P. D., Francis, D., & Blusztajn, J. (2010). Evidence for the survival of the oldest terrestrial mantle reservoir. *Nature*, *466*(7308), 853–856. https://doi.org/10.1038/nature09287

Jambon, A., Déruelle, B., Dreibus, G., & Pineau, F. (1995). Chlorine and bromine abundance in MORB: the contrasting behaviour of the Mid-Atlantic Ridge and East Pacific Rise and

implications for chlorine geodynamic cycle. *Chemical Geology*, *126*(2), 101–117. https://doi.org/10.1016/0009-2541(95)00112-4

Jarosewich, E., Nelen, J. A., & Norbers, J. A. (1980). Reference Samples for Electron Microprobe Analysis. *Geostandards Newsletter*, *4*(1), 43–47.

Jennings, E. S., Gibson, S. A., Maclennan, J., & Heinonen, J. S. (2017). Deep mixing of mantle melts beneath continental flood basalt provinces: Constraints from olivine-hosted melt inclusions in primitive magmas. *Geochimica et Cosmochimica Acta*, *196*, 36–57. https://doi.org/10.1016/j.gca.2016.09.015

Joachim, B., Pawley, A., Lyon, I. C., Marquardt, K., Henkel, T., Clay, P. L., … Ballentine, C. J. (2015). Experimental partitioning of F and Cl between olivine , orthopyroxene and silicate melt at Earth ' s mantle conditions. *Chemical Geology*, *416*, 65–78. https://doi.org/10.1016/j.chemgeo.2015.08.012

Joachim, B., Ruzié, L., Burgess, R., Pawley, A., Clay, P. L., & Ballentine, C. J. (2016). Bromine partitioning between olivine and melt at OIB source conditions : Indication for volatile recycling, *18*(2011), 6913.

Jochum, K., & Willbold, M. (2006). Reference Materials in Geoanalytical Research. Review for 2004 and 2005. *Geostandards and Geoanalytical Research*, 143–156. Retrieved from http://onlinelibrary.wiley.com/doi/10.1111/j.1751-908X.2006.tb01057.x/abstract

John, T., Layne, G. D., Haase, K. M., & Barnes, J. D. (2010). Chlorine isotope evidence for crustal recycling into the Earth's mantle. *Earth and Planetary Science Letters*, *298*(1–2), 175–182. https://doi.org/10.1016/j.epsl.2010.07.039

John, T., Scambelluri, M., Frische, M., Barnes, J. D., & Bach, W. (2011). Dehydration of subducting serpentinite: Implications for halogen mobility in subduction zones and the deep halogen cycle. *Earth and Planetary Science Letters*, *308*(1–2), 65–76. https://doi.org/10.1016/j.epsl.2011.05.038

Kendrick, M. a., Kamenetsky, V. S., Phillips, D., & Honda, M. (2012). Halogen systematics (Cl, Br, I) in Mid-Ocean Ridge Basalts: A Macquarie Island case study. *Geochimica et Cosmochimica Acta*, *81*, 82–93. https://doi.org/10.1016/j.gca.2011.12.004

Kendrick, M. a., Jackson, M. G., Hauri, E. H., & Phillips, D. (2015). The halogen (F, Cl, Br, I) and H2O systematics of Samoan lavas: Assimilated-seawater, EM2 and high-$^{3}He/^{4}He$ components. *Earth and Planetary Science Letters*, *410*, 197–209. https://doi.org/10.1016/j.epsl.2014.11.026

Kendrick, M. A., Hémond, C., Kamenetsky, V. S., Danyushevsky, L., Devey, C. W., Rodemann, T., … Perfit, M. R. (2017). Seawater cycled throughout Earth's mantle in partially serpentinized lithosphere. *Nature Geoscience*, *10*(February). https://doi.org/10.1038/ngeo2902

Kurz, M. D., Jenkins, W. J., & Hart, S. R. (1982). Helium isotopic systematics of oceanic islands and mantle heterogeneity. *Nature*, *297*, 43–47. https://doi.org/10.1038/297043a0

Lassiter et al 2002 Le Gall, B., Tshoso, G., Jourdan, F., Féraud, G., Bertrand, H., Tiercelin, J. J., Maia, M. (2002). Chlorine-potassium variations in melt inclusions from Raivavae and Rapa, Austral Islands: Constraints on chlorine recycling in the mantle and evidence for brine-induced melting of oceanic crust. *Earth and Planetary Science Letters*, *202*(3–4), 525–540. https://doi.org/10.1016/S0012-821X(02)00826-9

Layne, G. D., Godon, A., Webster, J. D., & Bach, W. (2004). Secondary ion mass spectrometry for the determination of $\delta^{37}Cl$ Part I. Ion microprobe analysis of glasses and fluids. *Chemical Geology*, *207*(3–4), 277–289. https://doi.org/10.1016/j.chemgeo.2004.04.002

Layne, G. D., Kent, A. J. R., & Bach, W. (2009). δ37Cl systematics of a backarc spreading system: The Lau Basin. *Geology*, *37*(5), 427–430. https://doi.org/10.1130/G25520A.1

Le Bas, M. J. (2000). IUGS Reclassification of the High-Mg and Picritic Volcanic Rocks. *Journal of Petrology*, *41*(10), 1467–1470. https://doi.org/10.1093/petrology/41.10.1467

Le Voyer, M., Asimow, P. D., Mosenfelder, J. L., Guan, Y., Wallace, P., Schiano, P., Eiler, J. M. (2014). Zonation of H2O and F concentrations around melt inclusions in olivines. *Journal of Petrology*, *55*(4), 685–707. https://doi.org/10.1093/petrology/egu003

Luth, R. W., Heinrich, D. H., & Karl, K. T. (2003). Mantle Volatiles--Distribution and Consequences. *Treatise on Geochemistry*, *2*, 319–361. Retrieved from http://www.sciencedirect.com/science/article/B782S-4CJV6M2-1C/2/66f42f033e6cc095dc7a3a1eae27720e

Lyubetskaya, T., & Korenaga, J. (2007). Chemical composition of Earth's primitive mantle and its variance: 1. Method and results. *Journal of Geophysical Research: Solid Earth*, *112*(3), 1–21. https://doi.org/10.1029/2005JB004223

Mackwell, S. (2012). Melt inclusions in olivine: Reliable witnesses to earth's interior? *Geology*, *40*(10), 959–960. https://doi.org/10.1130/focus102012.1

Manzini, M., Bouvier, A., Barnes, J. D., Bonifacie, M., Rose-koga, E. F., Ulmer, P., John, T. (2017). SIMS chlorine isotope analyses in melt inclusions from arc settings. *Chemical Geology*, *449*, 112–122. https://doi.org/10.1016/j.chemgeo.2016.12.002

McDonough, W. F. (1990). Constraints on the composition of the continental lithospheric mantle. *Earth and Planetary Science Letters*, *101*(1), 1–18. https://doi.org/10.1016/0012-821X(90)90119-I

McDonough, W. F., & Sun, S. s. (1995). The composition of the Earth. *Chemical Geology*, *120*(3–4), 223–253. https://doi.org/10.1016/0009-2541(94)00140-4

Michael, P. J., & Schilling, J. G. (1989). Chlorine in mid-ocean ridge magmas: Evidence for assimilation of seawater-influenced components. *Geochimica et Cosmochimica Acta*, *53*(12), 3131–3143. https://doi.org/10.1016/0016-7037(89)90094-X

Mihalffy, P., Steinberger, B., & Schmeling, H. (2008). The effect of the large-scale mantle flow field on the Iceland hotspot track. *Tectonophysics*, *447*(1–4), 5–18. https://doi.org/10.1016/j.tecto.2006.12.012

Mundl, A., Touboul, M., Jackson, M. G., Day, J. M. D., Kurz, M. D., Lekic, V., Walker, R. J. (2017). Tungsten-182 heterogeneity in modern ocean island basalts. *Science*, *356*(6333), 66–69. https://doi.org/10.1126/science.aal4179

Palme, H., O'Neil, H. S. C., Holland, H. D., & Turekian, K. K. (2003). Cosmochemical estimatess of mantle composition. *The Mantle and the Core*, *2*, 1–38. https://doi.org/10.1016/B978-0-08-095975-7.00201-1

Palme, H., & O'Neill, H. (2013). *Cosmochemical Estimates of Mantle Composition*. *Treatise on Geochemistry: Second Edition* (2nd ed., Vol. 3). Elsevier Ltd. https://doi.org/10.1016/B978-0-08-095975-7.00201-1

Paton, C., Hellstrom, J., Paul, B., Woodhead, J., & Hergt, J. (2011). Iolite: Freeware for the visualisation and processing of mass spectrometric data. *Journal of Analytical Atomic Spectrometry*, *26*(12), 2508. https://doi.org/10.1039/c1ja10172b

Peate, D. W., Peate, I. U., Rowe, M. C., Thompson, J. M., & Kerr, A. C. (2012). Petrogenesis of high-MgO lavas of the lower mull plateau group, Scotland: Insights from melt inclusions. *Journal of Petrology*, *53*(9), 1867–1886. https://doi.org/10.1093/petrology/egs036

Porcelli, D., & Elliott, T. (2008). The evolution of He Isotopes in the convecting mantle and the preservation of high $^{3}He/^{4}He$ ratios. *Earth and Planetary Science Letters*, *269*(1–2), 175–185. https://doi.org/10.1016/j.epsl.2008.02.002

Pyle, D. M., & Mather, T. A. (2009). Halogens in igneous processes and their fl uxes to the atmosphere and oceans from volcanic activity : A review. *Chemical Geology*, *263*(1–4), 110–121. https://doi.org/10.1016/j.chemgeo.2008.11.013

Ransom, B., Spivack, A. J., & Kastner, M. (1995). Stable Cl isotopes in subduction-zone pore waters: implications for fluid-rock reactions and the cycling of chlorine. *Geology*, *23*(8), 715–718. https://doi.org/10.1130/0091-7613(1995)023<0715:SCIISZ>2.3.CO;2

Rizo, H., Walker, R. J., Carlson, R. W., Horan, M. F., Mukhopadhyay, S., Manthos, V., … Jackson, M. G. (2016). processes of core formation (5), which is arguably the most important chemical differentiation event to occur on a rocky planet. Only recently, however, have measurement techniques improved to the. *Science (New York, N.Y.)*, *352*(6287), 809.

Roberge, M., Bureau, H., Bolfan-Casanova, N., Frost, D. J., Raepsaet, C., Surble, S., … Fiquet, G. (2015). Is the transition zone a deep reservoir for fluorine? *Earth and Planetary Science Letters*, *429*, 25–32. https://doi.org/10.1016/j.epsl.2015.07.051

Roberge, M., Bureau, H., Bolfan-Casanova, N., Raepsaet, C., Surble, S., Khodja, H., … Fiquet, G. (2017). Chlorine in wadsleyite and ringwoodite: An experimental study. *Earth and Planetary Science Letters*, *467*, 99–107. https://doi.org/10.1016/j.epsl.2017.03.025

Robillard, I., Francis, D., & Ludden, J. N. (1992). The relationship between E- and N-type magmas in the Baffin Bay Lavas. *Contributions to Mineralogy and Petrology*, *112*(2–3), 230–241. https://doi.org/10.1007/BF00310457

Roedder, E., & Emslie, R. F. (1970). Olivine-liquid equilibrium. *Contribution to MIneralogy and Petrology*, *29*, 275–289.

Rollinson, H. R. 1. (1993). *Using geochemical data: evaluation, presentation, interpretation.* Harlow, Essex, England : New York: Longman Scientific & Technical.

Rose-Koga, E. F., Koga, K. T., Moreira, M., Vlastelic, I., Jackson, M. G., Whitehouse, M. J., Habib, N. (2017). Geochemical systematics of Pb isotopes, fluorine, and sulfur in melt inclusions from São Miguel, Azores. *Chemical Geology*, *458*(November 2016), 22–37. https://doi.org/10.1016/j.chemgeo.2017.03.024

Schauble, E. a, Rossman, G. R., & Taylor, H. P. J. (2003). Theoretical estimates of equilibrium chlorine-isotope fractionations, Geochimica et Cosmochimica Acta. *Geochim Cosmochim Acta*, *67*(17), 3267–3281. https://doi.org/10.1016/S0016-7037(00)01375-3

Scambelluri, M., Piccardo O, G., Philipot, P., Robiano, A., & Negretti, L. (1997). High salinity fluid inclusions formed from recycled seawater in deeply subducted alpine serpentinite. *Earth and Planetary Science Letters*, *148*(3–4), 485–499. https://doi.org/10.1016/S0012-821X(97)00043-5

Schilling, J. G., Unni, C. K., & Bender, M. L. (1978). Origin of chlorine and bromine in the oceans. *Nature*, *273*(5664), 631–636. https://doi.org/10.1038/273631a0

Selverstone, J., & Sharp, Z. D. (2015). Chlorine isotope behavior during prograde metamorphism of sedimentary rocks. *Earth and Planetary Science Letters*, *417*, 120–131. https://doi.org/10.1016/j.epsl.2015.02.030

Sharp, Z. D., Barnes, J. D., Brearley, A. J., Chaussidon, M., Fischer, T. P., & Kamenetsky, V. S. (2007). Chlorine isotope homogeneity of the mantle , crust and carbonaceous chondrites, *446*(April), 1062–1065. https://doi.org/10.1038/nature05748

Sharp, Z. D., & Draper, D. S. (2013). The chlorine abundance of Earth: Implications for a habitable planet. *Earth and Planetary Science Letters*, *369–370*, 71–77. https://doi.org/10.1016/j.epsl.2013.03.005

Sharp, Z. D., Mercer, J. A., Jones, R. H., Brearley, A. J., Selverstone, J., Bekker, A., & Stachel, T. (2013). The chlorine isotope composition of chondrites and Earth. *Geochimica et Cosmochimica Acta*, *107*, 189–204. https://doi.org/10.1016/j.gca.2013.01.003

Shimizu, K., Saal, A. E., Myers, C. E., Nagle, A. N., Hauri, E. H., Forsyth, D. W., Niu, Y. (2016). Two-component mantle melting-mixing model for the generation of mid-ocean ridge basalts: Implications for the volatile content of the Pacific upper mantle. *Geochimica et Cosmochimica Acta*, *176*, 44–80. https://doi.org/10.1016/j.gca.2015.10.033

Shirey, S. B., & Richardson, S. H. (2011). Start of the Wilson Cycle at 3 Ga Shown by Diamonds from Subcontinental Mantle. *Science*, *333*(6041), 434–436. https://doi.org/10.1126/science.1206275

Sobolev, A. V. (1996). Melt Incusions in Minerals as a source of principle petrological information. *Petrology*, *4*(3), 209–220.

Spivack, A. J., Kastner, M., & Ransom, B. (2002). Elemental and Isotopic Chloride Geochemistry and Fluid Flow in the Nankai Trough. *Geophysical Research Letters*, *29*(14), 4–7. https://doi.org/10.1029/2001GL014122

Stuart, F. M., Lass-Evans, S., Fitton, J. G., & Ellam, R. M. (2003). High $^{3}He/^{4}He$ ratios in picritic basalts from Baffin Island and the role of a mixed reservoir in mantle plumes. *Nature*, *424*(6944), 57–59. https://doi.org/10.1038/nature01711

Starkey, N. a., Stuart, F. M., Ellam, R. M., Fitton, J. G., Basu, S., & Larsen, L. M. (2009). Helium isotopes in early Iceland plume picrites: Constraints on the composition of high $^{3}He/^{4}He$ mantle. *Earth and Planetary Science Letters*, *277*(1–2), 91–100. https://doi.org/10.1016/j.epsl.2008.10.007

Starkey, N. A., Fitton, J. G., Stuart, F. M., & Larsen, L. M. (2012). Melt inclusions in olivines from early Iceland plume picrites support high 3He/ 4He in both enriched and depleted mantle. *Chemical Geology*, *306–307*, 54–62. https://doi.org/10.1016/j.chemgeo.2012.02.022

Staudacher, T., & Allègre, C. J. (1988). Recycling of oceanic crust and sediments: the noble gas subduction barrier. *Earth and Planetary Science Letters*, *89*(2), 173–183. https://doi.org/10.1016/0012-821X(88)90170-7

Straub, S. M., & Layne, G. D. (2003). The systematics of chlorine, fluorine, and water in Izu arc front volcanic rocks: Implications for volatile recycling in subduction zones. *Geochimica et Cosmochimica Acta*, *67*(21), 4179–4203. https://doi.org/10.1016/S0016-7037(03)00307-7

Stracke, A., Zindler, A., Salters, V. J. M., McKenzie, D., Janne, B. T., Albarède, F., & Grönvold, K. (2003). Theistareykir revisited. *Geochemistry, Geophysics, Geosystems*, *4*(2). https://doi.org/10.1029/2001GC000201

Sumino, H., Burgess, R., Mizukami, T., Wallis, S. R., Holland, G., & Ballentine, C. J. (2010). Seawater-derived noble gases and halogens preserved in exhumed mantle wedge peridotite. *Earth and Planetary Science Letters*, *294*(1–2), 163–172. https://doi.org/10.1016/j.epsl.2010.03.029

Sun, S ., & McDonough, W. F. (1989). Chemical and isotopic systematics of oceanic basalts: implications for mantle composition and processes. *Geological Society, London, Special Publications*, *42*(1), 313–345. https://doi.org/10.1144/GSL.SP.1989.042.01.19

Thériault, R. ., St-Onge, M. ., & Scott, D. . (2001). Nd isotopic and geochemical signature of the Paleoproterozoic Trans-Hudson Orogen, southern Baffin Island, Canada: implications for the evolution of eastern Laurentia. *Precambrian Research*, *108*(1–2), 113–138. https://doi.org/10.1016/S0301-9268(00)00159-5

Thirlwall, M. F., Gee, M. A. M., Taylor, R. N., & Murton, B. J. (2004). Mantle components in Iceland and adjacent ridges investigated using double-spike Pb isotope ratios. *Geochimica et Cosmochimica Acta*, *68*(2), 361–386. https://doi.org/10.1016/S0016-7037(03)00424-1

Urann, B. M., Le Roux, V., Hammond, K., Marschall, H. R., Lee, C. T. A., & Monteleone, B. D. (2017). Fluorine and chlorine in mantle minerals and the halogen budget of the Earth's mantle. *Contributions to Mineralogy and Petrology*, *172*(7), 1–17. https://doi.org/10.1007/s00410-017-1368-7

von Glasow, R., Bobrowski, N., & Kern, C. (2009). The effects of volcanic eruptions on atmospheric chemistry. *Chemical Geology*, *263*(1–4), 131–142. https://doi.org/10.1016/j.chemgeo.2008.08.020

White, W. M. (2010). Oceanic Island Basalts and Mantle Plumes : The Geochemical Perspective. https://doi.org/10.1146/annurev-earth-040809-152450

White, W. M. (2015). *Isotope Geochemistry*. https://doi.org/10.1007/978-3-319

Yaxley, G. M., Kamenetsky, V. S., Kamenetsky, M., Norman, M. D., & Francis, D. (2004). Origins of compositional heterogeneity in olivine-hosted melt inclusions from the Baffin Island picrites. *Contributions to Mineralogy and Petrology*, *148*(4), 426–442. https://doi.org/10.1007/s00410-004-0613-z

Appendix

Supplementary Figure 1

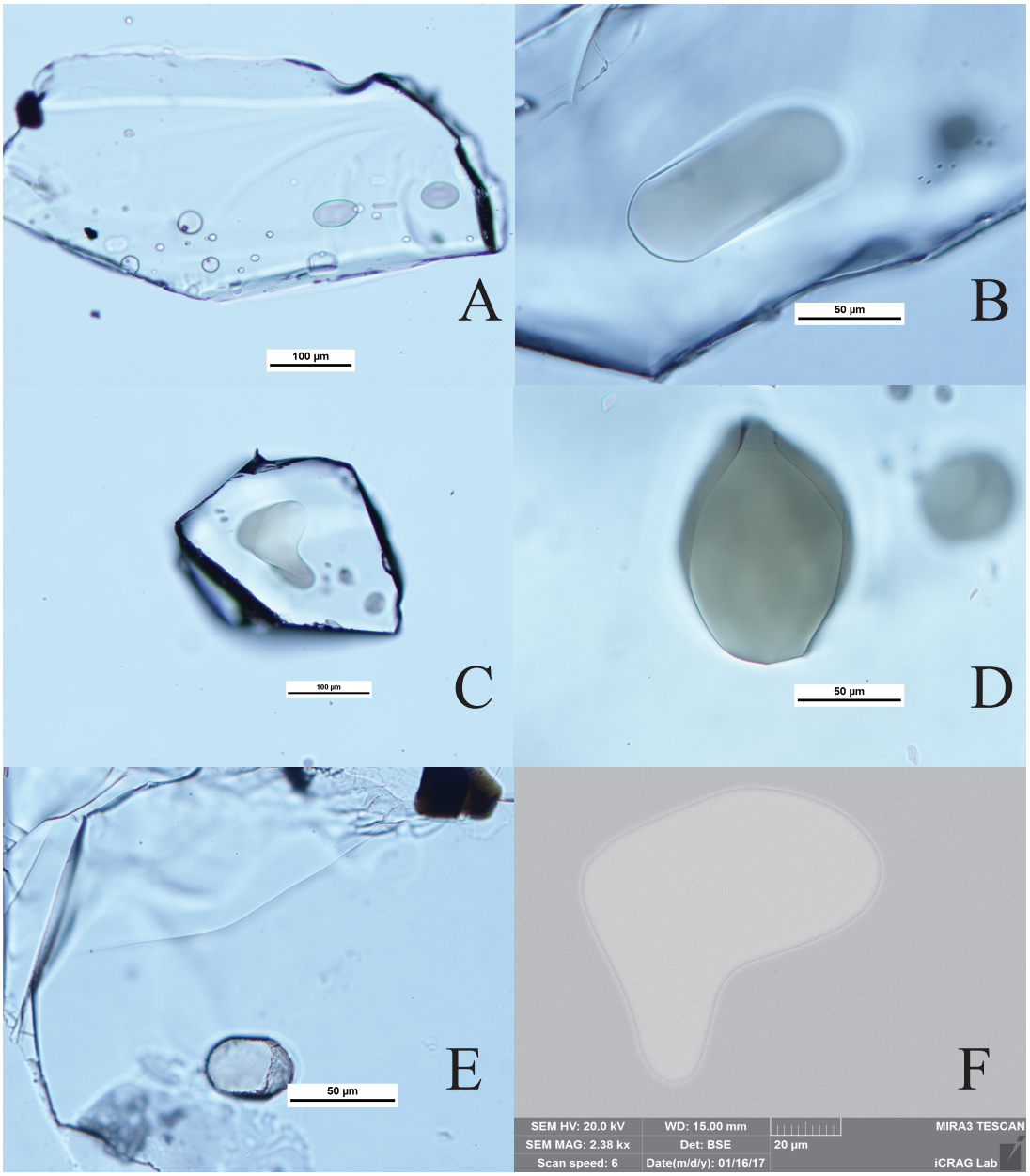

Supplementary Figure 1. 1A Typical sub 30µm oval inclusions. 1B: Wide aspect cylindrical inclusion; partially exposed. 1C: Orange-pink inclusion with irregular morphology. 1D:PI-25-1-6: Brown inclusion with irregular morphology; This 'enriched' inclusion was unique among the datset rrecording a highly positive δ37l composition. 1E: Heavily recrystallised inclusion prevalent in the CS5 phenocrysts. 1F: Backscattered electron image of inclusion with a recrystallised rim.

Supplementary Table 1: Olivine major element data

Sample	MgO	AL2O3	SIO2	CaO	TiO2	MnO	FeOt	Total
1.PI-25 1	45.73	0.04	38.97	0.36	0.01	0.23	14.80	100.23
1. PI-25 1	46.58	0.02	38.77	0.34	<LOD	0.20	13.87	99.86
1.PI-25 2	45.71	0.03	39.34	0.36	<LOD	0.27	14.62	100.42
1.PI-25 2	45.51	0.01	38.94	0.38	<LOD	0.25	14.53	99.71
1. PI-25 3	45.78	0.06	38.81	0.36	0.03	0.27	15.02	100.40
1. PI-25 3	45.59	0.01	39.01	0.35	<LOD	0.21	15.06	100.29
1. PI-25 4	45.74	0.02	38.26	0.35	0.03	0.22	14.90	99.60
1. PI-25 4	45.82	0.01	39.00	0.37	0.02	0.19	15.11	100.57
1.PI-25 5	44.93	0.29	39.99	0.57	0.01	0.27	14.95	101.05
1.PI-25 5	45.43	0.01	39.53	0.36	<LOD	0.26	15.19	100.85
1.PI-25 6	44.49	0.01	37.77	0.35	<LOD	0.23	16.49	99.38
1.PI-25 6	44.95	<LOD	38.74	0.42	0.01	0.24	15.14	99.56
1.PI-25 7	45.44	0.03	39.09	0.37	<LOD	0.22	15.39	100.61
1.PI-25 8	44.92	0.00	39.74	0.37	0.01	0.25	15.55	100.94
1.PI-25 8	45.04	0.03	39.56	0.35	0.02	0.17	15.57	100.84
1.PI-25 9	45.47	0.02	38.78	0.36	0.01	0.23	15.37	100.30
1.PI-25 10	45.51	0.01	39.58	0.36	0.01	0.17	15.11	100.79
1.PI-25 10	45.55	<LOD	38.85	0.35	<LOD	0.21	14.78	99.77
1.PI-25 11	45.62	0.03	39.41	0.37	0.03	0.23	15.37	101.16
1.PI-25 11	45.92	0.01	37.80	0.38	<LOD	0.18	14.78	99.15
1.PI-25 12	46.95	0.03	38.53	0.34	0.01	0.15	13.18	99.29
1.PI-25 12	46.94	0.04	38.22	0.36	<LOD	0.18	13.46	99.32
1.PI-25 13	45.46	<LOD	39.25	0.33	0.01	0.22	15.03	100.37
1.PI-25 13	45.30	0.01	39.06	0.39	0.01	0.27	14.98	100.11
1.PI-25 14	44.97	0.04	38.20	0.38	<LOD	0.24	15.71	99.61
1.PI-25 14	45.11	<LOD	38.88	0.36	0.01	0.30	15.24	99.95
1.PI-25 15	45.31	0.04	39.42	0.34	0.07	0.25	14.94	100.45
1.PI-25 15	45.41	0.01	38.92	0.40	0.02	0.23	15.03	100.10
1.PI-25 16	45.76	0.02	39.32	0.38	0.02	0.22	15.30	101.10
1.PI-25 16	45.48	0.04	38.42	0.38	0.02	0.22	14.84	99.49
1.PI-25 17	45.98	0.02	39.06	0.34	0.03	0.23	14.80	100.49
1.PI-25 17	46.11	0.03	39.44	0.35	<LOD	0.22	14.74	100.94
1.PI-25 18	45.23	0.05	39.95	0.35	<LOD	0.22	14.90	100.79
1.PI-25 18	45.86	0.02	38.93	0.35	<LOD	0.21	14.80	100.21
1.PI-25 19	46.19	0.01	39.14	0.36	<LOD	0.22	14.56	100.56
1.PI-25 19	45.50	0.01	39.53	0.34	0.01	0.26	15.02	100.73
1.PI-25 20	45.73	0.01	39.66	0.38	<LOD	0.24	15.12	101.24
1.PI-25 20	45.84	<LOD	39.21	0.38	<LOD	0.25	14.81	100.55

1.PI-25 21	45.70	0.02	39.55	0.38	<LOD	0.23	15.08	101.02
1.PI-25 21	45.16	0.01	39.20	0.36	0.02	0.28	15.29	100.38
2. PI-25 1	46.49	<LOD	38.46	0.39	<LOD	0.22	14.41	100.01
2. PI-25 2	46.02	0.01	37.84	0.38	0.01	0.21	14.58	99.11
2. PI-25 2	45.76	<LOD	39.04	0.35	<LOD	0.19	14.58	99.99
2. PI-25 3	45.66	0.02	38.12	0.36	<LOD	0.20	14.62	99.03
2. PI-25 3	45.43	0.02	38.01	0.38	0.01	0.24	14.91	99.05
2. PI-25 4	45.33	<LOD	39.88	0.37	0.02	0.21	15.02	100.85
2. PI-25 4	45.07	0.02	39.90	0.36	0.01	0.25	15.05	100.74
2. PI-25 5	45.39	<LOD	38.92	0.37	0.02	0.23	15.39	100.40
2. PI-25 5	45.96	0.02	38.60	0.36	<LOD	0.24	14.90	100.14
2. PI-25 6	45.76	0.07	38.43	0.36	0.04	0.26	15.01	100.03
2. PI-25 6	45.33	0.02	38.83	0.37	0.01	0.22	14.86	99.73
2. PI-25 7	45.74	0.03	38.74	0.36	<LOD	0.20	14.88	100.00
2. PI-25 7	46.02	<LOD	38.51	0.35	<LOD	0.21	14.58	99.74
2. PI-25 8	45.43	<LOD	39.81	0.35	<LOD	0.20	15.23	101.08
2. PI-25 8	44.80	0.01	39.53	0.34	<LOD	0.22	14.90	99.84
2. PI-25 9	45.36	0.02	39.95	0.36	<LOD	0.22	14.74	100.75
2. PI-25 9	45.96	0.01	38.52	0.36	<LOD	0.24	14.83	99.98
2. PI-25 10	45.38	<LOD	39.12	0.34	<LOD	0.21	14.81	99.93
2. PI-25 10	41.79	0.01	40.12	0.39	0.01	0.19	14.50	97.07
2. PI-25 12	45.36	0.02	39.62	0.36	0.01	0.27	14.92	100.65
2. PI-25 12	46.11	0.04	38.71	0.33	<LOD	0.26	14.59	100.11
2. PI-25 13	45.35	0.00	39.20	0.34	<LOD	0.25	15.01	100.22
2. PI-25 14	45.50	0.01	38.78	0.39	<LOD	0.21	14.51	99.45
2. PI-25 14	45.54	0.01	39.47	0.35	0.03	0.24	14.91	100.60
2. PI-25 15	45.26	0.03	38.81	0.39	<LOD	0.23	15.54	100.38
2. PI-25 15	45.11	<LOD	39.54	0.40	<LOD	0.24	14.79	100.11
3.CS-5 3	45.12	0.04	38.97	0.36	0.02	0.22	14.87	99.68
3.CS-5 3	45.30	0.02	38.93	0.34	<LOD	0.29	15.07	100.04
3.CS-5 3	45.12	0.04	38.97	0.36	0.02	0.22	14.87	99.68
3.CS-5 3	45.30	0.02	38.93	0.34	<LOD	0.29	15.07	100.04
3.CS-5 4	45.86	0.01	38.77	0.36	<LOD	0.24	14.63	99.92
3.CS-5 4	45.76	0.02	38.98	0.35	<LOD	0.22	14.33	99.78
3.CS-5 4	45.86	0.01	38.77	0.36	<LOD	0.24	14.63	99.92
3.CS-5 4	45.76	0.02	38.98	0.35	<LOD	0.22	14.33	99.78
3.CS-5 5	46.38	0.04	39.01	0.35	0.02	0.19	13.46	99.53
3.CS-5 5	46.44	0.01	39.06	0.36	<LOD	0.21	13.66	99.78
3.CS-5 5	46.09	0.02	39.03	0.36	0.02	0.21	14.55	100.33
3.CS-5 5	46.38	0.04	39.01	0.35	0.02	0.19	13.46	99.53
3.CS-5 5	46.44	0.01	39.06	0.36	<LOD	0.21	13.66	99.78
3.CS-5 5	46.09	0.02	39.03	0.36	0.02	0.21	14.55	100.33

Supplementary Table 1: Olivine phenocryst major element data. <LOD= Below limit of detection.

Supplementary Table 2: Uncorrected melt inclusion major element data

Label	Na2O	MgO	Al2O3	SiO2	K2O	CaO	TiO2	MnO	FeOt
1.PI25 5	2.09	8.25	15.28	49.18	0.20	13.08	1.28	0.08	10.32
1.PI25 6	2.21	7.70	14.44	49.94	0.65	11.85	1.39	0.22	11.19
*1.PI-25 7	2.10	7.71	15.11	49.52	0.19	13.05	1.29	0.14	10.19
1.PI-25 9	2.20	8.03	14.84	49.79	0.18	12.96	1.28	0.18	10.35
1.PI-25 10	2.36	6.41	15.52	49.78	0.17	13.68	1.28	0.20	10.32
1.PI-25 11	2.18	7.48	15.44	49.93	0.21	13.10	1.22	0.22	10.05
1.PI-25 12	1.93	8.13	15.69	48.86	0.13	13.15	1.05	0.15	9.18
*1.PI-2514A	2.09	7.47	14.87	49.28	0.14	13.54	1.30	0.24	10.90
1.PI-25 14B	1.94	7.60	14.74	49.85	0.22	13.24	1.20	0.09	10.64
*1.PI-25 15	2.10	7.91	15.12	49.92	0.19	13.18	1.29	0.17	10.21
1.PI-25 17	2.03	7.32	15.57	50.55	0.24	13.09	1.18	0.22	9.57
1.PI-25 19	2.24	7.72	15.53	50.30	0.29	12.71	1.17	0.14	9.59
1.PI-25 20A	1.92	7.34	15.75	50.59	0.24	12.76	1.28	0.21	9.65
1.PI-25 20B	1.83	7.60	15.52	50.52	0.23	12.86	1.28	0.20	9.70
2. PI-25 1	1.99	8.04	15.29	50.16	0.23	13.09	1.27	0.24	9.53
2.PI-25 2	1.92	8.21	15.42	49.70	0.21	13.11	1.16	0.20	9.98
2.PI-25 2B	1.95	8.09	15.46	49.44	0.12	13.71	0.90	0.18	10.03
2. PI-25 3	2.07	8.04	15.07	49.39	0.19	13.23	1.36	0.16	10.29
*2. PI-25 4	2.07	7.61	15.04	49.05	0.16	13.29	1.31	0.16	10.34
2.PI-25 7	2.10	8.07	15.41	49.49	0.17	12.91	1.30	0.31	10.02
2.PI-25 8	1.93	8.00	15.23	48.60	0.14	13.47	1.24	0.23	11.03
*2. PI-25 9	2.04	7.86	15.30	49.21	0.17	12.99	1.25	0.16	10.06
2.PI-25 10	2.23	7.57	15.21	49.42	0.21	13.44	1.26	0.12	10.19
2. PI-25 14	1.97	8.16	15.38	49.69	0.16	13.06	1.40	0.22	9.75
2. PI-25 14A	2.03	6.46	15.50	49.67	0.18	14.03	1.42	0.16	10.39
2.PI-25 14B	2.17	7.27	15.19	50.17	0.21	13.41	1.23	0.14	10.05
2. PI-25 14C	2.09	7.52	15.32	49.88	0.21	13.20	1.28	0.17	10.23
2.PI-25 14D	2.11	6.92	15.21	50.24	0.21	13.41	1.21	0.23	10.29
2.PI-25 15	2.09	7.84	14.78	49.71	0.24	12.87	1.27	0.21	10.75
2.PI-25 15B	2.18	7.78	14.76	49.35	0.19	13.04	1.35	0.27	10.90
3.CS5C3	2.18	3.09	17.02	50.59	0.21	15.55	1.49	0.16	8.62
3.CS5C4	1.98	2.74	17.97	51.59	0.23	15.50	1.37	0.19	8.16

3.CSC5A	2.06	6.37	15.84	49.71	0.21	13.86	1.30	0.29	9.80
3.CSC5B	1.25	4.23	16.93	51.89	0.34	14.47	1.21	0.08	9.17

*Supplementary Table 2: Melt inclusion data uncorrected for post entrapment crystallisation. *denotes substituted data (see methods)*

Supplementary Table 3: Corrected melt inclusion major element data

0.01% increments of olivine added until melts were in equilibrium with and olivine of Fo93									
Label	**Na2O**	**MgO**	**Al2O3**	**SiO2**	**K2O**	**CaO**	**TiO2**	**MnO**	**FeOt**
1.PI25 5	1.48	19.83	10.81	46.58	0.14	9.26	0.91	0.06	10.74
1.PI25 6	1.45	21.30	9.50	46.63	0.43	7.80	0.92	0.15	11.63
*1.PI-25 7	1.45	20.22	10.45	46.80	0.13	9.03	0.89	0.10	10.75
1.PI-25 9	1.53	20.25	10.29	46.88	0.12	8.99	0.89	0.12	10.80
1.PI-25 10	1.54	20.60	10.12	46.45	0.11	8.92	0.83	0.13	11.17
1.PI-25 11	1.49	20.08	10.61	46.91	0.14	9.00	0.84	0.15	10.65
1.PI-25 12	1.43	19.04	11.65	47.15	0.10	9.77	0.78	0.11	9.82
*1.PI-25 14A	1.39	20.86	9.90	46.26	0.09	9.01	0.87	0.16	11.38
1.PI-25 14B	1.31	20.69	9.94	46.77	0.15	8.92	0.81	0.06	11.17
*1.PI-25 15	1.45	20.14	10.47	46.91	0.13	9.13	0.89	0.12	10.68
1.PI-25 17	1.41	19.70	10.81	47.44	0.17	9.09	0.82	0.15	10.28
1.PI-25 19	1.58	19.60	10.96	47.41	0.20	8.97	0.83	0.10	10.21
1.PI-25 20A	1.32	19.91	10.86	47.41	0.16	8.80	0.88	0.14	10.35
1.PI-25 20B	1.27	19.88	10.79	47.43	0.16	8.94	0.89	0.14	10.33
2. PI-25 1	1.43	19.43	10.95	47.39	0.17	9.37	0.91	0.17	10.07
2.PI-25 2	1.36	19.85	10.91	46.97	0.15	9.28	0.82	0.14	10.43
2.PI-25 2B	1.38	19.75	10.95	46.79	0.09	9.71	0.64	0.13	10.49
2. PI-25 3	1.44	20.17	10.49	46.63	0.13	9.21	0.95	0.11	10.73
*2. PI-25 4	1.42	20.40	10.35	46.56	0.11	9.15	0.90	0.11	10.93
2.PI-25 7	1.31	20.82	10.31	45.90	0.09	9.12	0.84	0.16	11.35
2.PI-25 8	1.48	19.89	10.85	46.77	0.12	9.09	0.91	0.22	10.49
*2. PI-25 9	1.32	20.71	10.07	46.34	0.12	9.11	0.92	0.11	11.20
2.PI-25 10	1.48	20.12	10.35	47.02	0.15	9.14	0.84	0.10	10.70
2. PI-25 14	1.41	19.65	10.96	47.02	0.12	9.31	1.00	0.16	10.23
2. PI-25 14A	1.32	20.71	10.07	46.34	0.12	9.11	0.92	0.11	11.20
2.PI-25 14B	1.48	20.12	10.35	47.02	0.15	9.14	0.84	0.10	10.70
2. PI-25 14C	1.42	20.29	10.45	46.83	0.15	9.00	0.87	0.12	10.80

2.PI-25 14D	1.40	20.49	10.11	46.87	0.14	8.91	0.81	0.15	11.01
2.PI-25 15	1.41	20.71	10.00	46.64	0.16	8.71	0.86	0.14	11.18
2.PI-25 15B	1.47	20.81	9.93	46.37	0.13	8.77	0.91	0.18	11.31
3.CS5C3	1.37	18.90	10.70	46.77	0.13	9.78	0.94	0.10	11.16
3.CS5C4	1.23	18.78	11.11	47.05	0.14	9.59	0.85	0.12	10.97
3.CSC5A	1.46	18.41	11.19	47.01	0.15	9.79	0.92	0.21	10.75
3.CSC5B	0.80	19.14	10.86	47.62	0.22	9.28	0.78	0.05	11.07

Supplementary Table 3: Melt inclusion major element data corrected using the PETROLOG software (Danyushevsky et al., 2000). Equilibrium olivine was added to the melts in 0.01% increments until the melts were in equilibrium with an olivine of Fo93.

Supplementary Table 4: Combined halogen data

Label	$\delta^{37}Cl$	Cl ppm	Br ppb	Cl/K	Br/Clx10^3
3.CS5C3	0.81				
3.CS5C4	0.67				
3.CSC5A	-0.07				
3.CSC5B	1.01				
1.PI25 5	-0.97	62.50	<LOD	0.04	
1.PI25 6	**2.19**	923.11	1.29	0.17	1.39
*1.PI-25 7	0.21				1.73
1.PI-25 9	-0.09				
1.PI-25 10	0.03				
1.PI-25 11	-0.34				
1.PI-25 12	-0.31				
*1.PI-25 15	-0.22				
1.PI-25 17	-0.36				
1.PI-25 19	0.27	70.10	<LOD	0.032	
1.PI-25 20A	-0.28				
1.PI-25 20B	-0.08				
2. PI-25 3		123.27	0.33	0.07	2.69
2.PI-25 7		66.41	0.11	0.06	1.73
2. PI-25 14		108.84	0.43	0.05	3.98

Supplementary Table 4: Combined halogen data. The anomalously enriched inclusion is highlighted in red.

Supplementary Table 5: Nickel-corrected trace element data

Trace	**1.PI25 5**	**1.PI25 6**	***1.PI-25 7**	**1.PI-25 10**	**1.PI-25 12**
Cs	<LOD	0.462		6.969	<LOD
Rb	2.537	13.180	2.000	3.000	4.220
Ba	47.060	117.351	34.905	43.555	45.214
Th	0.445	1.831	0.569	0.447	0.904
U	0.128	0.434	<LOD	<LOD	0.151
Nb	5.168	11.2148	2.9807	4.839	5.210
La	5.085	10.0201	4.7259	4.878	5.942
Ce	11.285	16.5717	<LOD	9.679	12.961
Pr	1.624	2.0811	1.059	1.510	1.981
Nd	8.677	8.3244	7.452	10.453	11.024
Sr	142.247	84.0146	110.402	143.248	173.967
Hf	1.719	2.4279	1.275	1.200	1.292
Zr	66.263	95.5763	52.162	59.816	77.941
Sm	2.430	1.9847	1.039	2.187	2.153
Eu	1.102	0.7708	0.706	0.871	2.153
Gd	3.331	3.3914	2.667	3.059	5.297
Yb	2.134	1.9847	1.883	2.149	2.454
Y	20.033	17.9205	17.060	17.422	28.550
Pb	<LOD	<LOD	<LOD	<LOD	18.086

Trace	***1.PI-25 14A**	**1.PI-25 14B**	**1.PI-25 19**	**1.PI-25 20A**	**2. PI-25 1**
Cs	<LOD	<LOD	<LOD	<LOD	<LOD
Rb	2.494	2.662	3.210	3.160	3.537
Ba	43.625	32.780	39.600	42.800	77.574
Th	0.464	0.392	0.345	0.356	<LOD
U	0.072	<LOD	0.083	0.300	<LOD
Nb	4.5893	4.1140	4.440	4.900	7.571
La	4.4381	4.2900	3.500	4.200	6.516
Ce	11.88	10.25	7.810	9.820	26.685
Pr	1.512	1.628	1.140	1.544	2.544
Nd	8.855	7.832	4.890	5.800	11.419
Sr	156.576	104.500	68.600	129.800	186.176
Hf	1.944	1.364	1.010	1.520	7.447
Zr	68.894	58.080	37.200	58.800	89.985
Sm	2.602	2.530	1.470	1.940	<LOD
Eu	1.026	0.931	0.483	0.912	0.676
Gd	3.844	3.278	1.890	3.000	4.406

Yb	2.430	2.310	0.930	2.060	6.206
Y	24.512	20.900	9.410	18.340	29.788
Pb	<LOD	<LOD	0.630	<LOD	<LOD

Trace	**2.PI-25 2**	**2.PI-25 7**	**2.PI-25 8**	***2. PI-25 9**	**2.PI-25 10**
Cs	<LOD	0.210	1.725	<LOD	<LOD
Rb	7.4060	3.041	<LOD	3.138	2.382
Ba	76.8543	53.250	37.953	53.067	43.360
Th	0.6148	0.474	4.645	0.831	0.431
U	0.1481	0.158	1.592	0.923	<LOD
Nb	4.4715	4.799	3.981	6.080	5.038
La	4.1781	4.767	3.464	5.018	4.886
Ce	12.8556	12.31	14.465	12.009	10.535
Pr	1.9144	1.694	<LOD	1.684	1.832
Nd	6.4278	8.735	8.228	8.422	8.703
Sr	125.7616	152.59	144.648	143.051	137.410
Hf	1.3974	2.094	2.057	1.903	1.664
Zr	51.7020	66.93	60.513	61.835	68.247
Sm	<LOD	2.599	2.614	2.757	1.725
Eu	4.472	1.368	1.592	1.154	1.252
Gd	4.611	3.325	5.175	3.149	3.664
Yb	2.012	1.863	<LOD	2.480	2.428
Y	21.519	20.942	20.702	20.881	<LOD
Pb	4.332	<LOD	<LOD	3.346	<LOD

Trace	**2.PI-25 13a**	**2.PI25 13b**	**2.PI25 15**	**3.CS5C4**	**3.CSC5A**
Cs	0.229	<LOD	0.329	4.889	2.266
Rb	3.276	3.960	4.432	2.325	3.529
Ba	53.514	<LOD	47.032	48.225	70.371
Th	0.483	0.583	0.801	0.457	0.442
U	0.104	0.129	0.386	0.085	<LOD
Nb	5.690	5.137	6.719	4.069	6.251
La	5.854	4.950	7.720	4.426	5.992
Ce	12.636	12.651	13.438	10.702	12.719
Pr	1.747	1.760	2.430	1.533	1.832
Nd	9.502	8.691	7.720	9.116	7.730
Sr	149.622	148.514	142.382	151.809	158.542
Hf	2.053	2.024	3.860	1.559	1.749
Zr	68.258	69.857	63.472	66.193	68.612
Sm	3.167	2.783	10.579	2.537	2.670
Eu	1.092	1.067	1.487	1.414	0.993

Gd	3.287	3.663	3.903	3.528	3.249
Yb	1.824	2.134	2.445	3.092	1.925
Y	21.078	22.772	25.446	22.593	22.301
Pb	7.099	<LOD	6.147	<LOD	<LOD

Trace	**3.CSC5B**
Cs	0.871
Rb	3.827
Ba	76.747
Th	0.731
U	0.159
Nb	6.847
La	5.923
Ce	14.081
Pr	2.268
Nd	10.104
Sr	174.131
Hf	1.752
Zr	71.265
Sm	2.343
Eu	1.161
Gd	4.300
Yb	2.515
Y	22.465
Pb	<LOD

Supplementary Table 5: Nickel-corrected trace element data. Partial analysis of olivines resulted in poor concentrations so a simple correction factor based upon the percentage of nickel included in the analysis was employed to correct data. Ratios remain unaffected by this correction.